Differential effects of *Sutherlandia frutescens* subs. *microphylla* on cell numbers, morphology, gene and protein expression in a breast adenocarcinoma and a normal breast epithelial cell line

by
Barend Andre Stander
(25432614)

Submitted in fulfillment of part of the requirements for the degree

Masters of Science (Physiology)

in the Faculty of Health Sciences

University of Pretoria

Pretoria

November 2007

Supervisor: Prof AM Joubert

Co-supervisor: Prof F Joubert

Summary

Sutherlandia frutescens is a South African herbal remedy traditionally used for various ailments and lately to improve the overall health in cancer and HIV/AIDS patients. Relatively little is known about the mechanisms of action of the constituents present in *S. frutescens.*

The aim of this project was to examine the *in vitro* influence of crude ethanolic *S. frutescens* extracts in human breast adenocarcinoma (MCF-7) and non-tumorigenic breast epithelial (MCF-12A) cells after 48 h of exposure. Dose-dependent studies were conducted on cell numbers and metabolic activity by means of spectrophotometry. Morphological changes were determined with light-, fluorescent- and transmission electron microscopy (TEM). Cell cycle progression and apoptosis were analyzed using flow cytometry. The differential effects of *S. frutescens* extracts on gene expression levels in both the MCF-7 and MCF-12A cells were conducted utilizing microarray analysis. mTOR kinase activity was measured with an ELISA assay.

S. frutescens reduced cell proliferation in both the non-tumorigenic MCF-12A and the tumorigenic MCF-7 cell line in a dose-dependent manner. The tumorigenic MCF-7 cells were more susceptible to *S. frutescens* treatment compared to the non-tumorigenic MCF-12A cells. Morphological characteristics of apoptosis and autophagy, including cytoplasmic shrinking, membrane blebbing and an increase in autophagic vacuoles were observed in both cell lines with the MCF-7 cells being more susceptible to autophagy and the MCF-12A cells less susceptible to autophagy and apoptotic cell death. TEM confirmed ultrastructural characteristics of autophagy in both cell lines. Flow cytometry revealed a G_2/M arrest with no increase in apoptosis in MCF-7 cells and a G_2/M arrest with an increase in apoptosis in MCF-12A cells treated with 1.5mg/ml *S. frutescens* extract.

Microarray analyses revealed 325 statistically significantly differentially expressed genes in MCF-7 cells and 1467 genes in MCF-12A cells. The majority of *S. frutescens*-treated genes were down-regulated when compared to the vehicle-treated control in both cell

lines. Several genes involved in DNA replication and repair were differentially expressed in response to *S. frutescens* exposure. These include Poly (ADP-ribose) polymerase family, member 2 (PARP-2) (down-regulated in both cell lines), PCNA (down-regulated in MCF-7 cells) and growth arrest and DNA-damage-inducible beta (GADD45B) (up-regulated in MCF-12A cells). This suggests that abrogated expression of genes involved in DNA replication and repair play a role in inducing a G_2/M cell cycle arrest in *S. frutescens*-treated cells. ELISA analysis of the mTOR kinase revealed a decrease in mTOR kinase activity in both cell lines after *S. frutescens* exposure. Therefore, attenuated mTOR kinase activity as a result of *S. frutescens* treatment in both cell lines is regarded as a central mediator in inducing autophagy suppressing gene expression and inhibiting ribosome biogenesis.

Understanding of *in vitro* molecular mechanisms of *S. frutescens* enables researchers to focus on affected cellular mechanisms and identify active compounds with subsequent evaluation as possible candidates for use in anticancer therapy. The current study contributes to the unraveling of the *in vitro* molecular mechanisms and signal transduction associated with 70% ethanolic *S. frutescens* extracts, providing a basis for further research on this multi-purpose medicinal plant in Southern Africa.

Keywords: *Sutherlandia frutescens*, autophagy, cell cycle arrest, mTOR kinase, microarray, anticancer

Acknowledgements

To my family - Thank you for your unwavering love and support. Their support has not been only moral but also financial.

I would like to sincerely thank the following people:

- Professor Annie Joubert, supervisor and associate professor of the Department of Physiology. This work would not have been possible without her dedicated support, interest, professional guidance and resolute positive attitude. It has been a pleasure and an honor to work under Professor Joubert.

- Sumari Marais, technical assistant at the department of Physiology, for making the lab such an enjoyable environment to work in and always willing to help and provide a few words of wisdom and encouragement.

- Professor Fourie Joubert, supervisor and head of the Bioinformatics and Computational Unit in the Department of Biochemistry, for help and guidance with bioinformatics.

- Professor Dirk van Papendorp, head of the Department of Physiology, for allowing me the opportunity make use of the facilities at the department for this study.

- Doctor Carl Albrecht for providing raw as well as intellectual material.

- Professor Dave Berger, form the Department of Botany Forestry and Agriculture Biotechnology Institute, for allowing me to make use of the ACGT Microarray Facilities.

- Nicky Olivier, from the ACGT Microarray facility, for his help and guidance during the use of the facilities at the ACGT Microarray facility.

- Francina and Ezekiel for their help and excellent maintenance of the laboratory.

- The Cancer Association of South Africa and the National Reseaerch Foundation for providing financial support.

- Sanushka Naidoo, from the Forestry and Agricultural Biotechnology Institute, for always being so kind and willing to drop a few words of wisdom and technical expertise.

- Friends and relatives for always being there.

I wish to acknowledge God almighty. Without Him, nothing would have been possible.

Table of Contents

List of Figures

List of Tables

List of Abbreviations

4E-BP1	Eukaryotic translation initiation factor 4E-binding protein 1
53bp	p53 binding protein
ADAMTS20	Disintegrin-like and metalloprotease (reprolysin type) with thrombospondin type 1 motif 20
AIDS	Acquired Immunodeficiency Syndrome
AIF	Apoptosis inducing factor
Akt/PKB	Protein kinase B
AKT1S1	Akt1 substrate 1
AMP	Adenosine monophosphate
AMPK	AMP-activated protein kinase
Ap/D	Apoptosis/Death fraction
AP-1	Activator protein 1
Apaf-1	apoptotic protease activating factor
APC/C	Anaphase-promoting complex/cyclosome
Apo1	TNF receptor superfamily, member 6
Atg6	Autophagy-related protein 6
Atg8p	Autophagy-related protein 8 precursor
ATM	Ataxia telangiectasia mutated
ATP	Adenosine triphosphate
ATPase	Adenosine triphosphosphate-phosphatase
ATR	Rad3 related protein
Bad	Bcl-2 antagonist of cell death
bag-1	Bcl2-associated athanogene 1 protein
Bak	Bcl-2 homologous antagonist/killer
Bax	Bcl-2-associated X protein
Bcl-2	B-cell CLL/lymphoma 2
Bcl-2-A1	Bcl-2-related protein A1
Bcl-2-L2	B-cell lymphoma 2 like 2
BH3	Bcl-2 homology region 3

Bid	BH3-interacting domain death agonist
Bik	Bcl-2-interacting killer
Bim	Bcl2-interacting mediator of cell death
Bmf	Bcl-2-modifying factor
Bub1	Budding inhibited benzimidazole 1
Bub2	Budding inhibited benzimidazole 2
Bub3	Budding inhibited benzimidazole 3
BubR1	Budding inhibited benzimidazole receptor 1
C/EBPB	CCAAT/enhancer binding protein beta
Ca^{2+}	Calcium
CAD	Caspase-activated DNase
CAK	Cyclin activating kinase
cAMP	Cyclic adenosine monophosphate
CARD11	Caspase recruitment domain family, member 11
CARD11	Caspase recruitment domain family, member 11
CBP	CREB-binding protein
CD95	Clonal deletion 95
CD95L	CD95 ligand
Cdc	Cell division cycle
Cdc14	Cell division cycle 14
Cdc20	Cell division cycle 20
Cdc25A	Cell division cycle 25A
Cdc25B	Cell division cycle 25B
Cdc25C	Cell division cycle 25C
Cdc6	Cell division cycle 6
Cdh1	Cadherin 1
CDK	Cyclin Dependent Kinases
CDK1	Cyclin Dependent Kinase 1
CDK2	Cyclin Dependent Kinase 2
CDK4	Cyclin Dependent Kinase 4
CDK6	Cyclin Dependent Kinase 6

cDNA	complimentary DNA
Cdt1	Cdc10-dependent transcript
Chk1	Checkpoint kinase 1
Chk2	Checkpoint kinase 2
Cip	CDK-interacting protein
CMA	Chaperone-mediated autophagy
c-Myc	v-Myc myelocytomatosis viral oncogene homolog
CO2	Carbon dioxide
COX-2	Cyclo-oxygenase-2
CREB	cAMP responsive element binding protein
CSTA	Cystatin A
CV	Crystal violet
cyt-hsc70	Cytosolic heat shock protein of 70 kDa
DD	Death domain
DED	Death effector domain
Diablo	Direct IAP-binding protein with low pI
DISC	Death inducing signal complex
D-MEM	Dulbecco's minimum essential medium eagle
DMSO	Dimethyl sulfoxide
DNA	Deoxyribonucleic acid
DR4	Death receptor 4
DR5	Death receptor 5
DSB	Double-strand breaks
e2F	Elongation factor 2
EB	Elution Buffer
EDTA	Ethylenediaminetetraacetic acid
eIF-4G	Eukaryotic translation initiation factor 4 gamma 1
ELISA	Enzyme-Linked ImmunoSorbent Assay
Emi1	Early mitotic inhibitor 1
Endo G	Endonuclease G
ER	Endoplasmic reticulum

Erk1	Extracellular signal-regulated kinase 1
Fas	TNF receptor superfamily, member 6
FasL	Fas ligand
FCS	Fetal calf serum
FITC	Fluorescein isothiocyanate
FSC	Forward Scatter
GABA	Gamma-aminobutyric acid
GADD45B	Growth arrest and DNA-damage-inducible 45 beta
GAP	GTPase activating protein
GI50	50% growth inhibitory concentration
GO	Gene Ontology
GTPase	Guanosine-5'-triphosphate phosphatase
GβL	G protein ß -subunit-like protein
H&E	Haematoxylin and Eosin
HEPES	4-(2-hydroxyethyl)-1-piperazineethanesulfonic acid
HIF-1α	Hypoxia inducible factor 1 alpha
hip	hsc70-interacting protein
HIV	Human Immunodeficiency Virus
hop	hsc70-hsp90 organizing protein
hsc70	Heat shock cognate 70 (Heat shock protein 73)
hsp40	Heat shock protein of 40 kDa
hsp90	Heat shock protein of 90 kDa
IAP	Inhibitor of apoptosis
ICAD	Inhibitor of CAD
INK4	Inhibitor of cyclin-dependent kinase 4
INK4A	Inhibitor of cyclin-dependent kinase 4A
INK4B	Inhibitor of cyclin-dependent kinase 4B
INK4C	Inhibitor of cyclin-dependent kinase 4C
JNK	Janus kinases
junD	Jun D proto-oncogene
kDa	Kilodaltons

KIF2C	Kinesin family member 2C
KIFC1	Kinesin family member C1
Kip	Kinase-inhibitory protein
lamp2a	Lysosome-associated membrane protein type 2a
LARD	Lymphocyte associated receptor of death
LC3	Microtubule-associated proteins 1A/1B light chain 3B
LC50	50% lethal concentration
Limma	Linear Models for Microarray Data
LimmaGUI	Limma graphical user interface
lys-hsc70	Lysosomal heat shock protein of 70 kDa
Mad1	Mitotic arrest-deficient 1
Mad2	Mitotic arrest-deficient 2
MAP3K2	Mitogen-activated protein kinase kinase kinase 2
MAPK	Mitogen activated protein kinase
MAT1	Menage a trois 1
MCC	Mitotic checkpoint complex
MCM	Mini-chromosome
MDC1	Mediator of DNA damage checkpoint
MKK4	Dual specificity mitogen-activated protein kinase kinase 4
MKK7	Dual specificity mitogen-activated protein kinase kinase 7
MMP	Matrix metalloproteinase
MMP3	Matrix metalloproteinase 3 (stromelysin 1, progelatinase)
mob1	Mps one binder 1
MOPS	3-(N-morpholino)propanesulfonic acid
MPF	Mitosis promoting factor
MPS1	Maintenance of ploidy protein mob1
Mre11	Meiotic recombination 11 homolog (*S. cerevisiae*)
mRNA	Messenger RNA
mTOR	Mammalian target of rapamycin
mTORC1	mTOR complex 1
mTORC2	mTOR complex 2

MTT	3-(4,5-Dimethylthiazol-2-yl)-2,5-diphenyltetrazolium bromide
MYCL2	v-Myc myelocytomatosis viral oncogene homolog 2
Myt-1	Myelin transcription factor 1
NADH	Reduced nicotinamide adenine dinucleotide
NCI	United States National Cancer Institute
NCRL	National Chemical Research Laboratory
NFKB	Nuclear Factor-kappa B
Normexp	Normal+exponential convolution model
ORC	Origin recognition complex
PARP-1	Poly (ADP-ribose) polymerase family members 1
PARP-2	Poly (ADP-ribose) polymerase family members 2
PB	Phosphate buffer
PBS	Phosphate buffered saline
PCNA	Proliferating cell nuclear antigen
PCR	Polymerase chain reaction
PIAS1	Protein inhibitor of activated STAT1
PIKK	Phosphatidylinositol 3-kinase-like
PIP2	Phosphatidylinositol (4,5)-bisphosphate
PIP3	Phosphatidylinositol-(3,4,5)-trisphosphate
PKCα	Protein kinase C alpha
Plk-1	Polo-like kinase 1
PMT	Photomultiplier
post-RC	Post-replication state
PP2A	Ceramide-activated protein phosphatase 2A
PRA	Human replication protein A
pRB	retinoblastoma protein
pre-RC	Pre-replicative complex
PS	Phospholipid phosphatidylserine
PTEN	Phosphatase and tensin homolog (mutated in multiple advanced cancers 1)
Rad3	5' to 3' DNA helicase, subunit of RNA polymerase II transcription
Rad50	DNA repair protein Rad50

Raf	Ras-activated factor
Raf-1	Raf proto-oncogene serine/threonine-protein kinase
Raptor	Regulatory associated protein of mTOR
Ras	GTPase activating protein
RBBP5	Retinoblastoma binding protein 5
RBBP8	Retinoblastoma binding protein 8
RFC	Replication factor C
Rheb	Ras homolog enriched in brain protein
Rictor	Rapamycin-insensitive companion of mTOR
RIP1	Receptor-interacting protein 1
RNA	Ribonucleic acid
ROS	Reactive oxygen species
S. frutescens	*Sutherlandia frutescens*
S6K1	S6 Kinase 1
SAR	South African Rand
SBML	Systems Biology Markup Language
SBW	Systems Biology Workbench
SCF	Skp1/Cullin/F-box protein
SCFbTrCP	SCF beta-transducin repeat containing protein
SEM	Scanning electron microscopy
Ser	Serine
Ser214	Serine residue 214
Ser216	Serine residue 214
Ser259	Serine resdue 259
Skp1	S-phase kinase-associated protein 1
Smac	Second mitochondria derived activator of caspase
SSC	Side Scatter
STAT1	Signal transducer and activator of transcription 1
tBid	Truncated Bid
TBS	Tris buffered saline
TEM	Transmission electron microscopy

TGI	Total growth inhibitory
Thr	Threonine
Thr130	Threonine residue 130
Thr14	Threonine residue 14
Thr161	Threonine residue 161
TNF	Tumor necrosis factor
TNFR	Tumor necrosis factor receptor
TNFR-1	Tumor necrosis factor receptor-1
TNFR-L1	TNF-related apoptosis-inducing ligand 1
TNFR-2	Tumor necrosis factor receptor-2
TNFR-L2	TNF-related apoptosis-inducing ligand 2
TNFRSF10A	Tumor necrosis factor receptor superfamily, member 10a
TNFRSF10B	Tumor necrosis factor receptor superfamily, member 10b
TNFα	Tumor necrosis factor alpha
TopBP1	Topoisomerase binding protein
TOR	Target of rapamycin
TPA	12-O-tetradecanoylphorbol-13-acetate
TRADD	TNFR Associated Death Domain
TRAIL-r2	TNF-related apoptosis-inducing ligand receptor 2
TRAMP	TNF receptor apoptosis-mediating receptor protein
Tris	Hydroxymethylaminomethane
Tris HCl	Hydroxymethylaminomethane hydrochloride
TSC1	Tuberous sclerosis complex 1
TSC2	Tuberous sclerosis complex 2
Tyr	Tyrosine
Tyr15	Tyrosine residue 15
UV	Ultra-violet
Waf-1	Wild-type p53-activated fragment 1
Wee-1	Wee1-like protein kinase (wee: Scottish/Irish slang word meaning small)

Graphical representation of biochemical pathways

Graphical biochemical pathways were designed with CellDesigner 3.5.1. CellDesigner is a structured diagram editor for drawing gene-regulatory and biochemical networks [1]. Networks are drawn based on the process diagram, with the graphical notation system proposed by Kitano (2003) *et al.* and are stored using the Systems Biology Markup Language (SBML) [2]. Networks are able to link with simulation and other analysis packages through Systems Biology Workbench (SBW). CellDesigner was purely used for graphical purposes and no simulation or analyses were performed. Legends to the structures used in the representation of biochemical pathways are summarized in Figure A.

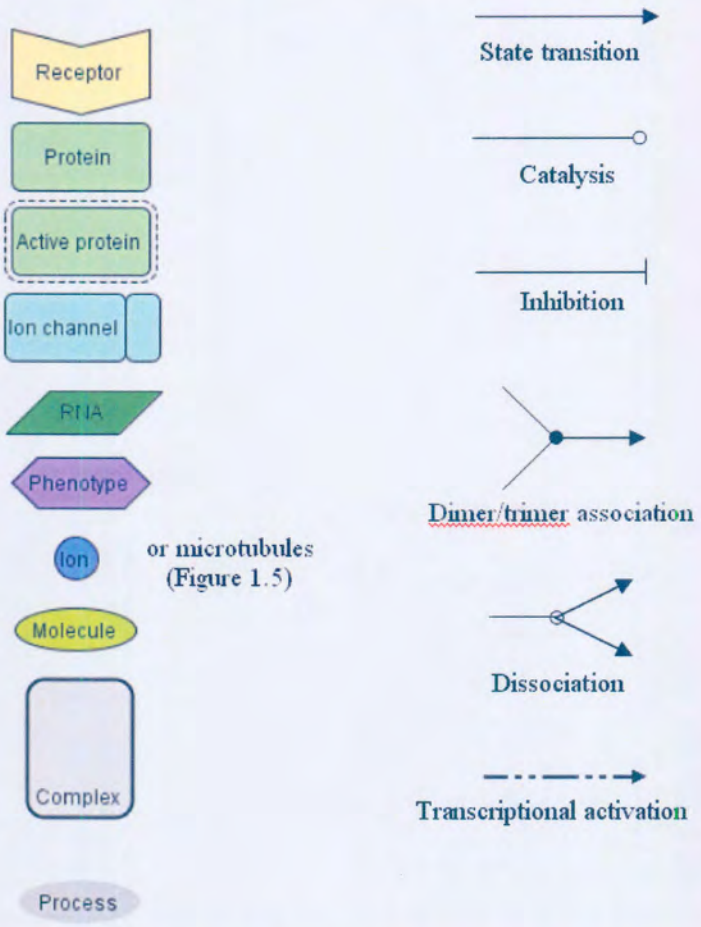

Figure A: Legend of important structures and reactions used in the representation of biochemical pathways.

Chapter 1

Literature review

1.1 History of ethnopharmacology

According to the world health organization, about three-quarters of the world population relies upon traditional remedies (mainly herbs) for the health care of its people [3]. By the middle of the nineteenth century at least 80% of all medicines were derived from herbs [4]. Plants have a long history of use in the treatment of many ailments including cancer [5]. The search for anticancer agents from plant sources in America started in earnest in the 1950s with the discovery and development of the several compounds including the vinca alkaloids, vinblastine and vincristine as well as the isolation of the cytotoxic podophyllotoxins (Figure 1.1).

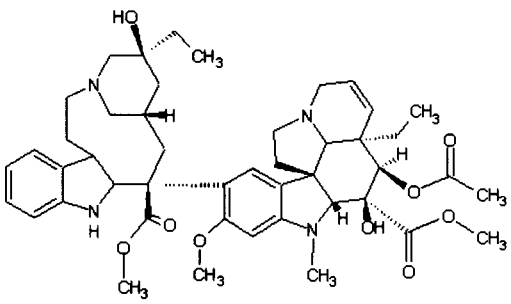

Vinblastine

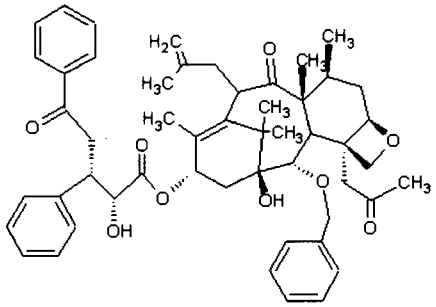

Taxol

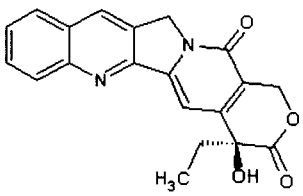

Camptothecin

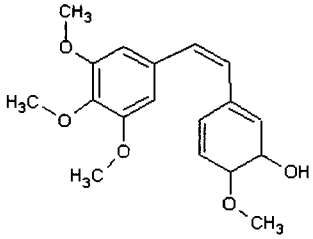

Combrestatin A_4

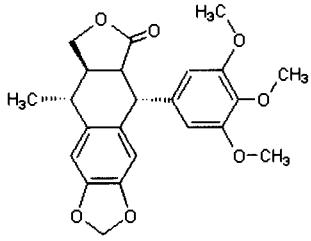

Podophylotoxin

Figure 1.1: Plant-derived antiproliferative molecules in clinical use and development. Structures were drawn with ACD/Labs ChemSketch 10.0 Freeware (ACD/Labs Toronto, Canada).

As a result, the United States National Cancer Institute (NCI) initiated an extensive plant collection program in 1960, focused mainly in temperate regions [6]. This led to the discovery of many novel chemotypes showing a range of cytotoxic activities, including the taxanes and camptothecins (Figure 1.1), but their development into clinically active agents spanned a period of some 30 years, from the early 1960s to the 1990s [7].

In southern Africa, there is an excellent historic research base to start from. Southern Africa is one of the richest centres of plant diversity in the world. The flora is rich and diverse (about 24,300 higher plant taxa), and also largely endemic in character [8]. The indigenous people of southern Africa have a long history of traditional plant usage for medicinal purposes, with ca. 4000 taxa being used for this purpose and it is estimated that there are 27 million indigenous medicine consumers [9]. A strong research basis in phytochemical investigation was established in the first half of the twentieth century because of the importance of stock farming to the economy. Cattle, sheep, horses and donkeys were killed in great numbers from diseases such as "slangkop" poisoning (*Homeria pallida)* [10], "stywe" siekte (liver damage and stiffness) caused by *Crotolaria burkeana* [11], "vermeersiekte" (*Geigera aspera*) from which a million sheep died between 1929 and 1930 [12], "geel dikkop" (*Tribulus terrestris*) killing some 600,000 sheep in the North-Western Cape in the years 1926–1927 [13] and "gifblaar" poisoning (fluoroacetate poisoning from the plant *Dichapetalum cymosum*) [14]. Most of the research took place in the National Chemical Research Laboratory (NCRL) or the Chemistry Laboratory of the Onderstepoort Veterinary Research Institute outside Pretoria which achieved world acclaim for its toxicological and chemical work.

In the 1970s the South African Biodiversity Institute working in collaboration NCI discovered the combretastatins in southern Africa as part of a random collection program. Combretastatins were isolated from the South African "bush willow", *Combretum caffrum* (Eckl. & Zeyh.) Kuntze (*Combretaceae*) and collected by the United States Department of Agriculture [15]. The basic structure of combrestatins has served as a model for the synthesis of a host of analogs containing the essential trimethoxy-aryl moiety (Fig. 1.1) linked to substituted aromatic moieties through a variety of two or three

atom bridges including heterocyclic rings and sulfonamides and provided an impressive display of the power of a relatively simple natural product structure to spawn a prolific output of medicinal and combinatorial chemistry [16].

The shift in research emphasis to the study of plants used in traditional medicine in South Africa has been very noticeable over the last decade. Centres of expertise where brought together to achieve high quality multidisciplinary research by the recent establishment of "A National Research and Development Platform for Novel Drug Developments from Indigenous Medicinal Plants" funded by the South African Department of Science and Technology through the National Research Foundation. Funding was awarded to a consortium of experts from nine South African universities and research organizations, including the South African Biodiversity Institute (formerly the National Botanical Institute) to investigate South African medicinal plants [9].

The studying of indigenous knowledge is considered a high priority of the South African National Research Foundation in which it is one of nine focus areas of research. It has allocated an amount of SAR 15 million to this area of research in 2005 and 44 postgraduate student grants in the area of indigenous medicine and health have been awarded [9].

1.2 *Sutherlandia frutescens*

Sutherlandia frutescens is a shrub mainly distributed in the Western Cape and Karoo regions of Southern Africa and has enjoyed a long history of use by many cultures because of its efficacy as a safe tonic for diverse health problems [17]. Traditionally it is a popular remedy for stomach problems, internal cancers, diabetes and various inflammatory conditions. Decoctions prepared by the Khoi and Nama people of South Africa are used externally to wash wounds, internally for fevers and is generally used as a tonic [18]. Advantages for the use of *S. frutescens* as an adaptogenic tonic are its relative safety and economical ways of acquiring the herb. A 3-month toxicity study of oral *S. frutescens* leaf powder was conducted on vervet monkeys by the Medical Research Council [19]. The report showed that doses up to 9 times the recommended dose have

been shown to be safe for consumption with no side effects. *S. frutescens* has been shown to be safe at high doses (lethal dose in 50% of animals at 1280 ± 71 mg/kg body weight) in mice [20]. A randomized, double-blind, placebo-controlled trial of *S. frutescens* in healthy adults concluded that consumption of 800 mg/d *S. frutescens* leaf powder capsules for 3 months was tolerated by healthy adults [21].

Recently, reports in South Africa have documented weight gains of 10-15kg in auto-immune deficient syndrome (AIDS) and cancer patients who were treated with *S. frutescens* twice daily in tablet form (300mg) as recommended [22]. Improvements in T-cell counts and a decrease in viral load in human immunodeficiency virus (HIV) - compromised patients have been acknowledged by clinicians in South Africa and Australia. However, data related to the mechanism whereby *S. frutescens* acts on the immune system have not been fully documented. Harnett *et al.* (2005) have shown that leaf extracts *of S. frutescens* inhibited reverse transcriptase and glycohydrolase enzyme activity and suggested that this was due to the presence of tannins in the extracts [23]. The study revealed a potential mechanism for the clinically observed improvement of HIV/AIDS sufferers when administered with *S. frutescens.* Nevertheless, Mills *et al.* (2005) suggested that the co-administration of traditional herbal drugs with antiretroviral agents may result in the early inhibition of drug metabolism and transport followed by the induction of decreased drug exposure with more prolonged therapy [24]. Thus it was highlighted that extreme caution should be taken when introducing herbal drugs into the routine care of HIV/AIDS patients [23].

Fernandez *et al.* (2004) described its antioxidant potential and concluded that *S. frutescens* leaf extracts possess significant superoxide, as well as hydrogen peroxide scavenging properties in cell-free and in stimulated neutrophil systems [25]. Antioxidant compounds have shown to act on modifying immune mechanisms by modulating activity and production of cytotoxic immune cells, enhancing the expression of cancer suppressor genes and inhibiting tumor angiogenesis, partly explaining the anticancer effect on some cancers according to preliminary clinical evidence [26]. In addition *S. frutescens* may exert its antitumor effects through its anti-inflammatory properties. It has been suggested

that inflammation and cyclo-oxygenase-2 (COX-2) is closely linked to carcinogenesis, which is a multistage process consisting of three apparently distinct phases: initiation, promotion and progression [27]. Inappropriate upregulation of COX-2, a rate limiting enzyme involved in prostaglandin biosynthesis and inflammation, has been frequently observed in various malignancies including those of the esophagus, stomach, breast, pancreas, lung, colon, skin, urinary bladder and prostate [28]. Numerous edible plant extracts and their active constituents exerting anti-inflammatory activity have been shown to inhibit COX-2 induction in *in vitro* and *in vivo* models of carcinogenesis [29,30]. Kundu *et al.* (2005) concluded that leaf extracts of *S. frutescens* inhibited 12-*O*-tetradecanoylphorbol-13-acetate (TPA)-induced COX-2 expression in mouse skin and inhibited TPA-induced expression of activator protein-1 [31]. The latter regulates induction of COX-2 expression. These findings lend mechanistic support to the antitumor promoting potential of *S. frutescens*. However, further investigation should follow to gain knowledge of the molecular mechanisms involved in COX-2 inhibition by *S. frutescens*.

Tai *et al.* (2004) demonstrated that ethanolic leaf extracts of *S. frutescens* exhibited concentration-dependent antiproliferative activities on several human cancer cell lines including the MDA-MB-468 human breast adenocarcinoma and leukemia (Jurkat and HL60) cell lines [32]. Chinkwo *et al.* (2005) showed that *S. frutescens* water extracts induced apoptosis in three different cell lines (CHO, Caski and Jurkat T lymphoma cells) and it was suggested that apoptosis occurred as a result of flip-flop translocation of phosphatidyl serine in the cell membrane [33]. In a study conducted by Tai *et al.* (2004) it was found that the leaves of the *S. frutescens* plant contain biologically active compounds namely L-canavanine, pinitol, gamma-aminobutyric acid (GABA), plant saponins, stigma-4-en-3-one and gamma-sitosterol, as well as several long chain alcohols [32]. Both *in vitro* and *in vivo* studies have demonstrated the anticancer properties of L-canavanine [34]. L-canavanine was found to be cytotoxic in the human lung adenocarcinoma cell line A549, the human bladder cancer cell line HTB9 and a human cervical cancer cell line, HeLa. Tai *et al.* (2004) demonstrated that 2mM L-canavanine was cytotoxic to MCF-7 cells and 1mM arginine supplementation protects MCF-7 cells from the effects of 2mM L-canavanine [32]. However, the latter was not observed in

S. frutescens treated MCF-7 cells. From this data Tai *et al* (2004) concluded that L-canavanine and its major metabolite canaline are likely only two of many factors contributing to the *in vitro* antiproliferative, antioxidant and apoptotic activity of *S. frutescens* [32].

Saponins are a group of glycosides widely distributed in higher plants including *S. frutescens* [17,35]. Liu and Henkel (2002) consider saponins as key ingredients in traditional Chinese medicines [36]. These compounds have been reported to be responsible for most of the observed biological effects *in vitro* and *in vivo* including anticarcinogenic, hypoglycemic, antioxidant, neuroprotective, anti-inflammatory and antiviral. Phytosterols are counterparts of cholesterol in animal products and the most common are sitosterol (beta and gamma), campersterol and stigmasterol [37]. Phytosterols are regarded as anticancer dietary components that may offer protection from the common cancers including colon, breast and prostate cancers [37]. Awad *et al.* (2000) proposed a mechanism through which beta-sitosterol inhibits tumor growth and stimulates apoptosis through the intracellular production of ceramide [37]. Therefore L-canavanine, phytosterols, plant saponins and other biologically active compounds present in *S. frutescens* may act synergistically to bring about the wide array of biological activity including growth inhibition and apoptosis induction. Tai *et al.* (2004) commented that the bioactivity of *S. frutescens* might be as a result of synergistic effects of compounds present in *S. frutescens* extracts and therefore that the bioactivity of the extracts may not be solely dependent on a single compound, but rather a host of phytocompounds, resulting in a relatively complex mechanism of action [32].

In 2005 a preliminary study of ethanolic extracts of *S. frutescens* was conducted as part of an honors project [38]. In the study it was demonstrated that 1.5mg/ml of the ethanol plant extract was required to inhibit cell proliferation to 50% (IC_{50}) of the vehicle-treated control in MCF-7 cells after 24h of exposure. A time-dependent study over 72h with intervals of 24, 36, 48 and 72h was conducted with the IC_{50} concentration and revealed a similar pattern of 40-50% growth inhibition over the entire period of the experiment compared to the medium only control. *S. frutescens*-treated cells exhibited an increase in

apoptotic cells compared to the vehicle-treated control, suggesting that apoptosis might play a role in the growth inhibitory effects of *S. frutescens* treated MCF-7 cells. The preliminary gene expression profile provided valuable insight into the possible mechanisms involved in the antiproliferative effects of *S. frutescens* and provided a basis for further study. Of particular interest amongst the differentially expressed genes were the Tumor necrosis factor receptor superfamily, member 10a and b (DR4, DR5), CARD11, Protein inhibitor of activated STAT1 (PIAS1), V-myc myelocytomatosis viral oncogene homolog 2, NF-κB inhibitor interacting Ras-like 2, NF-κB 1 substrate 1 and Neutral sphingomyelinase-2, all of which have been reported to play important roles in apoptosis, growth inhibition and Nuclear factor-kappa B (NF-κB) signaling [39,40,41,42,43]. From the above-mentioned data it was hypothesized that the formation of ceramide might play a central role in the growth inhibitory effects of *S. frutescens* extracts on MCF-7 cells after 24h of treatment *in vitro*.

1.3 Overview of the cell cycle

The cell cycle is the sequence of events by which a growing cell duplicates all its components and divides into two daughter cells, each with sufficient machinery to repeat the process. Eukaryotic cell division is a highly regulated process. One round of cell division consists of two "gap" phases termed G_1- and G_2-, an S-phase during which duplication of the three billion bases of DNA haendogenous retrovirus
ppen, and an M-phase where proper segregation of duplicated chromosomes and chromatid separation occur. When cells encounter specific growth inhibitory signals or there is an absence of appropriate mitogenic signaling, proliferation halts and enters a non-dividing, quiescent state known as G_0, or they can undergo apoptosis. Cell cycle progression is mediated by the activation of a highly conserved family of protein kinases, the cyclin dependent kinases (CDKs) [44]. Activation of a CDK requires binding to a specific regulatory subunit, termed a cyclin. The cyclin/CDK complexes are the central cell cycle regulators, with each complex controlling a specific cell cycle transition and at least nine CDKs and 15 cyclins have been described [45].

Extracellular stimuli, such as growth factors and hormones, elevate D-type cyclins (cyclins D1, D2, and D3), which bind to and activate CDK4 and CDK6 and stimulate quiescent cells to enter the cell cycle or proliferating cells to continue proliferation [46]. After elevation of D-type cyclins and activation of CDK4 and/or CDK6 in G_1, cyclin E levels increase and bind to CDK2. The cyclin E/CDK2 complexes regulate the transition from G_1 into S-phase [47]. Cyclin A expression is induced shortly after cyclin E and binds to CDK2 in S-phase and to CDK1 in G_2 and mitosis [48]. Cyclin A is involved in the regulation of S-phase entry, and is important in G_2- and M-phases. The entry into mitosis from G_2 is under the control of B-type cyclins, which also associate with CDK1 [48]. In normal cells, the CDKs are expressed throughout the cell cycle and each cyclin protein has a restricted period of expression. The limited expression of each cyclin proteins is due to cell cycle-dependent regulation of both cyclin gene transcription and protein degradation [45,49]. For CDKs to become active, they must bind a cyclin and undergo site-specific phosphorylation. The cyclin/CDK complex is regulated by a

number of phosphorylation and dephosphorylation events, resulting either in activation or inhibition of kinase activity [44]. Phosphorylation is carried out by cyclin-activating kinase and dephosphorylation is mediated by members of the Cdc25 family of dual-specificity protein phosphatases [44]. The CDK activating kinase (CAK) is responsible for the activating phophorylation of CDK1, CDK2, CDK4 and CDK6 and is composed of 3 subunits: CDK7, cyclin H and MAT1 [50]. Progression through the cell cycle is also dependent on the temporally controlled degradation of cyclins by the ubiquitin proteasome system. Two structurally related multiprotein E3 ligases, the anaphase-promoting complex/cyclosome (APC/C) and the Skp1/Cullin/F-box protein (SCF) complexes, drive progression through the eukaryotic cell cycle [51,52]. These complexes differ in that the activity of SCF ligases mainly controls the transition from G_1/S and G_2/M, while APC/C is primarily required for mitotic progression and exit [53].

Tai *et al.* (2004) demonstrated that 300mg *S. frutescens* tablets (PhytoNova, Cape Town, South Africa), extracted in 2.2ml 70% ethanol had a differential effect on cell cycle progression after 48h of the extract treatment [32]. MCF-7 breast tumor cells treated with a 1/200 (0.68mg/ml) dilution of the *S. frutescens* tablet extracts resulted in a small, but significant increase in G_0/G_1 fraction and a concomitant reduction in S fraction. The apoptosis/death (Ap/D) fraction was statistically insignificant increased. MDA-MB-468 breast tumor cells treated with 1/200 and 1/400 dilution of *S. frutescens* resulted in significant increase in G_0/G_1 fraction and a reduction in G_2/M fraction. The Ap/D fraction was not affected. Jurkat cells treated with 1/200 dilution of *S. frutescens* resulted in arrest in S-phase, 51.5% in treated cells versus 28.3% in control, and a reduction in G_2/M-phase. There was also a significant increase in Ap/D fraction. At a 1/400 dilution, the changes were not significant. HL60 cancer cells treated with 1/200 dilution of *S. frutescens* resulted in cell arrest in G_2/M-phase and reduction in S-phase. The Ap/D fraction was not increased. At 1/400 dilution, the same changes were observed.

Several genes involved in cell cycle dynamics were reported to be differentially expressed after 24h exposure to crude *S. frutescens* extracts [38]. These include Homo sapiens retinoblastoma binding protein 5 (RBBP5), Homo sapiens retinoblastoma binding

protein 8 (RBBP8), Akt1 substrate 1 (AKT1S1), V-myc myelocytomatosis viral oncogene homolog 2 (MYCL2), Kinesin family member 2C (KIF2C) and Kinesin family member C1 [38]. The effect on cell cycle dynamics was however not reported. Plant-derived biologically active molecules including flavanoids, phytosterols, polyphenols and saponins are known to affect cell cycle dynamics through several mechanisms. However, the effects that crude *S. frutescens* extracts have on cell division in MCF-7 and MCF-12A cells remain to be elucidated [54].

1.3.1 Cell cycle phases

1.3.1.1 G_1-phase

During the G_1 phase many signals intervene to influence cell division and the deployment of a cell's developmental program. Diverse metabolic, stress and environmental factors are interpreted during this period and on the basis of these inputs, the cell decides whether to enter S-phase or pause. A decision to enter S-phase is made at a time in mid-to-late G_1, called the restriction point, and this commitment to replicate DNA and divide is irreversible until the next G_1 phase [55]. Members of the retinoblastoma protein (pRB) family (pRB, p107, and p130) are key molecular switches that control transition from G_1 to S-phase and mediate their effect by binding to the elongation factor 2 (e2F) family of transcription factors [56]. The e2F family mediates transcription of genes required for DNA synthesis, including cyclin E, cyclin A, cyclin B, dihydrofolate reductase and thymidine kinase (Figure 1.2) [57]. Hypophosphorylated pRB acts as a transcriptional repressor by binding and inhibiting e2F-dependent transcription of S-phase genes [56]. Sequential phosphorylation of pRB is needed to inhibit the e2F repressor activity and ultimately results in the dissociation of e2F and pRB, and S-phase entry [56]. Phosphorylation of pRB is done by the cyclin D/CDK4 and CDK6 and cyclin E/CDK2 complexes (Figure 1.2) [58]. pRB can also be regulated by acetylation, which is mediated by histone acetylases such as p300/CBP [56]. The acetylases are under cell cycle control and prevent efficient pRB phosphorylation by cyclin E/CDK2 [59]. As cells progress into S-phase, maintenance of pRB hyperphosphorylation is necessary for the successful completion of DNA replication and the phosphorylation status of CDKs are tightly controlled by a group of functionally related proteins called CDK inhibitors [60,61].

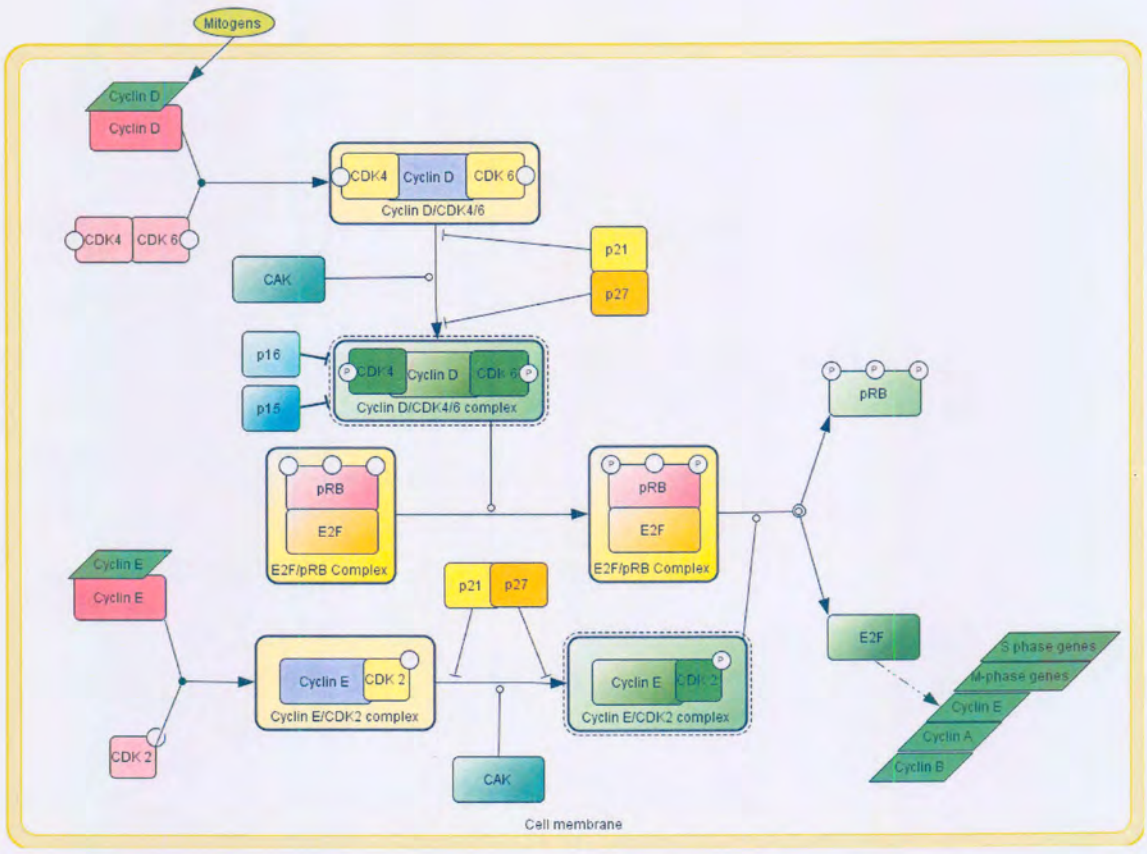

Figure 1.2: The G_1/S transition. During G_1 phase progression, activation of cyclin D/CDK4/6 and cyclin E/CDK2 complexes by CDK activating kinase (CAK) leads to sequential phosphorylation of the transcription factor RB. Hypophosphorylated pRB binds to the e2F transcription factor family to inhibit S-phase entry. Once hyperphosphorylated, pRB dissociates from e2F, resulting in activation of genes required for S-phase entry. Members of the INK4 and Cip/Kip CDK inhibitor families can inhibit the cyclin/CDK kinase complexes to mediate a G_1/S cell cycle arrest. (Adapted from Pietenpol and Kastan 2004 [62])

Two families of CDK inhibitors exist: the INK4 inhibitors and the Cip/Kip inhibitors. There are four known INK4 family members: p16/INK4A, p15/INK4B, p18/INK4C and p19/INK4D, and three known Cip/Kip family members: p21/Waf1/Cip1, p27/Kip1 and p57/Kip2 [60]. The INK4 family specifically inhibits CDK4 and CDK6 activity during the G_1 phase of the cell cycle, while the Cip/Kip family can inhibit CDK activity during all phases of the cell cycle. Both families of CDK inhibitors can arrest cells in the G_1 phase of the cell cycle by inhibiting the activities of CDKs and preventing their ability to phosphorylate and inactive pRB and other pRB-family proteins [60]. The levels,

subcellular localization and activity of these inhibitors can be regulated by various forms of cell stress and growth inhibitory signaling pathways.

1.3.1.2 S-phase

During the S-phase an exact copy of the genome is made through DNA replication. Replication of the human genome is a highly coordinated process that ensures inheritance of the genetic information. The initiation of DNA replication during the S-phase of the cell cycle takes place at multiple sites on the chromosomes, called the origins of replication [63]. The origin recognition complex (ORC) marks the position of replication origins in the genome and serves as the landing pad for the assembly of a multiprotein, pre-replicative complex (pre-RC) at the origins, consisting of ORC, cell division cycle 6 (Cdc6), Cdc10-dependent transcript (Cdt1) and mini-chromosome maintenance (MCM) proteins. The pre-RC is assembled during exit from mitosis, and is activated in a sequential manner by the action two families of kinases, cyclin-dependent kinases and the Cdc7-Dbf4 kinase [64]. After activation, the ORC protein complex at each origin changes to a post-replication state (post-RC), thereby activating DNA replication and preventing further activation events from the same origins for the rest of the cell cycle [63]. The MCM proteins serve as key participants in the mechanism that limits eukaryotic DNA replication to once-per-cell-cycle and its binding to the chromatin marks the final step of pre-RC formation [65]. After ORC activation, DNA polymerases, human replication protein A (PRA) and proliferating cell nuclear antigen (PCNA) assemble at the origins and the transition to DNA replication is irreversibly completed [63].

1.3.1.3 G_2/M-phase

After duplication of the genome in S-phase, cells transit through G_2 and prepare for mitosis. As cells enter into G_2 phase, the mitosis promoting factor (MPF) complex forms. The MPF complex is formed by the combination of cyclin B and CDK1 (Figure 1.3). CDK1 is constantly present throughout the cell division cycle, but its activity is finely tuned by means of protein-protein interactions and reversible phosphorylation [66]. At the end of G_2 phase, cyclin B/CDK1 complexes are activated by dephosphorylation

and cells enter into mitosis. CDK1 activity is inhibited by kinase phosphorylation of two residues, Thr14 and Tyr15, through the action of Wee-1 and Myt-1 kinases (Figure 1.3) [67]. Wee-1 and Myt-1 activity is upregulated by phosphorylation through checkpoint kinase 1 and 2 (Chk1, Chk2), proteins that operate in DNA structure checkpoint signaling [67]. Activation of CDK1 occurs after the simultaneous phosphorylation of Thr161 by cyclin activating kinase (CAK) and dephosphorylation of Thr14 and Tyr15 by dual-specificity phosphatases Cdc25C and Cdc25B (Figure 1.3) [67]. Cdc25C is phophorylated and activated at Ser214 and Thr130 by Polo-like kinase 1 (Figure 1.3) (Plk-1) and active CDK1, creating a positive feed-back loop between Cdc25C and CDK1 [68]. Cdc25C activity is also inhibited through phosphorylation at Ser216 by Chk1 and 2 [68]. Cdc25C is phosphorylated at Ser216 throughout interphase causing it to bind to 14-3-3σ, resulting in the cytoplasmic sequestration of Cdc25C [69]. Plk-1 activity in turn is regulated by DNA structure checkpoint signaling via Ataxia telangiectasia mutated (ATM) and Rad3-related (ATR) as well as checkpoint kinases 1 and 2 (Chk1 and Chk2) (Figure 1.3) [70].

The MPF complex plays a crucial role in nuclear envelope breakdown, centrosome separation, spindle assembly, chromosome condensation and Golgi fragmentation during mitosis (Figure 1.3). Activated cyclin B/CDK1 complexes can phosphorylate numerous substrates including nuclear lamins resulting in nuclear envelope breadown, condensins and various histones resulting in chromosome condensation, various Golgi matrix components resulting in Golgi fragmentation and various proteins involved in spindle dynamics and chromosome movements including kinesins and stathmin [71,72,73,74]. Inactivation of stathmin by phosphorylation is essential for formation of the mitotic spindle and progression through the cell cycle [74]. Furthermore, the cyclin B/CDK1 complex contributes to regulate the anaphase-promoting complex/cyclosome (APC/C), the core component of the ubiquitin-dependent proteolytic machinery that controls the timely degradation of critical mitotic regulators, in particular inhibitors of anaphase onset securins and cyclins [75]. MPF function is also regulated by its location. MPF accumulates in the cytoplasm, in association with microtubules and centrosomes, until

late prophase when it translocates to the nucleus and cause nuclear envelope breakdown [76].

1.3.1.4 M-phase

During the M-phase, the cell goes through five stages to ensure that each daughter cell will have a complete set of chromosomes. The five key stages of mitosis are:

1. Prophase, whereby the chromosomes become condensed and proteins begin to bind the kinetochores, preparing for spindle attachment.
2. Pro-metaphase, during which the mitotic spindle is formed and the chromosomes attach to microtubules in the spindle through their kinetochores after the nuclear envelope breakdown. Once attached, the chromosomes align along the metaphase plate in the center of the spindle.
3. Metaphase, whereby all of the chromosomes are attached to microtubules through their kinetochores and are aligned at the metaphase plate.
4. Anaphase, whereby the sister chromatids separate and move toward the poles of the spindle.
5. Telophase, whereby the parent cell is divided into two daughter cells by cytokinesis.

The MPF complex plays a crucial role during mitosis and as discussed orchestrates chromosome condensation (prophase), causes nuclear envelope breakdown (pro-metaphase) and controls spindle dynamics and centrosome separation (meta-anaphase transition). Mitotic exit requires sister chromatid separation (anaphase), spindle disassembly, and cytokinesis (telophase) and this is controlled by the APC/C. The APC/C is a multiprotein complex consisting of at least 11 core subunits and two cofactors namely Cadherin 1 (Cdh1) and cdc20 [77]. Phosphorylation of APC/C subunits regulates both the function and the assembly of the mature complex. Three kinases mediate APC/C subunit phosphorylation: protein kinase A (PKA), Polo-like kinase 1 (Plk1), and cyclin B/CDK1 (Figure 1.5) [78,79]. Phosphorylation of cdc20 by cyclin B/CDK1 leads to binding of Cdc20 to APC/C and disassociation of Cdh1 [78]. Plk1 also promotes APC/C-mediated ubiquitination, but only in synergy with cyclin B/Cdk1 [78].

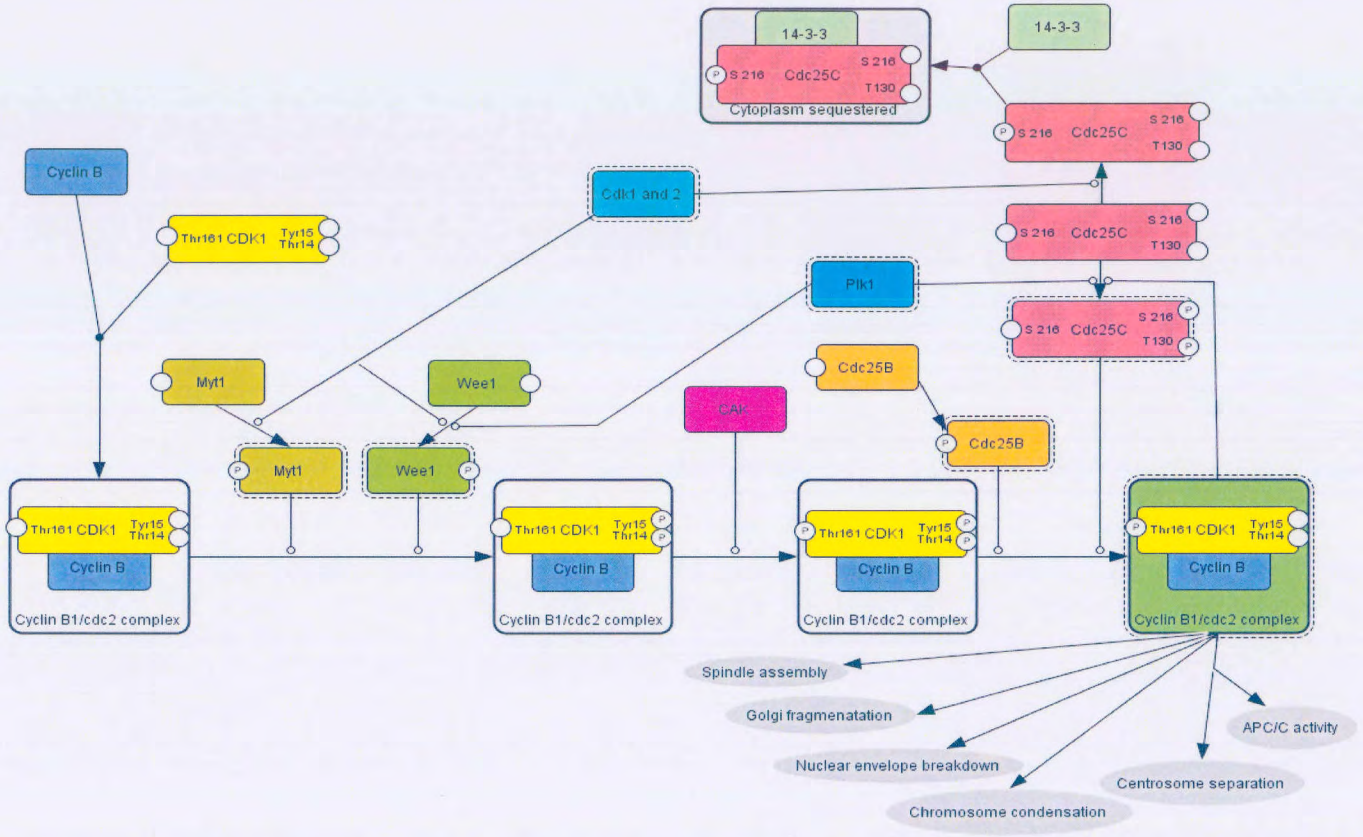

Figure 1.3: Cyclin B/CDK1 complex control during G_2/M-phase transition. CDK1 activity is controlled by consecutive sequences of phosphorylation and dephosphorylation events mediated by Myt1, Wee1, CAK and Cdc25B and Cdc25C. Wee1 and Myt1, and Cdc25B and Cdc25C compete for the phosphorylation status of same amino acid residues, and the balance in phosphorylation status is determined by DNA damage status and upstream regulators of Wee1, Myt1 and Cdc25C, including Plk1 and Chk1 and Chk2. Once CDK1 is activated it is able to phosphorylate several proteins involved in spindle assembly, chromosome condensation, nuclear envelope breakdown and APC/C activity.

PKA phosphorylation of APC/C inhibits the destruction of cyclin B, even when all activating cofactors are present [80]. APC/C-Cdc20 is active during the early stages of mitosis, whereas APC/C-Cdh1 is active in late mitosis and G_1 [81]. Cdh1 is phosphorylated by cyclin B/CDK1 which prevents its association with APC/C (Figure 1.5) [81]. Inhibitory phosphates are removed from Cdh1 by Cdc14 after APC/C-Cdc20-mediated destruction of cyclin A and B, thereby allowing the coactivator to associate with APC/C [82]. Catalytic activity of APC/C is controlled by early mitotic inhibitor 1 (Emi1) to prevent premature activation of the APC/C by interacting with newly synthesized Cdc20 (Figure 1.5) [83]. In prophase, Plk1 phosporylates Emi1 which allows Emi1 to be targeted for destruction by SCFbTrCP E3 ligase, and thereby leading to the formation of active APC/C-Cdc20 [84]. Activated APC/C-cdc20 targets cyclin B and APC/C-Cdh1 targets securin for ubiquitination and allows for a cell to transit from metaphase to anaphase (Figure 1.5) [81]. Cohesin, the protein responsible for binding the sister chromatids during mitosis after S-phase, is cleaved and inactivated by separase [85]. Securin binding and cyclin B/Cdk1-mediated phosphorylation inhibit the enzymatic activity of separase, thereby preventing premature sister chromatid separation [86]. Therefore APC/C/Cdh1 mediated degradation of the securing/separase complex is needed for separase mediated cohesion cleavage and subsequent sister chromatid separation (Figure 1.5).

1.3.2 Cell cycle checkpoints

At key transitions during eukaryotic cell cycle progression, signaling pathways monitor the successful completion of events in one phase of the cell cycle before proceeding to the next phase. These regulatory pathways are commonly referred to as cell cycle checkpoints [87]. Cells can arrest at cell cycle checkpoints temporarily to allow for any of the following:

• The repair of cellular damage
• The dissipation of an exogenous cellular stress signal
• The availability of essential growth factors, hormones, or nutrients.

When cellular damage is irreparable or cell stress is too much, checkpoint signaling could eliminate potentially hazardous cells by permanent cell cycle arrest and/or apoptosis [87]. After the transition through a checkpoint, cell cycling continues irreversibly until the next checkpoint. Four checkpoints exist, G_1/S checkpoint, S-phase checkpoint, G_2/M checkpoint and the spindle checkpoint. The cell cycle checkpoint pathways mentioned above are operational during the entire cell cycle and may slow down the cell cycle at any point during the four phases.

1.3.2.1 DNA structure checkpoint

The transition between phases is inhibited by DNA damage at the G_1/S, intra-S, and G_2/M checkpoints. These checkpoints are distinct and all respond to DNA damage and share many proteins. The intra-S-phase checkpoint differs from the G_1/S and G_2/M checkpoints, because it also recognizes and deals with replication intermediates, stalled replication forks and unreplicated DNA [88]. The signal for this checkpoint is unreplicated DNA rather than DNA damage and inhibits mitosis while DNA replication is ongoing or blocked. The DNA damage response during any phase of the cell cycle has the same pattern. After the detection of DNA damage by sensor proteins, signal transducer proteins transduce the signal to effector proteins (Figure 1.4). These effector proteins launch a cascade of events that causes cell cycle arrest, apoptosis, DNA repair, and/or activation of damage induced transcription programs [89]. Sensor proteins include proliferating cell nuclear antigen (PCNA)-like and replication factor C (RFC)-like protein complexes, which are able to bind to damaged DNA to form a scaffold for downstream repair proteins and checkpoint proteins including ATM and ATR [90]. The Rad50/Mre11/NBS1 complex is also loaded onto damaged DNA sites and mediates downstream checkpoint and repair proteins [90].

The ATM and ATR proteins belong to the phosphatidylinositol 3-kinase-like (PIKK) family of serine/ threonine protein kinases and ATM is the primary player in response to double-strand breaks (DSBs) caused by ionizing radiation and ATR plays a role in detecting DNA lesions such as those created by UV light [89]. In addition to damage sensors, signal transducers, and effector proteins, many other proteins are involved in the DNA damage response. They are mostly cell cycle-specific and associate with damage sensors, signal transducers, and effectors at particular phases of the cell cycle and, as a consequence, help provide signal transduction specificity. ATM and ATR phosphorylate most of these mediators [89].

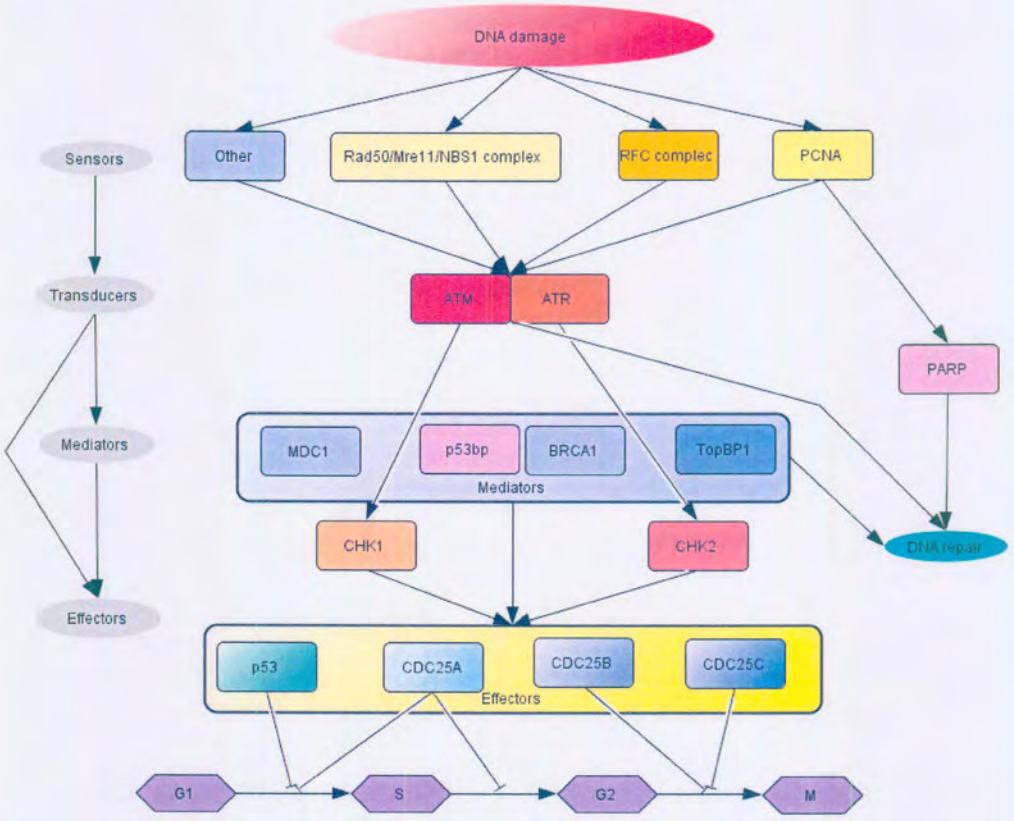

Figure 1.4: DNA-damage-induced checkpoint response. After the detection of a given damage by sensor proteins, this signal is transduced to the effector proteins Chk1 and Chk2 via the transducer proteins ATR and ATM. Depending on the phase of the cell cycle the cell is in, this can lead to activation of p53 and inactivation of CDC25, which eventually leads to cell cycle arrest. Mediator proteins mostly are cell cycle specific and associate with damage sensors, signal transducers, or effectors at particular phases of the cell cycle and, thus, help provide signal transduction specificity

Well known examples of mediators are p53 binding protein (53bp), the topoisomerase binding protein TopBP1, and mediator of DNA damage checkpoint (MDC1). Next to these mediators, many proteins fulfilling other functions have additional functions in checkpoint pathway [89]. Downstream of ATM and ATR transducers are the effector serine/threonine protein kinases Chk1 and Chk2 [90]. Chk1 and Chk2 transfer the signal of DNA damage to the phosphotyrosine phosphatases and cell division cycle proteins Cdc25A, Cdc25B, and Cdc25C. Phosphorylation of Cdc25A-C by Chk1 or Chk2 inactivates Cdc25A-C, and inhibits the G_1/S and G_2/M as a result of dephosphorylated CDKs directly involved in cell cycle transition as discussed. During the G_1/S checkpoint, DNA damage activates the ATM/ATR–Chk2/Chk1–Cdc25A–CDK2 pathway to prevent pRB dissociation [90]. ATM and ATR also phosphorylate p53, which leads to stabilization and accumulation of the p53 protein and promotes the transcription factor activity of p53. The target of the transcription factor p53 is p21, which, in turn, inhibits CDK2 activity, causing maintenance of arrest of the cell cycle. The ATM/ATR–Chk2/Chk1–Cdc25A–CDK2 pathway is also activated during the intra-S-phase checkpoint in order to attract DNA polymerase-α into prereplication complexes and thereby allowing DNA repair to take place. During the G_2/M checkpoint DSBs activate the ATM–Chk2–Cdc25C and DNA damage created by UV light activates the ATR–Chk1–Cdc25C, both upregulating Wee1 and Myt1 by phosphorylation, which together control Cdc2/CyclinB activity [90].

1.3.2.2 Spindle checkpoint

The spindle assembly checkpoint is a molecular system that ensures accurate segregation of mitotic chromosomes by delaying anaphase onset until each kinetochore has properly attached to the mitotic spindle. The kinetochore is a protein structure which assembles on the centromere and links the chromosome to microtubule polymers from the mitotic spindle. Accurate chromosome segregation requires bipolar attachment of sister chromatids to the mitotic spindle, mediated by connections between kinetochores and spindle microtubules [91]. Multiple protein kinases and checkpoint phosphoproteins are

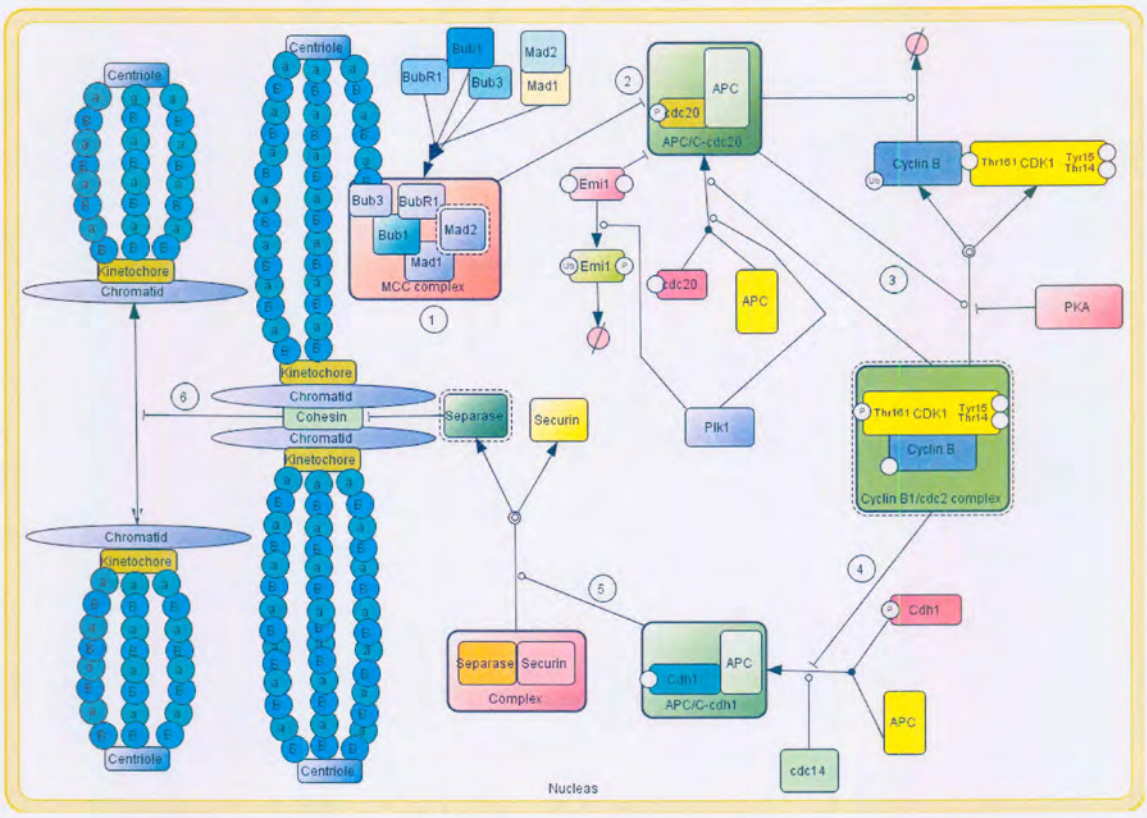

Figure 1.5: APC/C regulation and the spindle assembly checkpoint. 1) The mitotic checkpoint complex (MCC) assembles to mitotic microtubules unattached to kinetochores, as well as chromosome pairs that lack tension across sister chromatids and inhibits the APC/C-cdc20 complex. 2) Activation of APC/C is regulated by Emi1 and the MCC complex. 3) Cyclin B is ubiquitinylated and degraded and CDK1 activity abolished once the APC/C-cdc20 complex is activated. 4) CDK1 inhibition of Cdh1 is removed after Cyclin B degradation and Cdh1 dephosphorylation by cdc14 activates the APC/C-Cdh1 complex. 5) Active APC/C-Cdh1 targets securin for ubiquitination and activates securin. 6) Activated securin cleaves cohesin and allows chromatid segregation.

required for the function of the spindle assembly checkpoint and are summarized in table 1.1. The segregation of sister chromatids is controlled by the APC/C complex and the spindle assembly checkpoint proteins converge to control the activity of the APC/C complex [92]. To delay anaphase onset when there are unattached or relaxed kinetochores, the checkpoint blocks Cdh1-APC/C-mediated securin degradation [92]. Kinetochores that are not yet attached to mitotic microtubules and chromosome pairs that

lack tension across sister chromatids generated by the spindle poles activate the spindle assembly checkpoint. The established view is that the mitotic checkpoint complex (MCC), consisting of mitotic arrest-deficient 2 (Mad2), budding inhibited benzimidazole receptor 1 (BubR1) and budding inhibited benzimidazole (Bub3), bind to kinetochores that lack attachment or tension. Mad2 in the MCC undergoes conformational changes and inhibit Cdc20 activity and consequently inhibits APC/C mediated degradation of cyclins and securin (Figure 1.5) [93]. Mad1 interacts with Mad2 constitutively throughout the cell cycle and facilitates the formation of the Mad2–Cdc20 interaction [93]. The MCC is inactivated as each pair of sister kinetochores attaches to microtubules, and microtubule motors generate tension that stretches them, however how the MCC is disassembled after the checkpoint is inactivated remains unclear [93].

Table 1.1 Spindle assembly checkpoint genes and their function (Adapted from Lew and Burke 2003 [91]).

Gene	Protein function
MAD1	Coiled-coil protein that recruits Mad2 to kinetochores and is phosphorylated upon checkpoint activation. Facilitates Mad2 cdc20 interaction
MAD2	Interactions with Mad1 and Cdc20 to modulate APC/C activity
BubR1	Can inhibit APC/C activity by binding to Bub3 and Cdc20
BUB1	Protein kinase required to recruit Mad1, Mad2, and Bub3 to kinetochores
BUB2	Required for maintenance of spindle assembly checkpoint in response to spindle and kinetochore damage.
BUB3	Binds Bub1 and BubR1
MPS1	Protein kinase required for the spindle checkpoint and also required for spindle pole body duplication
Aurora B	Regulates microtubule attachment to kinetochores and promotes biorientation, required for cells to arrest in response to excess Mps1

1.4 Overview of mechanisms of cell death

Programmed cell death (PCD) is essential for the development and maintenance of multicellular organisms. Apoptosis, autophagy and mitotic catastrophe are types of PCD and are executed by active cellular processes that can be intercepted by interfering with intracellular signaling [94]. Necrosis and metabolic catastrophe are types of uncontrolled cell death.

1.4.1. Apoptosis

Apoptosis is an important process to the development and homeostasis of many living systems [94]. Dysregulation of apoptosis causes a number of human pathologies including cancer, autoimmune diseases, and neurodegenerative disorders [95,96,97,98]. Research in the past two decades has led to the identification of hundreds of genes that govern the initiation, execution, and regulation of apoptosis in several species [94]. In mammalian cells, apoptosis comes in two forms, intrinsic and extrinsic, which are triggered by cell death stimuli from intra- and extracellular environments, respectively [99]. Intra- and extracellular apoptotic stimuli triggers the activation of caspases which are the core components of the apoptotic machinery [99]. Apoptosis can also be induced by caspase-independent effectors of apoptosis including proteases of the cathepsin family, the calpain family, granzymes, apoptosis-inducing factor and the mitochondrial EndoG nuclease [100]. The morphological features of apoptosis include changes in plasma membrane asymmetry and attachment, condensation of cytoplasm, nucleus and internucleosomal cleavage of DNA [101]. Another characteristic of apoptosis is externalization of phosphatidylserine governed by activation of a calcium-dependent phospholipid scramblase activity in concert with inactivation of the aminophospholipid translocase at the cell surface [102]. Externalization of phosphatidylserine prepares the dying cell for engulfment and elimination by phagocytes. In the final stage the cell gets converted into "apoptotic bodies" which are rapidly eliminated by phagocytosis without eliciting inflammation in the surrounding areas [103].

1.4.1.1 Caspase-dependent apoptosis

1.4.1.1.1 Caspases

There are 8 apoptosis related enzyme members of the caspase family and comprises of caspase 2, caspase 3, caspase 4, caspase 6, caspase 7, caspase 8, caspase 9 and caspase 10 [104,105,106,107]. The caspases 2, 4, 8, 9, and 10 trigger apoptosis and are known as upstream or initiator caspases; they activate the executioner or downstream caspases comprising of caspases 3, 6, and 7 which ultimately execute apoptotic cell death [108]. Caspase activation may precede through autoactivation via oligomerization, death receptor, mitochondrial or endoplasmic reticulum pathways induced transactivation and proteinases-evoked proteolysis (granzyme B, cathepsin G, calpains, and apoptotic serine proteinase [109]. The activated caspases initiate a death program by destroying key components of cellular infrastructure and activate factors, which damage the cell and results in the morphological characteristics of apoptosis. Caspase-activated DNase (CAD) is one of the nucleases primarily responsible for genomic DNA fragmentation during apoptosis [110].

1.4.1.1.2 Caspase activation: Death receptor pathway

Death receptors are cell surface receptors that transmit apoptotic signals initiated by specific death ligands. These receptors can activate the caspase cascade within seconds of ligand binding. The receptors belong to the tumor necrosis factor gene super family [111]. The characterized death receptors include CD95 (also called Fas, Apo1), tumor necrosis factor receptor-1 (TNFR-1, also called p55, CD120a), death receptor-3 (DR3, also called Apo3, TRAMP, LARD), and death receptor-4 and 5 (DR4, DR5, also called Apo TRAIL-r2, killer). These receptors contain a death domain in their intracellular region to recruit downstream apoptotic proteins [112].

Tumor necrosis factor alpha (TNFα) is produced by T-cells and macrophages in response to infection. It exerts its biological activity by binding to TNFR-1 and TNFR-2 receptors and activating several signaling pathways. TNFRs belong to a large family of nerve growth factor receptors [112]. These are transmembrane receptors with one to five

cysteine repeats in their extracellular domains and in their cytoplasmic tail a common death domain (DD) [112]. TNFR-1 contains DD whereas TNFR-2 lacks death domain. Fas/CD95 is a 45–52 kDa glycoprotein ubiquitously expressed in various tissues, but its ligand, CD95L, is expressed mainly in T lymphocytes and natural killer cells. The interaction of TNFα with its receptor leads to trimerization and clustering of the intracellular death domain (Figure 1.6). This allows the binding of intracellular adapter molecule called TNFR Associated Death Domain (TRADD) via interaction between death domains (Figure 1.6) [112]. CD95 undergoes trimerization upon binding to CD95L and both TRADD and CD95 in turn can associate with another adapter molecule namely, Fas associated death domain (FADD). FADD recruits procaspase 8 by protein–protein interaction via homologous death effector domain (DED) to form a death inducing signal complex (DISC) [113]. During DISC formation procaspase 8 is autolytically cleaved to yield caspase 8 (Figure 1.6). Active caspase 8 is rapidly released from DISC to the cytoplasm and serves as an enzyme for down stream effector caspase 3, 6, and 7. These effector caspases especially caspase 3 cleave a number of substrates resulting in morphological and biochemical features of apoptosis [103]. TNF-related apoptosis inducing ligand (TRAIL) binds DR4 and DR5. The signaling pathways of these are similar to Fas and are mediated by FADD. However DR3 shows similar pattern to that of TNFR-1 [114].

Antioxidant compounds have shown to act on modifying immune mechanisms by modulating activity and production of cytotoxic immune cells (macrophages and T-cells), enhancing the expression of cancer suppressor genes (*e.g.* TNFα, TNFR-1 and 2, TRAIL) receptor) and inhibiting tumor angiogenesis [115]. *S. frutescens* leaf extracts possess antioxidant properties with significant superoxide, as well as hydrogen peroxide scavenging abilities [25].

1.4.1.1.3 Caspase activation: Mitochondrial pathway

The participation of the mitochondria is a well-characterized pathway of caspase activation. A number of stimuli, including chemotherapeutic agents, UV radiation, oxidative stress and growth factor withdrawal, mediate apoptosis via the mitochondrial

pathway. Mitochondria are comprised of a matrix surrounded by inner membrane, the intermembrane space and the outermembrane. The inner membrane contains molecules such as ATP synthase, electron transport chain, and adenine nucleotide translocator [112]. Under normal physiological conditions these molecules allow the respiratory chain to create an electrochemical gradient or membrane potential. The intermembrane space contains cytochrome *c*, certain procaspases, adenylate kinase-2, endonucluase G (Endo G), Dialbo/Smac, and apoptosis inducing factor (AIF) [116]. The permeabilization of the outer membrane results in the release of these molecules in the cytoplasm. The release of cytochrome *c* is one of the major events in apoptosis associated with permeabilization of the mitochondrial outer membrane [112]. Cytoplasmic cytohrome *c* promotes the formation of an apoptosome which in turn orchestrates apoptosis (Figure 1.6). The components of an apoptosome are cytochrome *c*, an adapter molecule apoptotic protease activating factor (Apaf-1) and procaspase 9. The binding of cytochrome *c* to Apaf-1 leads to the activation of procaspase 9. Active caspase 9 cleaves executioner caspases to induce apoptosis mainly through the activation of caspase 3 [103,117].

The B-cell lymphoma (Bcl) family members consist of antiapoptotic proteins including Bcl-2, Bcl-2-L2 and Bcl-2-A1, and proapoptotic proteins including Bid, Bim, Bik, Bmf, Bax, Bad and Bak. These proteins control mitochondrial apoptosis by regulating mitochondrial permeability. Overactivation of B-cell CLL/lymphoma 2 (Bcl-2) has shown to prevent cytochrome *c* release, while Bax promotes cytochrome *c* release (Figure 1.6) [103,117]. The intrinsic and extrinsic apoptosis signaling pathways communicate with each other through truncated Bid (tBid) (Figure 1.6). Caspase 8 has been shown to cleave the proapoptotic Bcl-2 family member Bid [118]. Bid can be cleaved by caspase 8 and the translocation of truncated Bid to the mitochondria promotes cytochrome *c* release through interaction with Bax and Bak. [119]. This can amplify the apoptotic signal following death receptor activation, and different cell types may be more reliant on this amplification pathway than others. Conversely, activators of the intrinsic pathway can sensitize cells to extrinsic death ligands [118]. Ceramide regulate Bcl-2 and Bax simultaneously by modulating their phosphorylation states and thereby induce apoptosis through the caspase activation via the mitochondrial pathway (Figure 1.6).

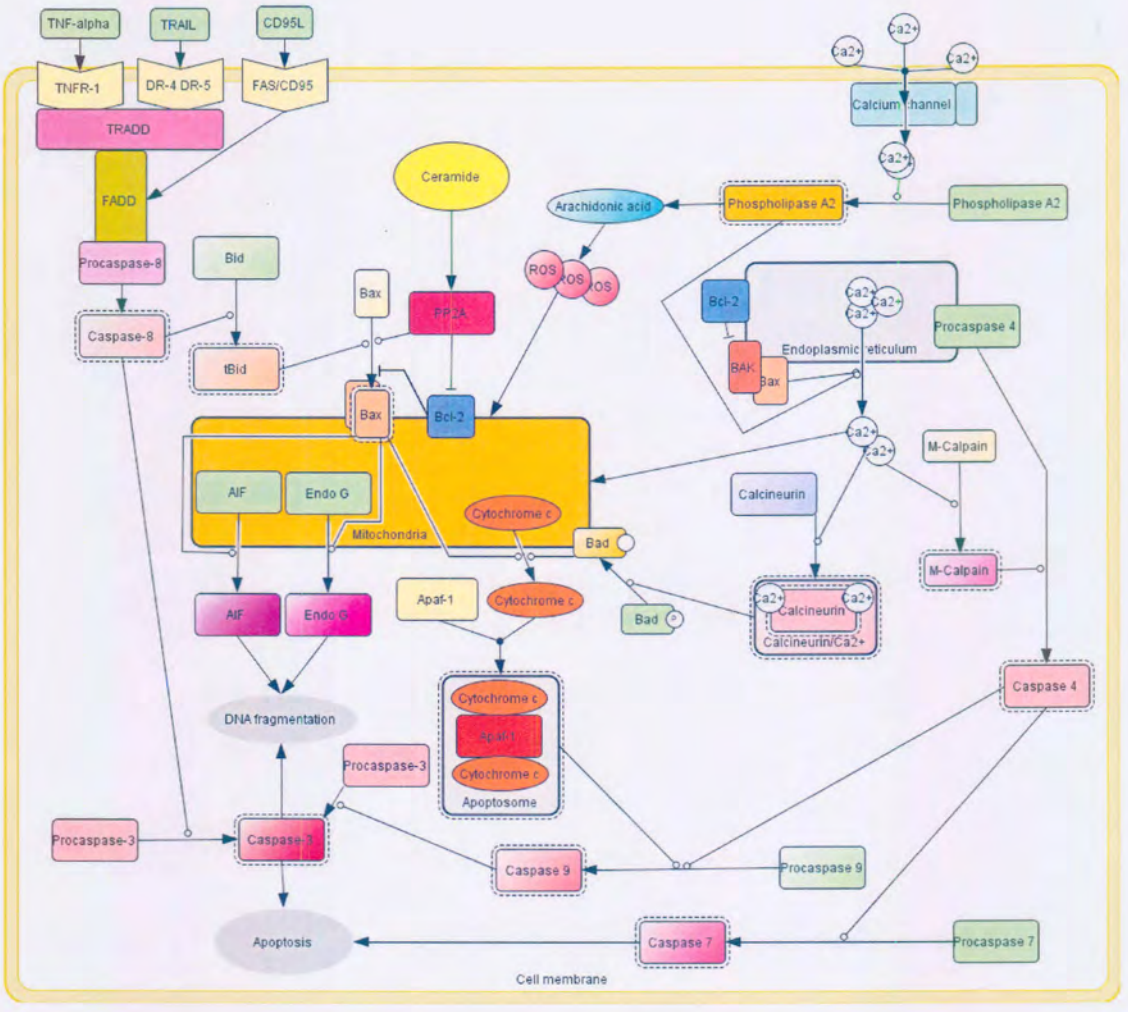

Figure 1.6: Steps in signaling of the pathways of apoptosis. In the extrinsic pathway, death receptors interact with their ligands and recruit adaptor protein and initiator caspases. Active initiator caspase activate the effector caspase to induce apoptosis. In the intrinsic mitochondrial and ER pathway, death signals stimulate mitochondria directly resulting in the release of cytochrome *c* that bind to an adaptor protein Apaf-1 and recruit initiator caspase 9. Active caspase 9 activates effector caspases to induce apoptosis. Elevation in cytoplasmic Ca^{2+} concentration as a result of ER stress results in the activation of caspase 4. Therefore distinct initiator caspases are activated in each pathway in order to activate effector caspases that are common to both the pathways. Truncated Bid (tBid) activated by caspase 8 enables intrinsic and extrinsic apoptosis signaling pathways to communicate with each other. Ceramide and other signals activated by cell stress affect mitochondrial permeability by interacting with the Bcl-2 family proteins.

Bcl-2, whose phosphorylation by protein kinase C alpha (PKCα) at serine 70 is required for its antiapoptotic function, becomes dephosphorylated in response to ceramide [120].

Recent work suggests that ceramide-activated protein phosphatase 2A (PP2A) may inhibit Bcl-2 via its dephosphorylation and proteasomal degradation [121]. On the other hand, Bax may also be regulated via PP2A, because Xin *et al.* (2006) showed that Bax is dephosphorylated following ceramide treatment in a PP2A-dependent manner [122]. Dephosphorylation of Bax was associated with its conformational change and subsequent release of cytochrome *c* from the mitochondria. These studies indicate a connection between ceramide, Bcl-2, and Bax, and imply that ceramide may be a regulator of Bcl-2 family members and their control over cell death pathways. Stander *et al.* (2007) reported that ceramide might play a central role in the growth inhibitory effects of *S. frutescens* extracts on MCF-7 cells and it is therefore possible to hypothesize that apoptosis might be induced via ceramide signaling in *S. frutescens* treated MCF-7 cells (Figure 1.2) [38].

1.4.1.1.3 Caspase activation: Endoplasmic reticulum pathway

The endoplasmic reticulum (ER) is the site of assembly of polypeptide chains destined for secretion or routing into various subcellular compartments. The ER represents the primary storage site for calcium (Ca^{2+}) within the cell [123]. Within the ER, Ca^{2+} functions in protein folding and when improperly regulated, Ca^{2+} has been shown to play a role in several cell death pathways [124]. High levels of Ca^{2+} uptake by mitochondria can activate the permeability transition pore and release cytochrome *c*, thereby inducing cell death (Figure 1.6) [125]. Calcineurin, a Ca^{2+}/calmodulin-dependent phosphatase, can dephosphorylate and activate the pro-apoptotic BH3-only protein Bad, inducing cell death through the mitochondrial pathway (Figure 1.6) [126]. Phospholipase A_2 can be activated by influx of extracellular Ca^{2+} to produce intracellular signaling lipids (*e.g.* arachadonic acid) which can induce reactive oxygen species (ROS) and ER Ca^{2+} release, followed by mitochondrial Ca^{2+} uptake and cytochrome *c* release (Figure 1.6) [127]. The cytoplasmic protease, M-calpain, is activated by calcium. Once activated, cleaves and activates caspase 12 (Figure 1.6) [128]. Caspase 12 plays the central role in

ER-mediated pathway of apoptosis induction in murine cells [129]. Once activated, caspase 12 can initiate downstream apoptotic pathways by inducing the activation of caspase 9 independent of Apaf-1 [128]. Caspase 4 is the human homolog of murine caspase 12 and is localized to the ER membrane and is specifically activated by and required for ER stress-induced apoptosis [107].

The Bcl-2 family of proteins is also able to control cell death at the ER through regulation of calcium homeostasis. Bcl-2 family members are also localized to the ER. Antiapoptotic bcl-2 is present in the ER membrane and contributes to ER membrane permeability by maintaining the pro-death bak and bax in their inactive conformations [130,131]. ER stress induces oligomerization of bax and bak to their active states and can then induce an ER Ca^{2+} leak that triggers apoptosis [130].

1.4.1.2 Caspase-independent apoptosis

Non-caspase proteases have been implicated as effectors of apoptosis. These include the cathepsins, calpains, granzymes and apoptosis inducing factor [100]. The cathepsin family of proteases consists of cysteine, aspartate, and serine proteases. Cathepsin B and cathepsin L, both cysteine proteases, and cathepsin D, an aspartate protease, are most frequently linked to apoptosis [132]. Cathepsin activity is associated with mitochondrial membrane permeability, chromatin condensation, the degradation of the intracellular matrix, the processing of procaspases, and the externalization of PS on the plasma membrane of apoptotic cells [100]. The calpain family of cysteine proteases resides in the cytosol and is activated by irregular increases in intracellular free Ca^{2+} [133]. Calcium activated M-calpain cleaves and activates caspase 12 and thereby activating downstream apoptotic pathways (Figure 1.6) [128]. Granzyme B promote caspase-independent DNA fragmentation by directly cleaving inhibitor of CAD (ICAD) allowing CAD to trigger nucleosomal DNA fragmentation [134]. Granzymes are also able to cleave the proapoptotic Bcl-2 family members Bid and Bax, thereby inducing mitochondrial membrane permeabilization [135]. Apoptosis-inducing factor (AIF) is a mitochondrial flavoprotein that is released from the intermembrane space during apoptosis. Once

liberated from the mitochondria, AIF translocates to the nucleus where it induces chromatin condensation and DNA fragmentation [100].

Mitochondrial EndoG is a mitochondrial nuclease that assists with the maintenance of the mitochondrial genome by participating in mitochondrial DNA duplication and repair [136]. After EndoG is released from the mitochondria into the cytoplasm as a result of apoptotic stimuli, it is translocated to the where it induces DNA fragmentation that is similar to CAD-induced DNA fragmentation [137]. However, unlike CAD, EndoG does not require caspase processing to be activated.

1.4.2 Autophagy

Normal cellular development and growth require a well-regulated balance between protein synthesis and degradation. Eukaryotic cells have two major avenues for degradation, the proteasome and autophagy. Autophagy literally means 'self-eating' and is involved in the bulk degradation of long-lived cytosolic proteins and organelles, whereas the ubiquitin–proteasome system degrades specific short-lived proteins. The term 'autophagy' includes several mechanisms, such as chaperone-mediated autophagy, microautophagy and macroautophagy. Chaperone-mediated autophagy is a mechanism that allows the degradation of cytosolic proteins that contain a particular pentapeptide consensus motif and has a limited degradative capacity [138]. Microautophagy involves the direct engulfment of cytoplasm at the surface of the degradative organelle by protrusion and/or invagination of the limiting membrane. Microautophagy is thought to contribute to the overall autophagic degradation of cytoplasm in intact cells, but its physiological significance or molecular properties have never been well characterized [139]. Macroautophagy is the major lysosomal route for the turnover of cytoplasmic components and is commonly referred to as only autophagy [140]. Autophagy is not constitutively active and needs to be induced. Known inducers include starvation and certain hormones. Phosphatidylinositol 3-phosphate kinases and target of rapamycin (TOR) are on the signal transduction pathways regulating autophagy.

1.4.2.1 Chaperone-mediated autophagy

Chaperone-mediated autophagy (CMA) involves the selective delivery of cytoplasm proteins to the lysosome/vacuole in a process which depends upon the recognition by lysosomal receptors of a sequence motif present in cytosolic proteins. CMA differs from the other lysosomal degradation pathways in that vesicular traffic is not involved and only soluble proteins, not organelles, are degraded [141]. The targeting motif of the CMA substrates is a series of five consecutive amino acids biochemically related to the pentapeptide KFERQ (Lys-Phe-Glu-Arg-Gln) [142]. The Q residue is always located at the beginning or at the end of the sequence followed by four amino acids consisting of a basic, an acidic, a bulky hydrophobic and a repeated basic or bulky hydrophobic amino acid [143]. Sequence analyses revealed that about 30% of the proteins in the cytosol contain this targeting motif and can be, in theory, substrates for CMA [143]. The signal transduction and the transcriptional cascades that activate CMA have not been fully elucidated however the components identified to date include lysosomal heat shock protein of 70 kDa (lys-hsc70), and lysosome-associated membrane protein type 2a (lamp2a), cytosolic heat shock protein of 70 kDa (cyt-hsc70) and associated cochaperones including; the heat shock protein of 40 kDa (hsp40), the heat shock protein of 90 kDa (hsp90), the hsc70-interacting protein (hip), the hsc70-hsp90 organizing protein (hop), and the Bcl2-associated athanogene 1 protein (bag-1) [141]. Cytosolic proteins with an exposed pentapeptide sequence related to KFERQ bind to cyt-hsc70 and associated cochaperones to form a molecular chaperone complex that binds to lamp2a (Figure 1.7) [141]. Hip stimulates the assembly of hsc70 with hsp40 and the protein substrate. Hsp40 stimulates the ATPase activity of hsc70 leading to increased rates of binding and release of substrate proteins [144]. Hsp90 recognizes unfolded regions within proteins and prevents substrate protein aggregation. Hop acts as a linker for hsc70 and hsp90 and may also act as a nucleotide exchanger. After protein unfolding, the protein is pulled into the lysosomal lumen with the help of lys-hsc70 (Figure 1.7).

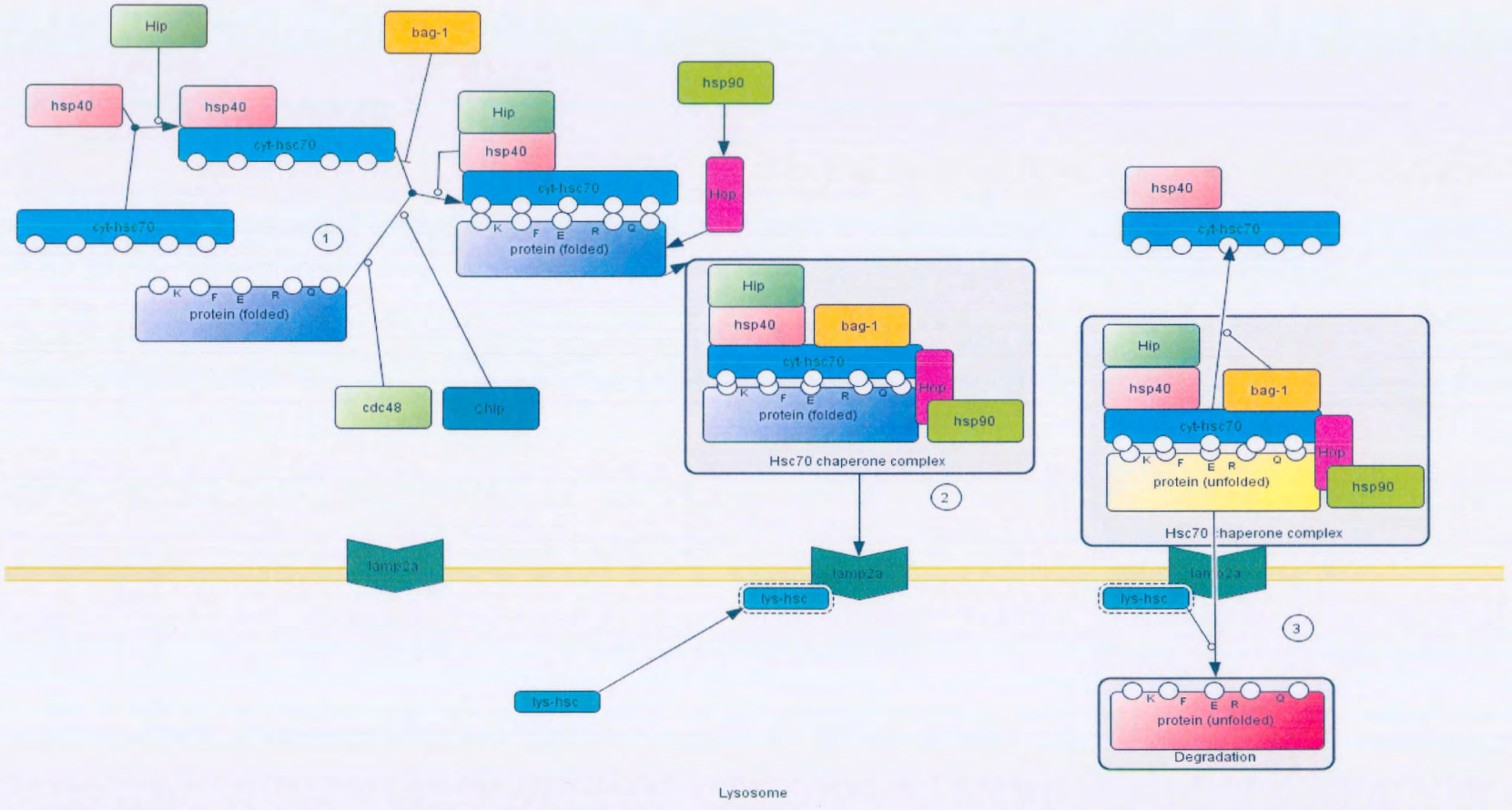

Figure 1.7: Mechanism of chaperone-mediated autophagy. 1) Hsc70 is activated by Hip to form an active hsc70-hsp40 complex. 2) The hsc70-hsp40 complex binds to substrate-proteins with a KFERQ motif and forms an hsc70-chaperone complex that binds to lamp2a. 3) After substrate-protein unfolding, lamp2a-bound lys-hsc70 pulls the unfolded substrate-protein into the lysosomal lumen for degradation.

1.4.2.2 Microautophagy

In microautophagy, portions of the cytoplasm are sequestered by invagination of the lysosomal membrane and subsequently degraded. Microautophagy does not appear to directly require autophagy-related (Atg) proteins in *Saccharomyces cerevisiae*, and its exact physiological role is not known. It is thought that it may play a role in removing the outer autophagosome membrane from the vacuole limiting membrane following autophagosome fusion [145].

1.4.2.3 Macroautophagy

In mammals, cells undergo autophagy during short-term starvation. By degrading non-essential components, cells get nutrients for vital biosynthetic reactions. Autophagy also contributes to cell homeostasis in muscle, liver and pancreas, as well as development and growth regulation and the down-regulation of macroautophagy observed in cancer cells is associated with tumor progression [140]. After an induction signal, autophagy starts when a flat membrane cistern wraps around a portion of cytosol and organelles to form a closed double-membrane bound vacuole containing cytosol and organelles. Such a vacuole is also known as an autophagosome and does not contain lysosomal proteins [146]. Autophagosomes are formed by phagophores or isolation membranes [146]. Autophagosomes undergo a stepwise maturation process by fusing the segregated cytosol and organelles with endosomal and/or lysosomal vesicles. Autophagosomes that have fused with endosomes are called amphisomes [147]. Autophagosomes and/or amphisomes that have fused with lysosomes are called autolysosomes [146]. Collectively autophagosomes, amphisomes and autolysosomes are called autophagic vacuoles (Figure 1.8) [148]. Both the segregated cytosol and organelles are then degraded by lysosomal hydrolases and the degradation products are transported back to the cytoplasm to be used for metabolic purposes.

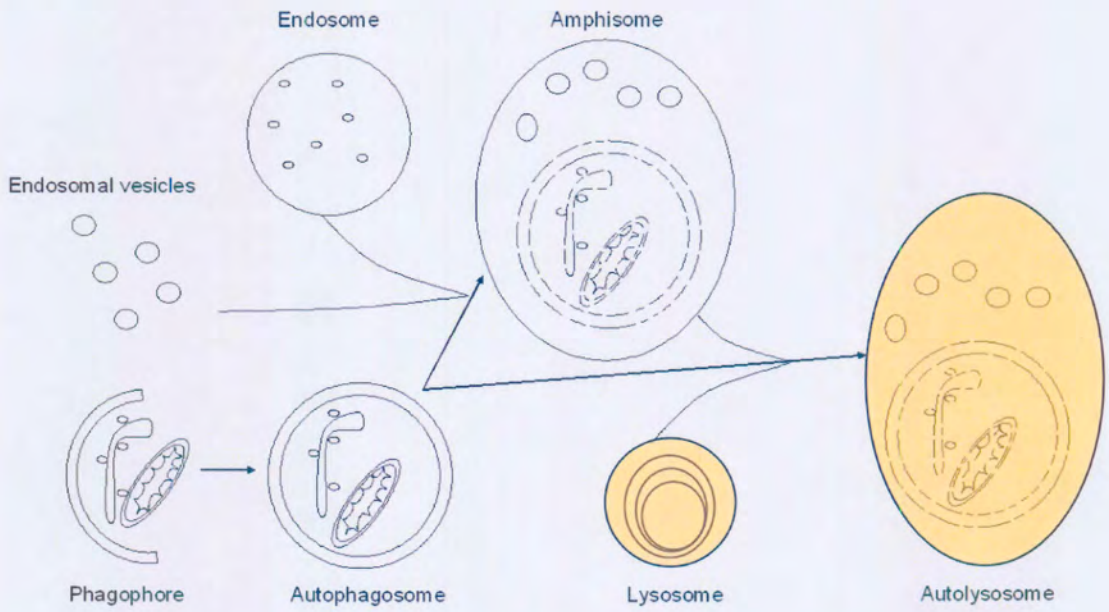

Figure 1.8: Schematic representation of the formation of autophagic vacuoles (Adapted from Eskelinen 2005 [148]).

Cells in the early stages of autophagy contain several autophagic vacuoli, and both the nucleoplasm and the cytoplasm appear slightly darkened while the nuclear structure still appears normal. Mitochondria and the endoplasmic reticulum are sometimes dilated, and the Golgi apparatus is often enlarged. The plasma membrane loses specializations such as microvilli and junctional complexes, and blebbing can occur. During late stages, both the number and size of vacuole increase, and many of them contain myelin figures or are filled with lipids, which appear as pale gray inclusions in the cytoplasm under electron microscopy. The nucleus of a cell undergoing autophagic cell death can become pyknotic and identifiable as such by light and fluorescence microscopy. However, nuclear condensation is not as common or as remarkable as that of apoptosis [149].

1.4.2.3.1 Signaling and regulation of macroautophagy

The kinase, mammalian TOR (mTOR), is a major sensor in the mammalian autophagy signaling pathway [150,151]. Once activated, mTOR can activate pathways that promote mRNA synthesis, protein synthesis, cell cycle progression, nutrient uptake and glyscolysis, while inhibiting apoptosis and autophagy [151]. The molecular mechanism and proteins involved in vesicle formation downstream of TOR has been well categorized in yeast, however, the functions of mammalian homologs and how they interact in mammalian autophagy needs to be clarified [152]. The most outstanding discovery is LC3, a mammalian homolog of the yeast Atg8p, and serves an index of autophagosome formation [153]. Similarly to the yeast homolog, LC3 is required for the formation process of autophagosomes, and is the only molecule controlled by nutrient supply and deprivation in the autophagy-related gene products. LC3 is clearly induced under conditions of autophagy stimulation like starvation and mTOR inhibition, implying that amino acid signaling and mTOR are upstream regulators of LC3 activity and expression (Figure 1.9) [153].

Two distinct mTOR kinase complexes exist, mTOR complex 1 and 2 (mTORC1/2). mTORC1 contains regulatory associated protein of mTOR (Raptor) and mTORC2 contains rapamycin-insensitive companion of mTOR (Rictor) (Figure 1.9). Both mTORC1 and mTORC2 contain the protein GβL [154]. Another protein that is associated with mTORC1 is the small GTPase Ras homolog enriched in brain protein (Rheb) [155]. GTPase Rheb in its active, GTP-bound form, positively regulates mTORC1 activity by direct interaction [155]. Rheb's activity is regulated by the tuberous sclerosis complex tumor suppressors TSC1 and TSC2, which form a GTPase activating protein (GAP), converting Rheb from its active to its inactive (GDP-bound) form (Figure 1.9) [155]. Growth factor and insulin signaling through receptor-mediated phosphoinositide-3 kinase (PI3K) activation leads to phosphorylation and activation of the oncogenic kinase Akt/PKB, which in turn inactivates TSC2, thereby activating Rheb and mTORC1 [155]. The energy sensor AMP-activated protein kinase (AMPK) inhibits mTORC1 by activating TSC2 in response to high AMP/ATP ratios, therefore AMPK serves as a sensor

for energy (ATP) status within the cell (Figure 1.9) [156]. High levels of AMP (low-energy status) activate AMPK which leads to the downstream inactivation of mTOR and ultimately upregulation of autophagy in order to regain energy through catabolic means. Both mTORC1 and 2 are similar in function however the exact mechanism of control of mTORC2 needs to be clarified [157].

mTOR kinase is also activated by amino acids, however, the exact mechanism by which amino acids control mTOR is still a matter of debate. The TSC1/TSC2 complex may integrate amino acid signaling upstream of mTOR [158]. Amino acids may also act at the level of mTORC1 by controlling the stability of it (Figure 1.3) [159]. The stability of this complex is increased in cells starved of amino acids, and is correlated with the inhibition of mTOR-dependent signaling. Amino acids have also been shown to mediate mTORC1 signaling by activating class III PI3K [160]. Beclin1, the mammalian homolog of Atg6 involved in autophagosome formation, is found in a complex with PI3K class III (Figure 1.9) [161]. In order to be able to bind to PI3K class III and to stimulate autophagy, Beclin 1, which is found in association with the antiapoptotic protein Bcl-2, must first dissociate from the inhibitory Beclin 1-Bcl-2 complex [162]. The Beclin 1-PI3K class III complex activity is also inhibited by the availability of amino acids (Figure 1.9) [163]. In MCF-7 cells, ceramide is able to induce autophagy through upregulation of Beclin-1 and inhibition of PKB/Akt [164]. Ras-dependent activation of the MAP-Erk1/2 pathway has a stimulatory effect on starvation-induced autophagy in colon carcinoma cells [165]. However, amino acids stimulate the phosphorylation of Ser259 of Raf-1 kinase and thereby inactivate the Erk1/2 MAPK kinase Raf-1 and down-regulate autophagy [165].

The tumor suppressor genes phosphatidylinositol-3,4,5-trisphosphate 3-phosphatase and dual- specificity protein phosphatases (PTEN) and p53 act in the mTOR signaling network to stimulate autophagy by inhibiting mTOR through TSC1/2 activation (Figure 1.9) [166,167]. PTEN inhibits autophagy by hydrolyzing phosphatidylinositol-(3,4,5)-trisphosphate (PIP3) to phosphatidylinositol (4,5)-bisphosphate (PIP2) and p53 inhibits mTOR activity through activation of AMPK. c-Myc, a proto-oncogene that

controls cell division and cell growth, increases autophagic activity when overexpressed in rat 3Y1 fibroblasts and is not dependent on its apoptogenic or tumorigenic functions [168]. Overexpression of p27kip1 (a cyclin-dependent kinase inhibitor that down-regulate cell cycle progression) induced autophagic cell death in human glioma cell lines, whereas the same treatment did not affect the viability of nonmalignant cultured astrocytes or induce autophagy inferring an interplay between autophagy and cell proliferation (Figure 1.9) [169].

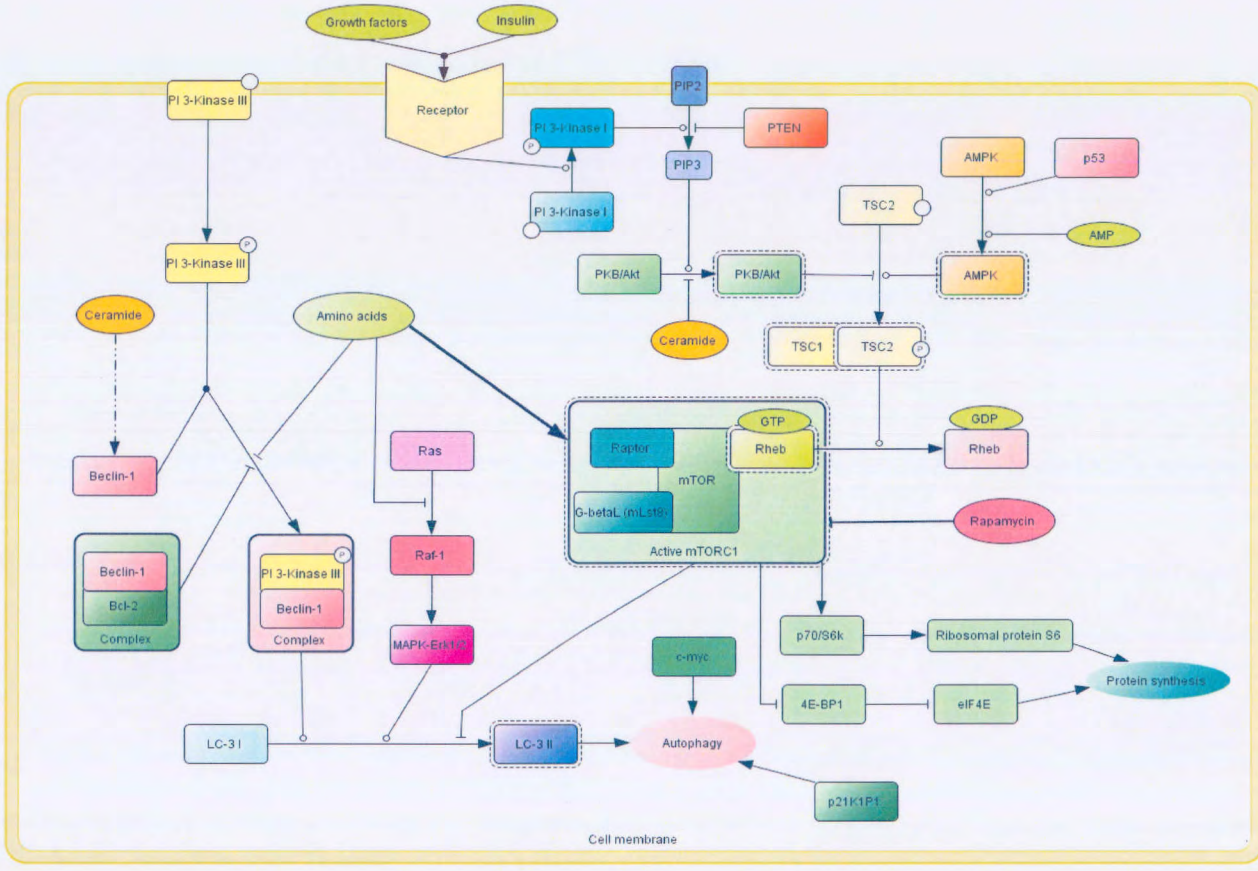

Figure 1.9: Signaling and the regulation of autophagy. Amino-acid-dependent activation of mTOR plays a crucial role in repressing autophagy. Insulin suppresses autophagy through the PI-3K-I/Akt/TSC1 and 2 mTOR pathway. Amino acid signaling controls autophagy in various ways; including mTOR stability, TSC1/2 pathway, the PI-3k-III pathway to inhbit Beclin1 activity and by inhibiting Ras-Raf1 signaling. smay be recognized at the plasma membrane by specific sensor/receptor(s). AMPK serves as an energy sensor and is able to induce autophagy when the intracellular energy status is low. mTOR plays a crucial role in initiation ribosomal activity and protein synthesis.

1.4.2.4 Autophagy and cell death

The precise role that autophagy plays in programmed cell death is unclear and seem to vary according to cell types [140]. During the initial stages of tumor growth autophagy may be increased to maintain cell metabolism and viability because insufficient vascularization limits nutrient supply to the cancer cells [170]. If nutrient deprivation persists, progressive autophagy can lead to autophagic cell death. Suppression or inactivation of the autophagy pathway can also contribute to cancer cell growth [170]. Many chemotherapeutic agents are able to induce autophagic cell death. Death-inducing agents, such as TNF and staurosporin, kill MCF-7 cells without producing apoptotic changes [171]. Tamoxifen and its downstream mediator ceramide induce autophagic cell death in MCF-7 cells [164]. Ceramide, as well as the proapoptotic Bcl-2 family protein BINP3, induces autophagic cell death in malignant glioma cells [172]. Anticancer drugs such as paclitaxel and vinblastine, induces autophagic cell death as well as apoptotic cell death [173,174]. Resveratrol is able to induce autophagic cell death in ovarian cancer cells, coupled, in part, with apoptotic cell death [175]. Rapamycin and its analogues, CCI-779, RAD001, and AP23573, specifically target the autophagy-regulated protein mTOR and preclinical studies indicate that mTOR inhibitors have a broad spectrum of antitumor activity [176]. However, mTOR inhibitors have been shown to induce tumor progression in patients with metastatic renal cancer [176].

The effects that *S. frutescens* extracts have on autophagic activity are yet to be analyzed. Stander *et al.* (2007) indicated that *S. frutescens* extracts inhibited growth with morphological hallmark of cytoplasmic shrinking and hypercondensed chromatin [38]. These are also morphologic characteristics of autophagy, and the hypothesis that ceramide might play a central role *S. frutescens* induced growth inhibition opens the possibility that autophagic cell death might occur in concert with apoptosis.

1.4.3 Oncosis

Oncosis, derived from the Greek word for swelling, is the common pattern of cellular changes in infarcts and zonal cell death following chemical toxicity [177]. Oncosis can occur as a result of the activation of specific signal transduction cascades and subsequently can be overt or revealed only on inhibition of apoptosis and/or autophagy [178]. A proposed sequence of events during oncosis includes early signs of mitochondrial dysfunction; namely, production of reactive oxygen species (ROS) by mitochondria and swelling of mitochondria; ATP depletion; failure of Ca^{2+} homeostasis; perinuclear clustering of organelles; activation of a few proteases, in particular calpains and cathepsins; lysosomal rupture; and ultimately plasma membrane rupture [178]. Plasma membrane blebbing, dilation of the ER, mitochondrial swelling, and clumping of nuclear chromatin are morphological changes associated with oncosis [177]. These morphological changes are followed by the breakdown of the plasma membrane, release of intracellular constituents, and inflammation. Lui *et al.* (2004) defined oncotic cell death as the point in the oncotic process in which respiration (mitochondrial function and associated ATP formation) and ion homeostasis cannot be restored [179]. Loss of mitochondrial function as a result of ischemia and toxicant exposure in tissues that generate ATP exclusively through oxidative phosphorylation is catastrophic. In contrast, cells in tissues that are capable of generating ATP from oxidative phosphorylation and glycolysis are more resistant to the effects of ischemia and mitochondrial-directed toxicants [179]. Cultured cells *in vitro* generate a significant amount of their ATP through glycolysis and it was found that if ATP decreases are less than 80%-85%, cells will either die by apoptosis or survive if mitochondrial function can be restored, and if ATP depletion is greater than 80%-85%, oncosis will occur [180]. Therefore ATP levels must be depleted beyond 80%-85% to initiate oncosis.

Death receptor-mediated oncosis has been described and is mediated by the TNFR superfamily [178]. One of the DISC components, FADD, has been shown to be involved not only in TNFα-induced apoptosis, but also in oncosis. Receptor-induced oncosis have been reported in L929 mouse fibrosarcoma cell line treated with TNFα [181]. In this model, cells initiate a complex multistep signal transduction pathway in

which FADD is recruited to the TNF-R1 and induces oncosis, presumable through its death domain [181]. In L929 cells, TNFα-induced necrosis is accompanied by a rapid burst in mitochondrial ROS production. ROS have been implicated in apoptotic as well as oncotic cell death, and damage to mitochondria by ROS leads to impaired ATP production via oxidative phosphorylation and ultimately oncotic cell death [133] In the presence of caspase inhibitors, enforced oligomerization of FADD can induce necrosis, and this death is blocked in FADD-deficient T cells [182,183]. Receptor-interacting protein 1 (RIP1) is also involved in death receptor-induced necrosis, as RIP1-deficient T cells are also resistant to death induced by TNFα and FasL in the presence of caspase inhibitors [183]. The kinase activity of RIP appears to be required for necrosis induction, although its targets remain to be identified.

Intracellular Ca^{2+} is an important signaling molecule for numerous cell responses including oncosis. Increased cytoplasmic Ca^{2+} concentration through endoplasmic reticulum Ca^{2+} release and/or extracellular Ca^{2+} influx play an important role in oncosis and calcium-activated neutral proteases (calpains) have been implicated in the mediation of oncosis in different cellular models subjected to diverse insults and in a limited number of *in vivo* models [184,185]. Two ubiquitous isoforms, μ- and m-calpain, have been identified and studied extensively and μ- and m-calpains are activated by μM and mM Ca^{2+} concentrations *in vitro*, respectively [133]. Calpain activity during oncosis is regulated by autolysis, translocation from the cytosol to the cell membrane and the endogenous inhibitor protein calpastatin [179]. In the autolysis/dissociation model, Ca^{2+} binds to calpains, inducing dissociation of the calpain subunits and two successive autolytic events (80 kDa to 78 kDa to 76 kDa) producing two active calpain enzyme forms with different cell localization [186]. A growing body of evidence indicates that calpains play a critical role in plasma membrane permeability during cell injury and death. For example two calpain inhibitors, PD-150606 and SJA-7029, prevented increased plasma membrane permeability to propidium iodide and lactate dehydrogenase in the late stage of renal cell oncosis produced by diverse toxicants or insults, suggesting that calpain mediates the increased plasma membrane permeability [187,188,189]. Activated calpains have a large number of substrates that play a role in calpain-mediated

disruption of ion homeostasis, calpain-mediated progressive plasma membrane permeability, and calpain-mediated mitochondrial dysfunction in oncosis [179].

1.4.4 Metabolic catastrophe

Regulation of cell growth is explicitly linked to regulation of metabolism and a common feature of human tumors is their reliance on glycolysis even under aerobic conditions which is commonly known as the Warburg effect [190]. A wide body of evidence shows that mitochondria from rapidly growing tumors are generally smaller and show less cristae than mitochondria from well differentiated tumors or normal tissues [191]. Pedersen (1978) further emphasized that tumors have a significantly reduced number of mitochondria [191]. Evidence also exists indicating increased glycolytic activity in cancer cells and it was found that glycolysis is triggered by oncogene activation including activation of Ras, Akt, c-Myc, and by hypoxia in the tumor environment through hypoxia inducible factor 1 alpha (HIF-1α) induction [192,193,194]. Glycolysis may also be triggered by the accumulation of damaged mitochondria that have impaired capacity for ATP generation through oxidative phosphorylation [195]. Glycolysis is a substantially less efficient means for ATP generation compared with oxidative phosphorylation, however many of the mechanisms involved in promoting glycolysis (oncogene activation) also facilitate uptake of nutrients from extracellular sources [196]. Metabolic stress is a potent activator of apoptosis and is mediated by AMP-activated protein kinase (AMPK) [197]. Activated AMPK can induce apoptosis in a p53-dependent manner and in cancerous cells with apoptotic defiencies. AMPK can induce autophagy through mTOR inhibition. However, both apoptotic and autophagic pathways are deficient in many tumors and the unrelenting demand for energy, exacerbated by inefficient ATP production, can result in the oncotic pathway to cell death in energy starved tumor cells [198,199]. This is termed metabolic catastrophe and represents a means to induce death in tumor cells resistant to apoptosis and deficient of autophagy. Metabolic catastrophe can be induced by various methods in tumor cells with constitutive activation of the PI-3-kinase pathway. Angiogenesis inhibitors such as Avastin targets vascular endothelial growth factor and reduces nutrient availability [200,201]. Increase in energy requirements to increase metabolic stress can be induced by DNA alkylating agents that stimulate

poly-(ADP-ribose) polymerase which consumes ATP [202]. These and other means for acute induction of oncotic cell death in tumor cells are an attractive means for cancer therapy, however controlling necrosis as a result of oncotic cell death and modulating appropriate inflammatory response to favor tumor regression remains the challenge (Figure 1.10) [203].

1.4.5 Mitotic catastrophe

Mitotic catastrophe is a type of cell death occurring during mitosis, as a result of DNA damage or deranged spindle formation coupled to the debilitation of different checkpoint mechanisms that would normally arrest progression into mitosis and hence suppress catastrophic events until repair has been achieved [204]. Gross abnormalities of chromosome segregation, formation of large cells with multiple micronuclei and decondensed chromatin are characteristics mitotic catastrophe. As discussed, the DNA structure checkpoint arrests cells at the G_2/M transition in response to unreplicated DNA or DNA damage, and the spindle assembly checkpoint prevents anaphase until all chromosomes have obtained bipolar attachment. The combination of checkpoint deficiencies and specific types of damage would lead to mitotic catastrophe. The pharmacological inhibition or genetic suppression of several G_2 checkpoint genes such as ATM, ATR, Chk1, Chk2 and polo-like kinases (Plks) 14-3-3-s can promote DNA-damage-induced mitotic catastrophe [205,206]. At least two subtypes of mitotic catastrophe can be distinguished. Firstly, mitotic catastrophe can kill the cell during, or close to the metaphase in a p53-independent manner, as this occurs in Chk2-inhibited syncytia or Plk2-depleted cells [206]. Activated Chk2 due to DNA damage can act in a pleiotropic manner to phosphorylate the transcription factor E2F1, which in turn facilitates the induction of at least two proapoptotic proteins, Apaf-1 and p73 [204,206]. Second, mitotic catastrophe can occur after failed mitosis, during the activation of the polyploidy checkpoint, in a partially p53-dependent manner. Therefore failure to activate the G_2/M checkpoint, cells with DNA lesions (or incomplete DNA replication) activates an apoptotic program that leads to the phenotypic manifestation of mitotic catastrophe, during the metaphase of the cell cycle. Suppression of the apoptotic program (and of the spindle checkpoint) then may lead to asymmetric cell division or mitotic slippage,

resulting into the generation of tetraploid cells. Formation of tetraploid cells activates the polyploidy checkpoint, in a p53-dependent manner which results in G_1/S arrest and ultimately apoptosis [204]. The generation aneuploid offspring as a result of an inactive polyploidy checkpoint can result in cancerous growth of cells (Figure 1.10) [207].

1.5 Cross-talk between programmed cell death pathways and the cell cycle

Molecular linkages between cell death, cell survival, and cell cycle have become an object of intense research in recent years. Tumorigenesis is a dynamic process that is driven by complex interactions between oncogene activation, tumor suppressor inactivation and responses to cellular stress. How cancer cells choose their fate from options such as cell cycle arrest, apoptosis, necrosis, autophagy and mitotic catastrophe in response to anticancer agent is an important question in the successful treatment of tumors. Many anticancer drugs induce apoptosis, and the magnitude of cell death is well correlated with tumor response. The molecular mechanisms by which anticancer drugs induce apoptosis are mediated by mitochondrial dysfunction, which is regulated by the balance of proapoptotic and antiapoptotic proteins in the Bcl-2 family as discussed. DNA damage to cancer cells induces the activation of proapoptotic proteins such as Bax and Bak in a p53 dependant manner, which translocate from the cytosol to mitochondria. A functional defect of a proapoptotic protein or overexpression of an antiapoptotic protein causes resistance to apoptosis in many tumorigenic cells [208]. Nonapoptotic cell death in cells lacking apoptotic machinery is mainly attributed to autophagy. Many chemotherapeutic agents are able to induce autophagic cell death and it has been reported that treatment with anticancer drugs such as paclitaxel and vinblastine induced autophagic cell death as well as apoptotic cell death (Figure 1.10) [174]. Targeting mTOR is an attractive and promising means for cancer treatment and preclinical studies indicate that mTOR inhibitors have a broad spectrum of antitumor activity [176]. Many tumors however lack sufficient apoptotic and autophagic activity and these pathways are usually defective. Cell death can be induced in an oncotic fashion directly through receptor-mediated pathways which result in ROS release and ultimately mitochondrial damage; causing metabolic catastrophe and ultimately oncotic cell death.

Figure 1.10: Possible interactions between cell cycle arrest and programmed cell death pathways. After cell cycle arrest due to various cell stresses, apoptosis can be directly induced or indirectly induced via mitotic catastrophe, apoptosis can begin with autophagy, autophagy can end with apoptosis, blockage of caspase activity can result in autophagic cell death from apoptosis, and insufficient autophagy can result in metabolic catastrophe and ultimately oncotic cell death.

Oncosis can also be induced as a result of insufficient autophagy when cells are under metabolic stress, resulting in insufficient energy production through catabolism and loss of function of organelles as a result of insufficient energy supplies (Figure 1.10). Ca^{2+} release from dysfunctional ER can then result in the induction of calpains, leading to oncotic cell death [187]. Cancer cells often have a defect in a particular cell death pathway, but are still able to die through the many possible mechanisms discussed. However, the nature of the cell death defect ultimately affects the clinical outcome of

treatment, depending on which mechanism is missing. Several questions remain concerning the interactions between apoptotic and non-apoptotic cell death pathways. Are apoptosis, senescence, oncosis, autophagy and mitotic catastrophe entirely independent programs, or do they overlap to some degree? Do these responses occur successively or simultaneously? Can one mechanism compensate for another that is inactivated by a tumorigenic mutation? If these cell death pathways overlap significantly and are commonly modified in tumor progression, anticancer therapies that are designed to restore function to a key program will restore them all, and therefore greatly improve the efficacy of the treatment. However, if these cell death mechanisms are independent, identifying and targeting only the pathway that most efficiently inactivates the cancer cells in question might be the most effective approach [209].

1.6 Relevance and aim of the study

The use of traditional medicine for the treatment of various maladies in many parts of Africa is an inherent characteristic of the continent. However, there is relatively little scientific evidence to support anecdotal evidence of efficacy. Therefore, the need exists to investigate the mechanism through which these biologically active compounds synergistically activate growth inhibitory and programmed cell death pathways.

The purpose of this study is to investigate and compare the possible differential actions of crude *S. frutescens* extracts in MCF-12A and MCF-7 cell lines by:

a) performing cell growth studies in order to determine the effect of *S. frutescens* extracts on cell numbers and metabolic activity.
b) studying morphological changes induced by *S. frutescens* extracts with haematoxylin and eosin staining, Hoechst 33342, Acridine orange and propidium iodide triple fluorescent staining and transmission electron microscopy techniques.
c) investigating the effects that *S. frutescens* extracts have on the cell cycle, apoptosis, autophagy and oncosis.

d) investigating the effects that *S. frutescens* extracts have on global gene expression changes and protein expression.

Unraveling the mechanism of crude *S. frutescens* extracts *in vitro* is an important avenue of research in order to provide a basis for future research in looking for promising anticancer compounds. It is thus an important avenue to explore in order to support the use of traditional medicine as an alternative to often expensive conventional medicine.

Chapter 2

Materials and methods

Experiments were conducted in the Department of Physiology of university of Pretoria in conjunction with the African Centre for Gene Technologies. (ACGT) Microarray facility and the Bio-informatics and Computational Biology Unit of the University of Pretoria. Electron microscopy was conducted at the Electron Microscopy Unit of the University of Pretoria. Flow cytometry analysis was conducted at the department of Pharmacology of the University of Pretoria.

2.1 Cell lines

The effects of *S. frutescens* extracts were investigated in the following cell lines:

a) MCF-7: Cell line derived from a pleural effusion of human breast adenocarcinoma.

b) MCF-12A: Non-tumorigenic epithelial cell line established from tissue taken at reduction mammoplasty from a nulliparous patient with fibrocystic breast disease that contained focal areas of intraductal hyperplasia.

The MCF-7 cell line was supplied by Highveld Biological Pty (Ltd) (Sandringham, Johannesburg, South Africa) and the MCF-12A cell line was obtained as a gift from Professor MI Parker (Department of Cancer Biology of the University of Cape Town, Cape Town, South Africa).

In vitro studies using continuous cell lines aim at describing the effects of an experimental variable on a well established model. *In vitro*-type studies are best suited for deducing the mechanisms of action of a test substance and test conditions may not directly correspond to *in vivo* conditions. In order to evaluate the diagnostic and/or prognostic value of results, it has to be assumed that *in vitro* results would be representative of *in vivo* conditions.

2.2 General laboratory procedures

2.2.1 Materials

Dulbecco's minimum essential medium eagle (D-MEM), Trypsin-EDTA and crystal violet were supplied by Sigma Chemical Co. (St. Louis, MO, USA). Heat-inactivated fetal calf serum (FCS), sterile cell culture flasks and plates were obtained through Sterilab Services (Kempton Park, Johannesburg, South Africa). Penicillin, streptomycin and fungizone were purchased from Highveld Biological Pty (Ltd) (Sandringham, SA). All other chemicals were of analytical grade and will be purchased from Sigma Chemical Co. (St. Louis, MO, USA), Southern Cross Biotechnology Pty (Ltd) (Cape Town, SA), Amersham Biosciences Pty (Ltd) (Pittsburgh, PA, USA) and Agilent Technologies Pty (Ltd) (Palo Alto, CA, USA).

2.2.2 General cell culture procedures

Cell were grown and maintained in $25cm^2$ tissue culture flasks in a humidified atmosphere at 37°C, 5% CO_2 in a Forma Scientific water-jacketed incubator (Ohio, United States of America). MCF-7 cells were cultured in DMEM and supplemented with 10% heat-inactivated FCS (56°C, 30min), 100U/ml penicillin G, 100µg/ml streptomycin and fungizone (250µg/l). MCF-12A maintenance medium consisted of a 1:1 mixture of DMEM and Ham's-F12 medium, 20ng/ml epidermal growth factor, 100ng/ml cholera toxin, 10µg/ml insulin and 500ng/ml hydrocortisone, supplemented with 10% heat-inactivated FCS (56°C, 30min), 100U/ml penicillin G, 100µg/ml streptomycin and fungizone (250µg/l).

Phosphate buffered saline (PBS) was prepared by diluting a ten times concentrated solution consisting of 80g/l NaCl, 2g/l KCl, 2g/l KH_2PO_4 and 11.5g/l Na_2HPO_4 (purchased from Merck (Munich, Germany)) to a 1 times concentrated solution. The diluted PBS solution was autoclaved (20min, 120°C, 15psi) before use.

Hydroxymethylaminomethane (Tris) buffered saline (TBS) was prepared by diluting a ten times concentrated solution (pH=7.4) consisting of 61g/l Tris (purchased from Sigma

Chemical Co. (St. Louis, MO, USA)) and 90g/l NaCl, (purchased from Merck (Munich, Germany) to a 1 times concentrated solution. The pH was adjusted to 7.4 with 6N HCl.

Growth medium of the cells were replaced at one to three day intervals and the cells were trypsinized when confluent. When confluent, cells were trypsinized by removing the growth medium, washing with sterile PBS and incubating in trypsin/versene for ±10min or when the cells appeared round and detached easily. The trypsin solution was removed and the tissue culture flask was gently tapped against the hand in order to detach the cells. The detached cells were resuspended in fresh medium and either divided into subcultures, used in experiments or frozen away in cryotubes in a -70°C freezer. The freeze medium consists of 10% growth media, 10% DMSO and 80% FCS.

Aseptic techniques were applied throughout, with all work being carried out in a laminar flow cabinet from Labotec (Midrand, South Africa), all solutions were filtered-sterilized (0.22µm pore size) and all glassware and non-sterile equipment sterilized by autoclaving (20min, 120°C, 15psi)

2.2.3 General methods for experiments

2.2.3.1 Preparation of *S. frutescens* extracts

Specimens of *S. frutescens* were harvested and air-dried in the shade in the vicinity of Murraysburg in the Karoo, South Africa by W Grobler. The plants were identified as *S. frutescens* (L.) R. Br. Var. *microphylla* (Burch. Ex DC) Harv., by BE van Wyk of the Botany and Biotechnology department of the University of Johannesburg (voucher specimen from W. Grobler: C. Albrecht s.n. sub. BE van Wyk 4126 JRAU). The leaves and small twigs were ground to obtain a fine powder with an electrical grinder. 3g of the *S. frutescens* powder was weighed, autoclaved and mixed with 10ml, 70% ethanol and extracted for 24h at room temperature. After extraction, the supernatant was transferred to a 50 ml tube and centrifuged at 3000rpm for 5 min to further remove any debris. The supernatant was filtered twice with a 0.22µm filter to obtain a purified stock solution with a concentration of 300mg/ml.

2.2.3.2 General methods for experiments

For experiments, cells were seeded in a 96-well (5000 cells per well) tissue culture plates, on heat-sterilized coverslips in 6-well culture plates (500 000 cells per well) or in 25cm^2 tissue culture flasks (1.5x10^6 cells per flask). Cells were incubated for 24h to allow for attachment after which medium was removed and the cells were exposed to *S. frutescens* extract concentrations between 1.0mg/ml to 2.0mg/ml. Cells were harvested by tripsinization as described above and were counted by making use of a haemocytometer as desribed by Freshney (1995) (210). 20µl of the suspended cells where mixed with 80µl PBS and 100µl Trypan blue to give a concentration of cells with 10 times dilution factor. Dead cells take up the dye and are consequently stained blue, which is then left uncounted.

The number of viable cells per ml is determined by:

Cells/ml = Average count of viable cells in the corner squares x dilution factor x 10^4

2.3 Analytical experimental protocols

2.3.1 Cell growth studies

2.3.1.1 DNA staining – crystal violet

Quantification of fixated monolayer cells were spectrophotometrically determined employing crystal violet as a DNA stain. Staining cell nuclei of fixed cells with crystal violet allows for rapid, accurate and reproducible quantification of cell number in cultures grown in 96-well plates [211,212]. Absorbance of the dye measured spectrophotometrically at 570nm will correspond to cell numbers. According to Berry *et al.* (1996) crystal violet staining of samples containing an abnormally high proportion (>30%) of stationary binucleated cells will yield higher cell concentrations than trypan blue or Coulter counter methods [213]. MCF-7 and MCF-12A cells contain less than 1% stationery binucleated cells [214,215] and will therefore not lead to anomalous results.

a) Materials

Glutaraldehyde, crystal violet and Triton X-100 were purchased from Merck (Munich, Germany).

b) Methods

Exponentially growing MCF-7 and MCF-12A cells were seeded in 96-well tissue culture plates at a cell density of 5000 cells per well. Cells were incubated at 37°C for 24h to allow for attachment. After 24h attachment the medium was discarded and the cells were exposed to concentrations ranging between 1.0mg/ml and 2.0mg/ml of *S. frutescens* extract, and incubated for 48h, before the assay was performed. A baseline measurement was obtained before exposure in order to determine the starting amount of cells.

After 48h the medium was discarded and 100µl of 1% glutaraldehyde (in PBS) was added to each well and incubated at room temperature for 15min. The glutaraldehyde was discarded and 100µl 0.1% crystal violet (in PBS) was added and left at room temperature for 30min. The crystal violet was discarded and the microtiter plates were immersed under running tap water for 10min and left overnight to dry. 200µl 0.2% Triton X-100 was added to solubilize the cells and incubated at room temperature for 30 min. 100µl of the solution was transferred to a clean micrometer plate and the absorbance was read at 570nm with an EL_x800 Universal Microplate Reader from Bio-Tek Instruments Inc. (Vermont, United States of America).

2.3.1.2 Metabolic activity - MTT assay

3-(4,5-Dimethylthiazol-2-yl)-2,5-diphenyltetrazolium bromide (MTT) was used to determine the metabolic effects of *S. frutescens* extracts on MCF-7 and MCF-12A cells. MTT is oxidized to purple by the reduced nicotinamide adenine dinucleotide (NADH), therefore conversion is directly related to the metabolic activity of cells [216]. The amount of converted MTT was spectrophotometrically measured at a wavelength of 570nm with background subtraction at 650nm [216].

a) Materials

3-(4,5-Dimethylthiazol-2-yl)-2,5-diphenyltetrazolium bromide (MTT) was supplied by Sigma-Aldrich (St. Louis, United States of America). All other chemicals were from Merck (Munich, Germany).

b) Methods

Exponentially growing MCF-7 and MCF-12A cells were seeded in 96-well tissue culture plates at a cell density of 5000 cells per well. Cells were incubated at 37°C for 24h to allow for attachment. After 24h attachment the medium was discarded and the cells were exposed to concentrations ranging between 0.5mg/ml and 2.25mg/ml of *S. frutescens* extract, and incubated for 48h, before the assay was performed. A baseline reading was conducted before exposure to determine the starting number of cells.

After 48h of exposure, 20µl MTT (5mg/ml in PBS) was added to each well containing 200µl medium. The microtiter plates were incubated for 4h at 37°C in a CO_2 incubator. The medium was carefully removed without disturbing the cells. 200µl DMSO was added to each well by gently pipetting up and down. 100µl of the solution was transferred to a clean micrometer plate and the absorbance was read at 570nm (reference 630nm) with an EL_x800 Universal Microplate Reader from Bio-Tek Instruments Inc. (Vermont, United States of America).

2.3.2 Morphology studies

2.3.2.1 Light microscopy – haematoxylin and eosin cell staining

The influence of crude ethanolic *S. frutescens* extracts on cell morphology was conducted by staining the nucleus and cytoplasm of MCF-7 and MCF-12A with haematoxylin and eosin (H&E) staining [217].

a) Materials

Bouins's fixative was purchased from Sigma-Aldrich ((St. Louis, United States of America). Haematoxylin, eosin, ethanol, xylol and Entellam® fixative were purchased from Merck (Munich, Germany).

b) Methods

Exponentially growing MCF-7 and MCF-12A cells were seeded at 500 000 cells per well in 6-well plates on heat-sterilized coverslips. After 24h attachment the medium was discarded and the cells were exposed to 1.5mg/ml of *S. frutescens* extract, and incubated for 48h, before the cells were stained. The coverslips were transferred to staining dishes and fixed with Bouin's fixative for 30min. The Bouin's fixative was discarded and the coverslips where left in 70% ethanol for 20min before they were rinsed with tap water. Mayer's haemalum was added and left for 20min and discarded. The coverslips were rinsed with tap water for 2 min then with 70% ethanol before being subjected to 1% eosin for 5min. The eosin was discarded and the coverslips were consecutively rinsed twice for 5 min with 70%, 96%, 100% and xylol. The coverslips were mounted on microscope slides with resin and left to dry before evaluation with a Zeiss Axiovert MRc microscope (Zeiss, Germany)

2.3.2.2 Fluorescent microscopy – apoptosis, autophagy and oncosis detection

Fluorescent microscopy was employed to differentiate between viable, apoptotic, autophagic and oncotic cells. A triple fluorescent dye staining method was developed utilizing acridine orange (green), Hoechst 33345 (blue) and propidium iodide (red) fluorescent dyes. Acridine orange is a lysosomotropic fluorescent compound that serves as a tracer for acidic vesicular organelles including autophagic vacuoles and lysosomes [218]. Cells undergoing autophagy will have an increased tendency for acridine orange staining when compared to viable cells, however acridine orange is not a specific marker for autophagy and therefore other techniques are needed to verify the appearance of increased autophagic activity. Hoechst 33342 is a fluorescent dye that can penetrate intact cell membranes of viable cells and cells undergoing apoptosis and stain the nucleus. Propidium iodide is a fluorescent dye that is unable to penetrate an intact membrane and

therefore stains the nucleus of cells that have lost their membrane's integrity due to oncotic or necrotic processes.

a) Materials

bisBenzimide (Hoechst 33342), acridine orange and propidium iodide were purchased from Sigma-Aldrich (St. Louis, United States of America).

b) Methods

Exponentially growing MCF-7 and MCF-12A cells were seeded at 500 000 cells per well in 6-well plates on heat-sterilized coverslips. After 24h attachment the medium was discarded and the cells were exposed to 1.5mg/ml of *S. frutescens* extract, and incubated for 48h, before the cells were stained. After 48h exposure, 0.5ml of Hoechst 33342 solution (3.5µg/ml in PBS) was added to the medium to give a final concentration of 0.9µM and incubated for 30min at 37°C C in a CO_2 incubator. After 25min, 0.5ml of acridine orange solution (4µg/ml) was added to the medium to give a final concentration of 1µg/ml and incubated for 5min at 37°C. After 30min, 0.5ml of propidium iodide solution (40µg/ml in PBS) was added to the medium to provide a final concentration of 12µM. Within 5min the coverslips were mounted on microscope slides with mounting fluid (90% glycerol, 4% N-propyl-gallate, 6% PBS). The cells were examined with a Zeiss inverted Axiovert CFL40 microscope and Zeiss Axiovert MRm monochrome camera under Zeiss Filter 2 for Hoechst 33342 (blue) stained and Zeiss Filter 9 for acridine orange-stained (green) and Zeiss filter 15 for propidium iodide-stained (red) cells. In order to prevent fluorescent dye quenching, all procedures were performed in a dark room.

2.3.2.3 Transmission electron microscopy

Transmission electron microscopy (TEM) was used to determine the ultra structure of intracellular components of exposed and control cells. TEM is an imaging technique whereby a beam of electrons is focused onto a specimen. The electron beam is partially transmitted through the very thin specimen and carries information about the inner structure of the specimen. [219].

a) Materials

Aqueous osmium tetroxide, glutaraldehyde, phosphate buffer quetol, Reynolds' lead citrate, aqueous uranyl acetate were purchased by the Electron Microscopy Unit of the University of Pretoria from Merck Co. (Munich, Germany). The Multi-purpose Philips 301 transmission electron microscope (TEM) of the Electron Microscopy Unit of the University of Pretoria was used for viewing the prepared samples.

b) Methods

Exponentially growing MCF-7 and MCF-12A cells were seeded at $1{,}5x10^6$ cells per $25cm^2$ flask. After 24h attachment the medium was discarded and the cells were exposed to 1.5mg/ml of *S. frutescens* extract and incubated for 48h. After 48h cells trypsinized and resuspended in 1ml growth medium in 1.5ml eppendorfs. Cells were fixed in 2.5% glutaraldehyde in 0.075M phosphate buffer (pH 7.4-7.6) for 1 h and rinsed 3 times for 5 min each with 0.075M phosphate buffer. Thereafter the cells were fixed in 0.25% aqueous osmium tetroxide for 30 min and rinsed three times in distilled water in a fume cupboard. The samples were dehydrated with increasing concentrations of ethanol (30%, 50%, 70%, 90%, 100%, 100%, 100%) and infiltrated with 30% quetol in ethanol for 1h. Thereafter the samples were infiltrated with 60% quetol for 30min and thereafter pure quetol for 4h. The samples were polymerized at 60°C for 36h or longer. Ultra-thin sections were prepared with a microtome and mounted on a copper grid. The samples were contrasted with 4% uranyl acetate for 10min and rinsed with water. Enhancement of contrast was obtained by placing samples in Reynolds' lead citrate for 2min and rinsing with water. Samples were viewed with a Multi-purpose Philips 301 TEM.

2.3.2.4 Scanning electron microscopy

Scanning electron microscopy (SEM) was used to determine surface features of the exposed and control cells. SEM is a technique capable of producing high resolution images of a sample surface. The sample to be viewed is coated by a thin layer of an electron dense substance (*e.g.* gold). Electrons are emitted from a tungsten cathode and are accelerated towards an anode. After emission, low energy (<50 eV) secondary

electrons originate within a few nanometers from the surface and are detected by a scintillator-photomultiplier device and the resulting signal is rendered into a two-dimensional intensity distribution that can be viewed and saved as a digital image [220].

a) Materials

Aqueous osmium tetroxide, glutaraldehyde, phosphate buffer and gold were purchased by the Electron Microscopy unit of the University of Pretoria from Merck Co. (Munich, Germany). The Cryo-SEM (JEOL 840 with Cryostage) Scanning electron microscope (SEM) of the Electron Microscopy unit of the University of Pretoria was used for viewing the prepared samples.

b) Methods

Exponentially growing MCF-7 and MCF-12A cells were seeded at 500 000 cells per well in 6-well plates on heat-sterilized coverslips. After 24h attachment the medium was discarded and the cells were exposed to 1.5mg/ml of *S. frutescens* extract, and incubated for 48h. Cells were fixed in 2.5% glutaraldehyde in 0.075M phosphate buffer (pH 7.4-7.6) for 1 h and rinsed 3 times for 5 min each with 0.075M phosphate buffer. Thereafter the cells were fixed in 0.25% aqueous osmium tetroxide for 30 min and rinsed three times in distilled water in a fume cupboard. The samples were dehydrated with increasing concentrations of ethanol (30%, 50%, 70%, 90%, 100%, 100%, 100%). Samples were dried utilizing critical point drying whereby the samples are mounted in a chamber and liquid Carbon dioxide (CO_2) was fed into the chamber until it was full. Ethanol was then expelled from the chamber by opening a valve and thereby releasing CO_2 dissolved ethanol. The valve was closed and the sample left in liquid CO_2 for an hour. The vessel was then warmed to 34°C so that the CO_2 becomes a gas. The pressure was released slowly and the sample remained in its natural shape and was completely dry. The dried coverslips were mounted on a stub and sprayed with a thin layer of gold. The samples were viewed with a Cryo-SEM (JEOL 840 with Cryostage).

2.3.3 Flow cytometry studies

2.3.3.1 Cell cycle analysis

Flow cytometry was employed to analyze the influence of *S. frutescens* extracts on cell cycle progression of MCF-7 and MCF-12A cells. Analysis was conducted by ethanol fixation and propidium iodide staining of cells. Propidium iodide was used to stain the nucleus in order to determine the amount of DNA present. The amount of DNA present correlates with the stages of the cell cycle during cell division. In flow cytometry a laser beam of a single frequency is directed onto a hydrodynamically focused stream of fluid. A number of detectors are aimed at the point where the stream passes through the light beam; one in line with the light beam (Forward Scatter or FSC) and several perpendicular to it Side Scatter (SSC) and one or more fluorescent detectors. Each suspended particle passing through the beam scatters the light and fluorescent chemicals in the particle may be excited into emitting light at a lower frequency than the light source. This combination of scattered and fluorescent light is detected by the detectors. By analyzing fluctuations in brightness at each detector (one for each fluorescent emission peak) it is possible to deduce the size, quantity and fluorescent intensity (DNA content when stained with propidium iodide) of cells. FSC correlates with the cell volume and SSC depends on the inner complexity of the particle *e.g.* amount of DNA, shape of nucleus, etc.

a) Materials

99.9% ethanol was from Merck Co. (Munich, Germany). Propidium Iodide was purchased from Sigma-Aldrich (St. Louis, United States of America).

b) Methods

Exponentially growing MCF-7 and MCF-12A cells were seeded at $1.5x10^6$ cells per $25cm^2$ flask. After 24h attachment the medium was discarded and the cells were exposed to 1.5mg/ml of *S. frutescens* extract and incubated for 48h. After 48h the cells were trypsinized and resuspended in 1ml growth medium. $1x10^6$ cells were centrifuged for 5min at 300xg in order to pellet them. The supernatant was discarded and the cells were resuspended in 200µl of ice cold PBS containing 0.1% FCS. 4ml of ice cold 70% ethanol was added in a drop wise manner and the cells were stored at 4°C for 24h. After 24h, the

cells were pelleted by centrifuging them at 300xg for 5min. The supernatant was removed and the cells were resuspended in 1ml of PBS containing propidium iodide (40µg/ml) and incubated at 37°C, 5% CO_2, for 45min.

Propidium iodide fluorescence (relative DNA content per cell) was measured with a fluorescence activated cell sorting (FACS) FC500 System flow cytometer (Beckman Coulter South Africa (Pty) Ltd) equipped with an air-cooled argon laser excited at 488nm. Data from at least 10 000 cells were analyzed with CXP software (Beckman Coulter South Africa (Pty) Ltd). Data from cell debris (particles smaller than apoptotic bodies) and clumps of 2 or more cells was removed from further analysis. Cell cycle distributions were calculated with WEASEL version 2.4 software (F. Battye, Walter and Eliza Hall Institute (WEHI), Melbourne, Australia) by assigning relative DNA content per cell to sub-G_1, G_1, S and G_2/M fractions. Propidium iodide molecules emit light at 617nm therefore, data obtained from the log forward scatter detector nr 3 (Fl3 log, detects 600nm emissions) was represented as histograms on the *x*-axis.

2.3.3.2 Apoptosis detection analysis

Flow cytometry was employed to analyze apoptosis in MCF-7 and MCF-12A cells. Cells were stained with Annexin V and propidium iodide. One of the earliest indications of apoptosis is the translocation of the membrane phospholipid phosphatidylserine (PS) from the inner to the outer leaflet of the plasma membrane. Once exposed to the extracellular environment, binding sites on PS become available for Annexin V, a 35-36 kDa, Ca^{2+}-dependent, phospholipid binding protein with a high affinity for PS. Annexin V is conjugated to a fluorochrome, fluorescein isothiocyanate (FITC) and used for identification by flow cytometry for stages of apoptosis. Propidium iodide is used to distinguish between necrotic and apoptotic cells.

a) Materials

Annexin V-FITC Kit was purchased from BIOCOM biotech Pty (Ltd) (Clubview, South Africa).

b) Methods

Exponentially growing MCF-7 and MCF-12A cells were seeded at $1.5x10^6$ cells per $25cm^2$ flask. After 24h attachment the medium was discarded and the cells were exposed to 1.5mg/ml of *S. frutescens* extract and incubated for 48h, before the cells were stained. After 48h cells were trypsinized and 10^6 cells were resuspended in 1mL of 1x Binding Buffer and centrifuged at 300×g for 10 minutes. The supernatant was removed and the cells resupended in 100µL of 1x Binding Buffer. 10µl of Annexin V-FITC was and incubated for 15 minutes in the dark at room temperature. After 15mins the cells were washed by adding 1ml of 1x Binding Buffer and centrifuged at 300×g for 10 minutes. The supernatant was carefully pipetted off and the cells were resuspended in 500µl of 1x Binding Buffer solution. Immediately prior to analysis 5µl of propidium iodide (100µg/ml) was added and gently mixed.

Propidium iodide fluorescence (oncotic cells) and annexin V fluorescence (apoptotic cells) was measured with a fluorescence activated cell sorting (FACS) FC500 System flow cytometer (Beckman Coulter South Africa (Pty) Ltd) equipped with an air-cooled argon laser excited at 488nm. Data from at least 30 000 cells were analyzed with CXP software (Beckman Coulter South Africa (Pty) Ltd). Data from cell debris (particles smaller than apoptotic bodies) and clumps of 2 or more cells was removed from further analysis. Propidium iodide molecules emit light at 617nm and FITC emit at 530nm therefore, data obtained from the log forward scatter detector nr 1 (Fl Lin, detects 515-545nm emissions) and the log forward scatter detector nr 3 (Fl3 Lin, detects 600nm emissions) was represented as a single dot-plot. FL3 log (propidium iodide) was represented on the *x*-axis and FL1 log (FITC) was represented on the *y*-axis. The FL3 log/FL1 log dot-plot was divided into for quadrants. The bottom-left quadrant was assigned to measure the viable cells with minimal propidium iodide and FITC staining. Medium only control MCF-7 cells were calibrated to include 98% of cells within the

viable cell quadrant. MCF-12A cells have a higher rate of apoptosis than MCF-7 cells therefore, the medium only control MCF-12A cells were calibrated to include 96% of cells within the viable cell quadrant. The top left quadrant was assigned to cells in the early stages of apoptosis, the bottom-right quadrant was assigned to cells undergoing oncosis and the top-right quadrant was assigned to cells in the late stages of apoptosis which have become necrotic. Distributions of cells within the quadrants were calculated with WEASEL version 2.4 software (F. Battye, Walter and Eliza Hall Institute (WEHI), Melbourne, Australia).

2.3.5 Gene expression analysis

2.3.5.1 Microarray and bioinformatics

Gene expression changes induced by *S. frutescens* were studied using microarray technology. Agilent's Human 1A Oligo Microarray (V2) slides were used to collect genomic information from *S. frutescens* and vehicle-treated MCF-7 and MCF-12A cells. These slides represent 20,173 60-mer oligonucleotide probes that span conserved exons and are designed to truly represent genes in the human genome across the transcripts of the targeted full length genes.

a) Materials

RNeasy Minelute Cleanup Kit, Qiazol lysis reagent and QIAquick PCR Purification Kit were provided by Southern Cross Biotechnology Pty (Ltd) (Cape Town, SA). Cyscribe Post-Labeling kit was supplied by Amersham Biosciences Pty (Ltd) (Pittsburgh, PA, USA). Agilent's Human 1A Oligo Microarray slides were provided by Agilent Technologies Pty (Ltd) (Palo Alto, CA, USA). Powerscript reverse transcriptase enzyme was supplied by BD Clontech Biosciences Pty (Ltd) (Cape Town, SA). The Nanodrop ND-1000 spectrophtotometer (Nanodrop Technologies, Wilmington, USA) utilized for spectrophotometrical quantification of ribonucleic acid (RNA) and deoxyribonucleic acid (DNA), and the Axon Genepix 400B scanner (Molecular Devices, Sunnyvale, USA) utilized for microarray slide scanning were kindly provided for use by ACGT Microarray Facility of the University of Pretoria (Pretoria, South Africa).

b) Methods

I) RNA extraction

Total RNA was extracted from MCF-7 and MCF-12A cells. In order to obtain high quality pure RNA, a combined protocol utilizing Qiagen's Qiazol reagent and RNeasy plant Mini kit was used.

Exponentially growing MCF-7 and MCF-12A cells were seeded at $1.5x10^6$ cells per $25cm^2$ flask. After 24h attachment the medium was discarded and the cells were exposed to 1.5mg/ml of *S. frutescens* extract, and incubated for 48h, After 48h the cells were washed twice with PBS and lysed by adding 1ml RLT buffer (RNeasy Mini Kit) to each flask and the flask was decanted until all the cells were lysed. The lysate was pipetted into Qiashredder columns and centrifuged for 2min at 9000xg. 1ml Qiazol reagent was added to the flow-through. After being left for 5min at room temperature, 0.3ml chloroform was added; the sample was shaken vigorously and left at room temperature for 10min. After 10min the sample was centrifuged for 15min at 4°C at 12000xg. The upper aqueous phase was removed and 1 volume 70% ethanol was added and gently mixed. This solution was divided into Qiagen Plant Mini Kit columns (700µl per column) and centrifuged for 15s at 9000xg. The flow-through was discarded. 350µl RW1 buffer was added to each column in order to wash the column. The column was centrifuged for 15s at 9000xg. A DNase mixture was prepared utilizing Qiagen's RNase-free DNase Set, by adding 70µl RDD buffer to every 10µl DNase1. 80µl of this mixture was added in the middle of each column and left at room temperature for 15min. Another 350µl RW1 buffer was added and the column was centrifuged for 15 at 9000xg. Flow-through was discarded and columns transferred to new eppendorf tubes. A series of washing steps followed. 500µl RPE buffer was added to each tube and centrifuged for 15s at 12000xg, discarding the flow-through afterwards and replacing the eppendorf tubes. This step was repeated. The column was the then centrifuged at 9000xg for 1min. To elute the total RNA from the column 50µl RNase-free water was added to the column and centrifuged for 1min at 9000xg. The total RNA was suspended in 50µl RNase-free water and was

ready to be quantified with the Nanodrop and tested for integrity by means of electrophoresis.

II) RNA integrity

0.6g agarose powder was dissolved in 40ml RNase free water (1.5% gel). 6ml 10x 3-(N-morpholino)propanesulfonic acid (MOPS), 3.4ml formaldehyde and 14ml RNase free water was added. A sample mix to be loaded in the well was prepared by adding 3µg total RNA (±8µl), 2µl tracking dye (50% glycerol, 100mM Na_2EDTA, pH 8.0, 1% SDS, 0.1% bromophenol blue 0.1%) and 1µl ethidium bromide (0.5 µg/ml final concentration). The mix was heated for 15min at 55°C and rapidly chilled on ice afterwards. 15µl of each sample was pipetted into a well of the agarose-formaldehyde RNA gel and electrophoresis was conducted at 80mV for 45min.

III) Amino-allyl labeled cDNA synthesis

Total RNA extracted from MCF-7 and MCF-12A cells was used to synthesize cDNA. Oligo(dT) primers hybridizes to the polyadenylated tail of messenger RNA (mRNA), thereby allowing only mRNA to be transcribed into cDNA. Amino-allyl labeled dUTP was used to label the cDNA and allow for the incorporation of fluorescent dyes.

Synthesis of cDNA was done in two steps, primer annealing and an extension reaction. For primer annealing 10µg total RNA suspended in 13µl of RNase free water was mixed with 6µl (0.5 µg/µl) anchored oligo(dT) and 1µl (20U/µl) RNase inhibitor for a total volume of 20µl. This was gently mixed by pipetting up and down. This reaction was incubated at 70°C for 5min and susequently cooled at room temperature for 10min to allow primers and mRNA template to anneal and then centrifuged for 15s.

For the extension reaction the following components were added in this order, 8µl 5x powerscript buffer, 4µl 0.1M DTT, 2µl nucleotide mix (10mM dATP, dCTP, dGTP, 4mM dTTP), 2µl aa-dUTP (6mM aa-dUTP) and 2µl (200U/µl) powerscript reverse transcriptase enzyme. The reaction was mixed by gently pipetting up and down and incubated overnight at 42°C.

After the extension reaction the RNA was degraded by adding 2µl 2.5M NaOH to the reaction and mixed by vortexing and incubated for 15min at 37°C. 10µl 2M 4-(2-hydroxyethyl)-1-piperazineethanesulfonic acid (HEPES) buffer was added to neutralize the NaOH.

The cDNA was purified utilizing the Qiagen's PCR Clean-up Kit. 5 volumes PB Buffer was added to 1 volume of the prepared cDNA, and placed in a QIAquick spin column and centrifuged for 60s at 11000g. 750µl PE buffer was added and centrifuged for 60s. Flow-through was discarded and the column was centrifuged again for 60s to remove residual ethanol. The columns were placed into new eppendorf tubes and 30µl Elution Buffer (EB) was used to elute the purified cDNA. After adding the 30µl EB the reaction was left to stand for 1min. The column was centrifuged for 1min at 11000g. This step was repeated so that the cDNA was suspended in 60µl EB buffer. The cDNA was quantified spectrophotometrically with the Nanodrop. Sufficient quality and quantity amino-allyl cDNA was obtained and proceeded to couple the cDNA with CyDye.

IV) cDNA post-labeling coupling reaction

During the post-labeling coupling reaction the Cy-3 (green) and Cy-5 (red) fluorescent dyes were coupled to the amino-allyl molecules of the cDNA. The cDNA was dried in a vacuum and resuspended in 100µl 0.1M Sodium bicarbonate (pH=9). The cDNA was divided into two parts, of equal volume. One part was added to the Cy-3 dye and the other part was added to the Cy-5 dye and gently mixed. The reaction was incubated for 90min at room temperature without any light exposure. 15µl 4M hydroxyl amine was added to each reaction.

The Cy-dye labeled cDNA was purified with Qiagen's PCR Clean-up Kit as described above and quantified with the Nanodrop to determine the incorporation of the fluorescent dye onto the cDNA.

V) Hybridization of Cy-dye labeled cDNA

Hybridization of Cy-dye labeled cDNA was conducted with a sufficient amount of Cy-dye incorporated cDNA.

A hybridization mixture was prepared by adding equal amounts of Cy-3 and Cy-5 labeled cDNA to a final volume of 28µl. 7µl 10x control targets was added together with 35µl 2x hybridization buffer. A final volume of 70µl was obtained. This mixture was pipetted onto Agilent's 22k 60-mer human oligo slide with a cover slip on. The mixture propagated over the whole slide as a result of capillary action of the liquid and cover-slip. The slides were sealed in an incubation chamber and incubated for 16h at 42°C. Afterwards the slides were washed twice in Falcon tubes containing 6X saline sodium citrate (SSC), 0.005% Triton X-100 and washed once for 10min in a Falcon tube containing 0.1X SSC, 0.005% Triton X-100.

VI) Scanning of Agilent microarray slides

Slides were scanned with the Axon Genepix 4000B Scanner (Molecular Devices, USA) provided by the African Centre of Gene Technology (ACGT) Microarray Facility at the University of Pretoria.

VII) Spotfinding

Spotfinding was performed using Genepix Pro 6.1 (Molecular Devices Corporation, Sunnyvale, CA, USA). GenePix Pro 6.1 uses a set of proprietary feature-finding algorithms to find circular features. Every pixel in a region around the feature is examined by a local alignment algorithm and assigned to feature or background. Global alignment algorithms determine the translation, rotation and skew of blocks of features. Saturated spots, spots with an uneven background, non-uniform spots and spots with a low intensity vs back ground ratio were removed from further analysis by excluding the spots that satisfied the following parameters. The excluded spots were assigned as "Bad".

Saturated spots:

[F532 % Sat.] > 30 And

[Ratio of Means (635/532)] > 0.75 Or

[F635 % Sat.] > 30 And

[Ratio of Means (635/532)] < 1.3333

Spots with an uneven background:

([B635 Mean] > (1.5*[B635 Median]) Or

[B532 Mean] > (1.5*[B532 Median])) And

([B635 Median] > 40 Or

[B532 Median] > 40)

Non-uniform spots:

[Ratio of Medians (635/532)] > (4.0*[Rgn Ratio (635/532)]) Or

[Ratio of Medians (635/532)] < (0.25*[Rgn Ratio (635/532)])

Low intensity vs back ground ratio:

[% > B635+2SD] < 10 Or [% > B532+2SD] < 10

VIII) Limma statistical analysis

Statistical analysis after spotfinding was conducted using Limma with the LimmaGUI interface [221]. Background correction was done with the normal+exponential (Normexp) convolution model to observed intensities. The normal part represents the background and the exponential represents the signal intensities [221]. The Normexp offset value was set to 25. A value of 25 maximized the df.prior. df.prior is the numeric vector giving empirical Bayes estimated degrees of freedom associated with s2.prior for each gene. s2.post is the numeric vector giving posterior residual variances. A maximized df.prior is optimal and will allow for greater power to detect differentially expressed genes [221]. Spot quality weighting was performed and Genepix Flag weightings that were flagged as "Bad" were excluded from further analysis. Normalization within arrays was performed to remove dye-bias at higher and lower intensities by normalizing M-values (log-ratios) with the Global Loess method [222]. The M-value (M) represents a log2-fold change between two or more experimental conditions. The A-value (A) is the average log2-expression level for a gene across all the arrays and channels in the experiment.

The M-value is calculated as follows:

M = log2(Cy5)/Cy3) (Cy5/Cy3 are the normalized emission intensities of the spot)

The A-value is calculated as follows:

A = (log2(Cy5)*Cy3))/2

Aquantile normalization between arrays was performed in order to normalize expression intensities so that the intensities or log-ratios have similar distributions across a series of arrays [222]. Aquantile normalization ensures that the A-values (average intensities) have the same empirical distribution across arrays leaving the M-values (log-ratios) unchanged [222]. The Least squares linear model fit method was employed and the *P*-values were adjusted for multiple testing utilizing the Benjamini and Hochberg's step-up method for controlling the false discovery rate [223]. Genes that had a *B*-value of greater than zero were considered statistically significantly differentially expressed and were included in further analyses. The B-statistic is the log-odds that that gene is differentially expressed. A B-statistic of zero corresponds to a 50/50 chance that the gene is differentially expressed [222].

IX) Gene expression analysis

Biologic interpretation and functional analysis of gene lists were performed by mapping differentially expressed genes to biochemical pathways and Gene Ontology (GO) categories using Gene Annotation Co-occurrence Discovery (GENECODIS) [224]. GENECODIS is a web-based tool for finding sets of biological annotations that frequently appear together and are significant in a set of genes [224]. In order to determine common genes that were affected by the *S. frutescens* extracts between cell lines, differentially expressed gene lists were compared utilizing GeneVenn [225]. GeneVenn is a simple, web-based application creating Venn diagrams from two or three gene lists.

2.3.6 Enzyme activity

2.3.6.1 Enzyme-Linked ImmunoSorbent Assay (ELISA)

Gene expression profiles obtained from microarray data indicate relative mRNA levels of genes associated at the time of termination. Differentially expressed genes are then categorized according to their biological function and provide valuable information of gene expression under various conditions. However, gene expression does not necessarily correlate with protein translation or activity. An ELISA to detect mTOR kinase activity was chosen based on the results obtained from the growth studies, morphological hallmarks, cell death analysis, cell cycle analysis, microarray and bioinformatical analysis. Quantitative data from the ELISA will show the differences in the magnitude and of protein activation of mTOR.

a) Materials

The K-LISA mTOR Activity Kit, Protease cocktail inhibitor set III, Phopsphatase inhibitor cocktail set IV, Protein G agarose suspension, anti-mTOR/FAP (Ab-2) Mouse monoclonal antibody, sodium chloride and Tween®-20 detergent were purchased from Merck Chemical (Pty) Ltd. Hydroxymethylaminomethane hydrochloride (Tris HCl), β-glycerophosphate, glycerol and ethylenediamine tetraacetic acid (EDTA) were purchased from Sigma-Aldrich (St. Louis, United States of America).

b) Methods

I) Immunoprecipitation of mTOR

mTOR was immunoprecipitated from the cell lysate with the anti-mTOR/FAP (Ab-2) mouse monoclonal antibody. The anti-mTOR/FAP (Ab-2) mouse monoclonal antibody efficiently immunoprecipitates mTOR from crude biological samples without affecting the catalytic activity of the mTOR kinase.

Exponentially growing MCF-7 and MCF-12A cells were seeded at $1.5x10^6$ cells per $25cm^2$ flask. After 24h attachment the medium was discarded and the cells were exposed

to 1.5mg/ml of *S. frutescens* extract, and incubated for 48h. After 48h, the cells were washed twice with TBS. Cells were lysed by adding 1.0ml lysis buffer to 10^7 cells, scraping the cells loose with a cell scraper and forcing the lysate through a 22-gauge needle. The lysis buffer consisted of 50 mM Tris-HCl, (pH adjusted to 7.4 with 2N NaOH), 100mM NaCl, 50mM β-glycerophosphate, 10% glycerol (w/v), 1% Tween®-20 detergent (w/v), 1 mM EDTA, 25 mM NaF, a protease inhibitor cocktail consisting of 1mM AEBSF hydrochloride, 2.0µg/ml aprotinin, 10µM bestatin, 10µM E-64 protease inhibitor, 100µM leupeptin, 10µM pepstatin A, and a phosphatase inhibitor cocktail consisting of 25µM (-)-*p*-Bromotetramisole oxalate, 5µM Cantharidin and 10nM calyculin A.

Insoluble material was precipitated by centrifuging the lysate at 18 500xg for 11min. The supernatant was transferred to a clean tube and 0.5ml cell lysate was pre-cleared by adding 15µl Protein G-Plus agarose beads and incubated for 15min at 4°C. The pre-cleared lysate was centrifuged at 4000 rpm for 5min at 4°C to pellet the agarose beads and the supernatant was transferred to a fresh tube. 5µl (1µg/ml) of the anti-mTOR/FAP (Ab-2) mouse monoclonal antibody was added to the pre-cleared lysate and rotated for 1h at 4°C. After 1h rotation, 50µl Protein G-Plus agarose was added to capture the mTOR-bound anti-mTOR/FAP (Ab-2) mouse monoclonal antibody and rotated for 90min at 4°C. The agarose beads were carefully washed 3 times by centrifuging at 4000 rpm for 5min at 4°C and adding 0.5ml lysis buffer. After washing with lysis buffer, the beads were rinsed once with 1x Kinase assay buffer.

II) mTOR phosphorylation of p70S6K-GST fusion protein at Thr389

Active mTOR kinase activates p70S6-kinase at by phosphorylating p70S6K at Thr389 in the presence of ATP. Immunoprecipitated mTOR was suspended in 100µl containing 2.5µg/ml recombinant p70S6K-GST fusion protein, 0.2mM ATP, 2mM DTT, 1x Kinase assay buffer and TBS, and was incubated for 30 min at 30°C. 10µl kinase stop solution was added to each tube and mixed briefly by gently tapping the tube. The solution was centrifuged at 4000 rpm for 5 min at 4°C and the supernatant was transferred to a fresh tube. The supernatant contained the phosphorylated p70S6K-GST fusion protein.

III) Detection of Thr389-phosphorylated p70S6K-GST fusion protein

The phosphorylated p70S6K-GST fusion protein was detected with Anti-p70S6K-T389 antibody, followed by detection with horse-radish peroxidase (HRP)-Antibody Conjugate and the 3.3',5,5'-tetramethylbenzidine (TMB) substrate. 50µl supernatant containing the phosphorylated p70S6K-GST fusion protein was added to each well of a Glutathione-coated 96-well plate and incubated for 60min at 30°C. The wells were washed 3 times with 200µl TBS with 0.2% Tween®-20 detergent (v/v) (plate wash), and 100µl Anti-p70S6K-T389 (1µg/ml) was added to each well. The plate was covered with the plate sealer and incubated for 1h at room temperature. After 1h incubation, the wells were washed 3 times with 200µl plate wash and 100µl HRP Antibody-Conjugate was added and incubated for 1h at room temperature. After 1h incubation, the wells were washed 3 times with 200µl plate wash and 100µl TMB substrate was added and incubated for 20min at room temperature. 100µl ELISA Stop solution was simultaneously added to each well and the absorbance was read at 450nm, with a reference wavelength of 570nm.

2.4 Statistical analysis of data

2.4.1 Cell growth, metabolic activity, ELISA, mitotic indices and flow cytometry

Statistical analysis of the data was done as prescribed by Dr. Steve Olorunju of the Unit for Biostatistics at the Medical Research Council. Data was obtained from 3 independent experiments with an n-value of 6 for each repeat for crystal violet and MTT studies and an n-value of 3 for each repeat for the ELISA experiment. Data for mitotic indices was obtained by counting 1000 cells on each slide of the biological replicates. Obtained data was statistically analyzed for significance using the analysis of variance-single factor model followed by a two-tailed Student's *t*-test. Means are presented in bar charts, with T-bars referring to standard deviations. *p*-values, 0.05 were regarded as statistically significant and indicated by an * or number as indicated in the legends.

2.4.2 Microarray and bioinformatics

Microarray analysis was conducted in conjunction with Prof. Fourie Joubert of the Bioinformatics and Computational Biology Unit of UP. Prof. Fourie Joubert assisted with basic data analysis, statistical analysis and gene identification as described in chapter 2.3.5.1 VI-IX.

Chapter 3

Results

3.1 Cell growth studies

3.1.1 DNA staining – crystal violet

Quantification of fixated monolayer cells were spectrophotometrically determined employing crystal violet as a DNA stain. Cell numbers were expressed as a percentage of the ethanolic control in order to determine the antiproliferative effect of *S. frutescens* extracts on tumorigenic MCF-7 and non-tumorigenic MCF-12A cells. 5000 cells were seeded per well in 96-well plates and exposed to five different concentrations of *S. frutescens*, ranging from 1.0mg/ml to 2.0mg/ml. The concentration range is similar to studies conducted by Tai *et al.* (2004) and Stander *et al.* (2007) [32,38]. Staining cell nuclei of fixed cells with crystal violet allows for rapid, accurate and reproducible quantification of cell number in cultures grown in 96-well plates [211,212]. Absorbance of the dye measured spectrophotometrically at 570nm will correspond to cell numbers. According to Berry *et al.* (1996) crystal violet staining of samples containing an abnormally high proportion (>30%) of stationary binucleated cells will yield higher cell concentrations than trypan blue or Coulter counter methods [213]. MCF-7 and MCF-12A cells contain less than 1% stationery binucleated cells [214,215] and will therefore not lead to anomalous results.

The growth inhibitory effect was calculated as described by the the National Cancer Institute in order to compare the growth inhibition induced by *S. frutescens* between the two cell lines [226]. The growth inhibitory effect was calculated by:

Growth inhibitory effect = 100 x $(T - T_0)/(C - T_0)$

T is the optical density of the test well after background subtraction after 48h exposure to test conditions.

$\mathbf{T_0}$ is the optical density after background subtraction at time zero.

C is the control optical density after background subtraction of the vehicle treated-control.

The 50% growth inhibitory concentration (GI_{50}) is the concentration where:

$$\mathbf{100 \times (T - T_0)/(C - T_0) = 50}$$

The total growth inhibitory (TGI) concentration is the concentration where:

$$\mathbf{100 \times (T - T_0)/(C - T_0) = 0}$$

The 50% lethal concentration (LC_{50}) is the concentration where:

$$\mathbf{100 \times (T - T_0)/T_0) = -50}$$

S. frutescens reduced cell proliferation in both the non-tumorigenic MCF-12A and the tumorigenic MCF-7 cell line in a dose-dependent manner (Figure 3.1). A statistical significant difference (Student's t-test: p-value < 0.05) in growth inhibition was observed between the non-tumorigenic and tumorigenic cells at all the concentrations (1.0, 1.25, 1.5, 1.75, 2.0mg/ml) (Figure 3.1). *S. frutescens* extracts reduced cell proliferation at all tested concentrations in the MCF-7 cell line. *S. frutescens* extracts reduced proliferation to 47% at 1.0mg/ml, 35% at 1.25mg/ml, 24% at 1.5mg/ml, 17% at 1.75mg/ml and 14% at 2.0mg/ml when compared to the vehicle-treated control in the MCF-7 cell line. Stander *et al.* (2007) reported that *S. frutescens* extracts inhibited growth to 50% of the vehicle control at a 1.5mg/ml concentration after 24h and 26% after 48h [38]. An increase in the number of cells in telophase after 24h treatment with 1.05% ethanol was also noted [38]. The final concentration of ethanol for *S. frutescens*-treated and vehicle-treated cells in the latter study was however 1.05%, compared to the 0.35% ethanol being employed in the current study. A lower ethanol concentration was used in the current study, because ethanol stimulates cell growth through the activation of the mitogen-activated protein kinase signaling pathway at higher concentrations [227].

In the MCF-12A cells, *S. frutescens* extracts did not reduce proliferation at the 1.0mg/ml concentration. *S. frutescens* extracts reduced proliferation to 89% at 1.25mg/ml, 62% at 1.5mg/ml, 39% at 1.75mg/ml, and 25% at 2.0mg/ml when compared to the vehicle-treated control in the MCF-12A cell line. The GI_{50} concentration for the MCF-7 cell line was determined to be less than 1.0mg/ml and determined as 1.5mg/ml for the

MCF-12A cell line (Figure 3.2). The TGI concentration for the MCF-7 cell line was determined as 1.5mg/ml and 2.0mg/ml for the MCF-12A cell line (Figure 3.2). The LC_{50} concentration for both cell lines was calculated to be above 2.0mg/ml (Figure 3.3).

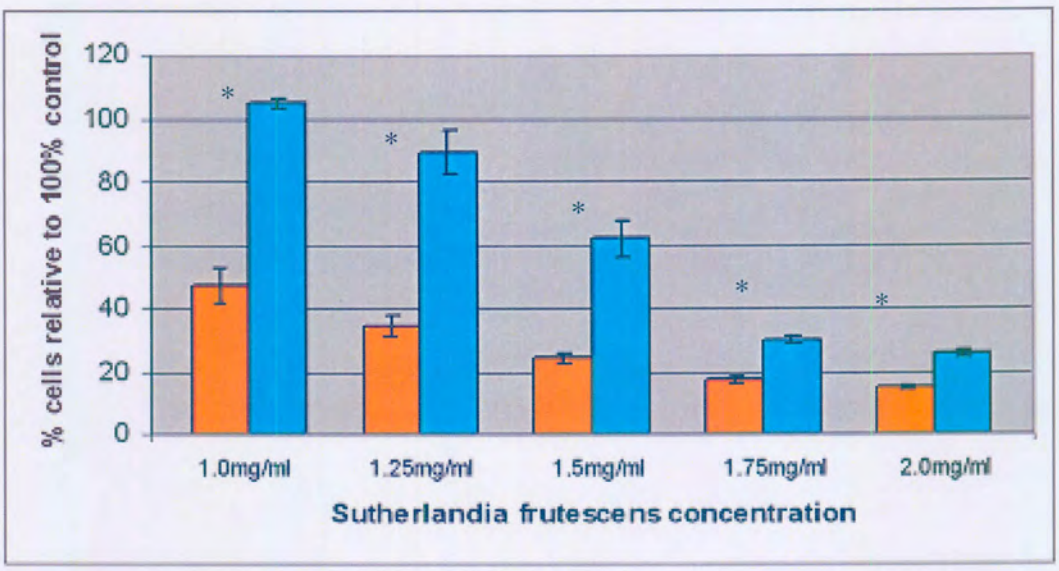

Figure 3.1: MCF-7 (orange) and MCF-12A (blue) cell numbers expressed as a percentage of cells relative to 100% control after exposure to different concentrations of *S. frutescens* (1.0, 1.25, 1.5, 1.75, 2.0mg/ml) for 48h. * Indicates a p-value < 0.05 for growth inhibition between cell lines.

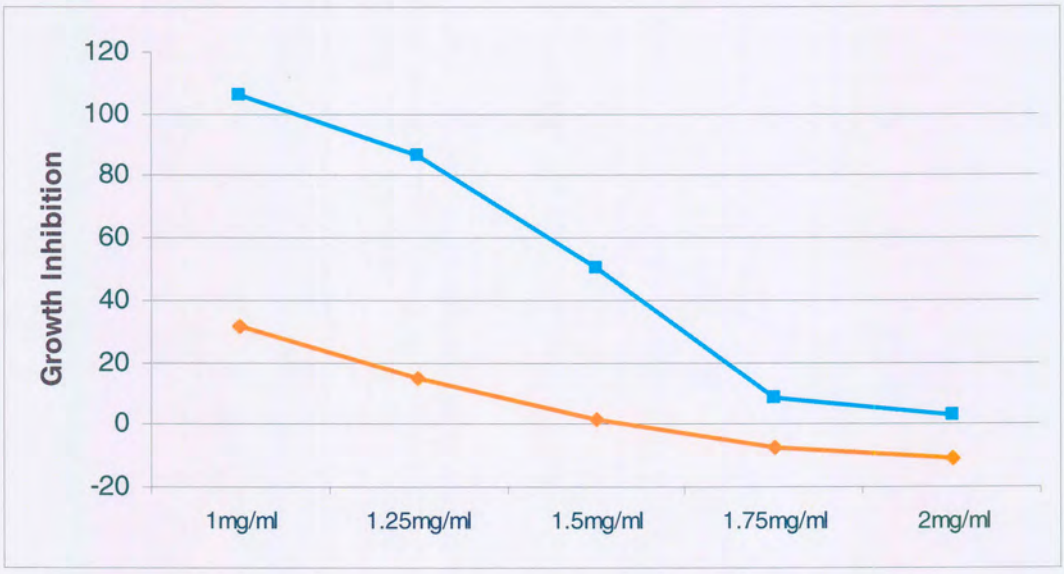

Figure 3.2: Growth inhibitory effect of *S. frutescens* on MCF-7 (blue) and MCF-12A (orange) cells. Growth inhibition = 100 x $(T-T_0)/(C-T_0)$.

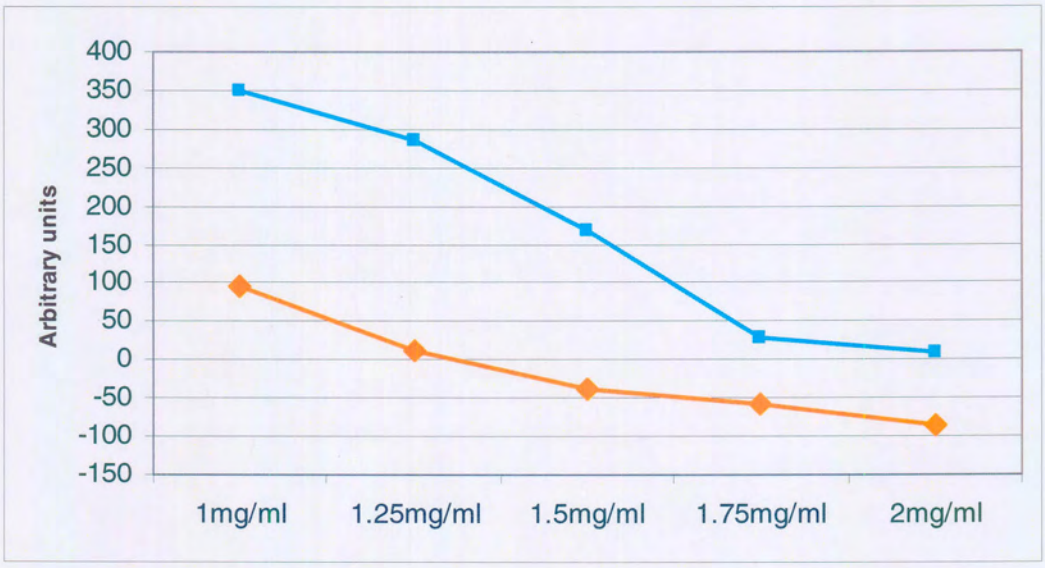

Figure 3.3: Cytotoxic effect of *S. frutescens* on MCF-7 (blue) and MC-12A (orange) cells. LC_{50} = 100 x $(T-T_0)/(T_0)$ = -50

3.1.2 Metabolic activity - MTT assay

3-(4,5-Dimethylthiazol-2-yl)-2,5-diphenyltetrazolium bromide (MTT) was used to determine the ability of MCF-7 and MCF-12A cells to reduce MTT to purple formazan crystals as measurement of metabolic activity after 48h of exposure to *S. frutescens* extracts. The reduced nicotinamide adenine dinucleotide (NADH) is responsible for most MTT reduction and MTT reduction is associated not only with mitochondria, but also with the cytoplasm and with non-mitochondrial membranes including the endosome/lysosome compartment and the plasma membrane [228,229]. The ability of MCF-7 and MCF-12A cells to reduce MTT to purple formazan crystals was expressed as a percentage of the ethanolic control in order to determine the effect that *S. frutescens* extracts have on metabolic activity in tumorigenic MCF-7 and non-tumorigenic MCF-12A cells. 5000 cells were seeded per well in 96-well plates and exposed to five different concentrations of *S. frutescens* ranging from 1.0mg/ml to 2.0mg/ml.

Metabolic activity was reduced in both cell lines in a dose-dependent manner (Figure 3.4). A statistical significant difference (Students *t*-test: p-value < 0.05) in metabolic activity was observed between the non-tumorigenic and tumorigenic cells at all the concentrations (1.0, 1.25, 1.5, 1.75, 2.0mg/ml) (Figure 3.4). *S. frutescens* extracts reduced metabolic activity at all tested concentrations in the MCF-7 cell line. Metabolic activity relative to the vehicle-treated control was reduced to 27% at 1.0mg/ml, 24% at 1.25mg/ml, 20% at 1.5mg/ml, 19% at 1.75mg/ml and 16% at 2.0mg/ml in the MCF-7 cell line. In the MCF-12A cells, metabolic activity was reduced to 84% at 1.0mg/ml concentration, 81% at 1.25mg/ml, 72% at 1.5mg/ml, 46% at 1.75mg/ml and 37% at 2.0mg/ml in *S. frutescens*-treated cells when compared to the vehicle-treated cells (Figure 3.4).

The GI_{50}, TGI and LC_{50} concentrations for metabolic activity were determined as described in 3.1.1. The GI_{50} metabolic activity concentration for the MCF-7 cell line was calculated as <1.0mg/ml and between 1.5mg/ml and 1.75mg/ml for the MCF-12A cell line (Figure 3.5). The TGI metabolic activity concentration for the MCF-7 cell line was determined to be between 1.25mg/ml and 1.5mg/ml, and larger than 2.0mg/ml for the

MCF-12A cell line (Figure 3.6). The LC_{50} metabolic activity concentration for both cell lines was determined to be above 2.0mg/ml (Figure 3.6).

A comparison between the inhibitory effect on growth and metabolic activity is demonstrated in Figure 3.7. *S. frutescens* extracts had a more pronounced negative effect on metabolic activity than on growth in MCF-7 and MCF-12A cells at *S. frutescens* extract concentrations lower than 1.5mg/ml.

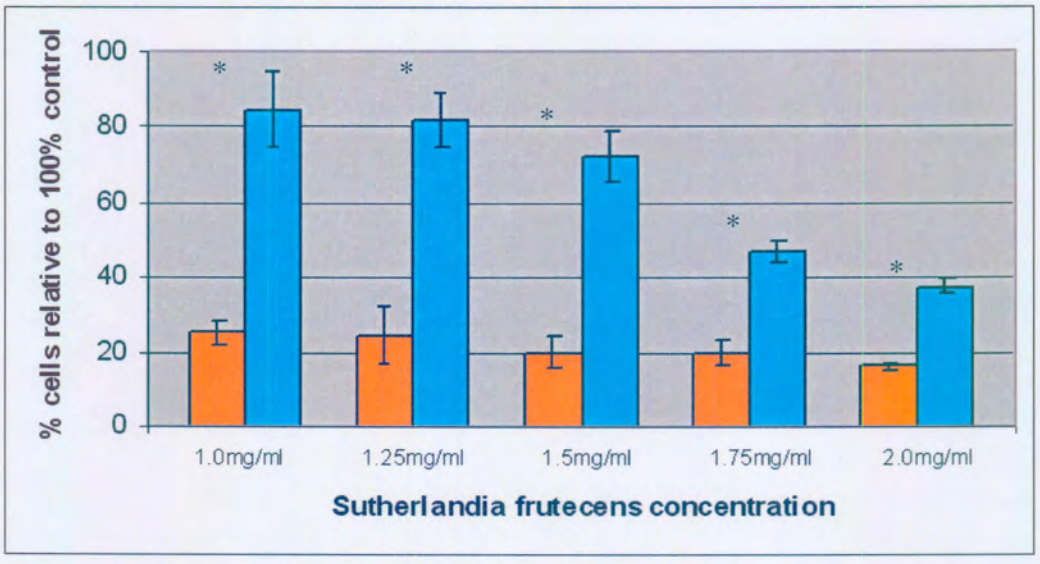

Figure 3.4: MCF-7 (blue) and MCF-12A (orange) metabolic activity expressed as a percentage of cells relative to 100% vehicle-control after exposure to different concentrations of *S. frutescens* (1.0, 1.25, 1.5, 1.75, 2.0mg/ml) for 48h. * Indicates a p-value < 0.05 for growth inhibition between cell lines.

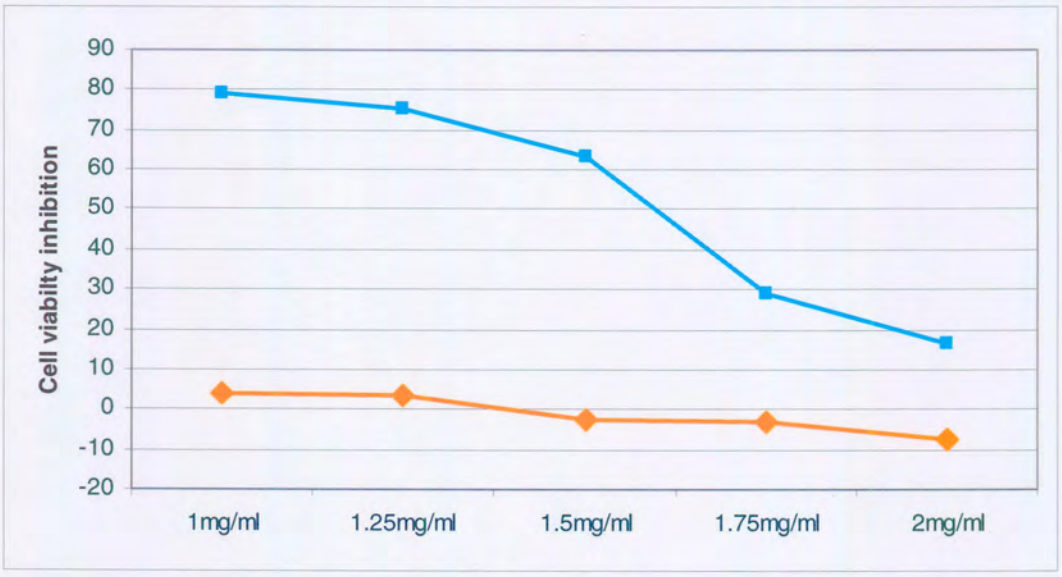

Figure 3.5: Effect of *S. frutescens* extracts on metabolic activity on MCF-7 (blue) and MCF-12A (orange) cells. Metabolic activity inhibition = 100 x $(T\text{-}T_0)/(C\text{-}T_0)$.

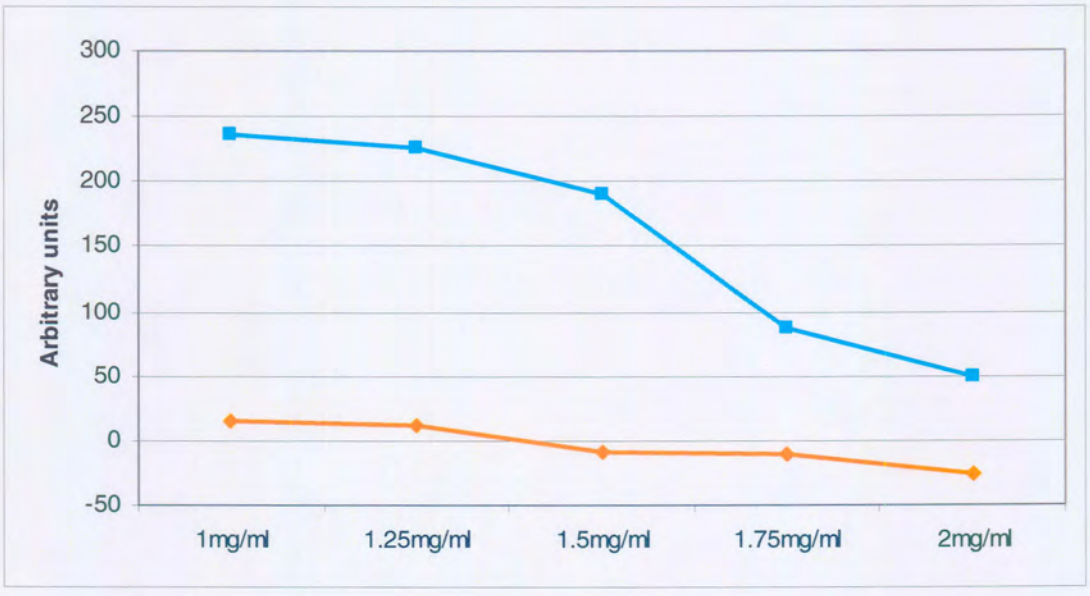

Figure 3.6: Cytotoxic effect of *S. frutescens* on metabolic activity of MCF-7 (blue) and MCF-12A (orange) cells. $LC_{50} = 100 \times (T\text{-}T_0)/(T_0) = -50$.

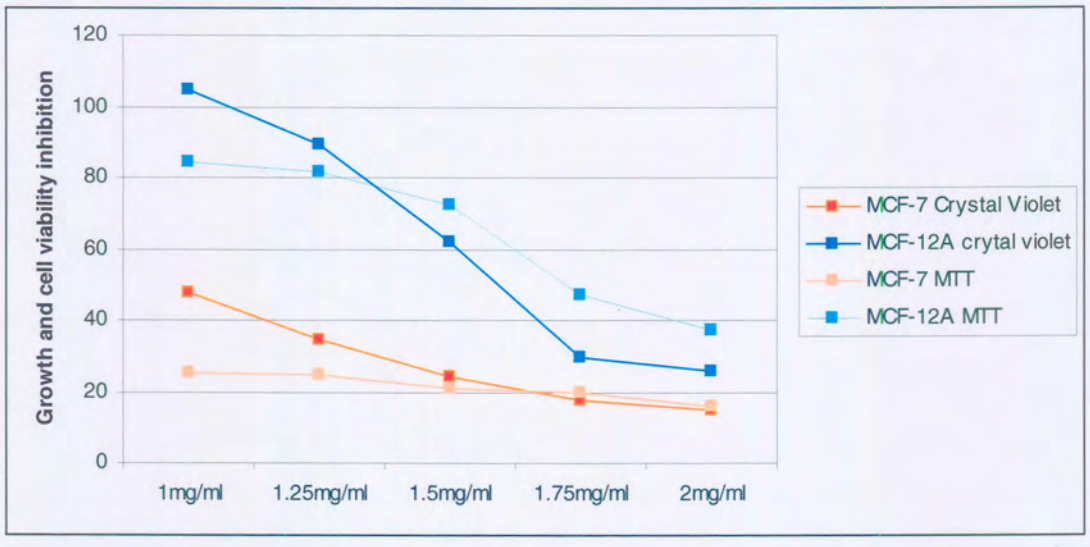

Figure 3.7: Comparison of the *S. frutescens* extracts inhibitory effect on growth (dark colour) and metacolic activity (light colour) between MCF-7 (orange) and MCF-12A (blue). Inhibition (CV and MTT) $= 100 \times (T\text{-}T_0)/(C\text{-}T_0)$.

3.2 Morphology studies

3.2.1 Light microscopy – haematoxylin and eosin cell staining

The effects that *S. frutescens* extracts have on cell morphology in both cell lines were investigated by H&E staining. The 1.5mg/ml exposure concentration was used in all subsequent studies for both cell lines in order to determine the differential effects of *S. frutescens* extracts. The concentration is consistent with the concentration used by Stander *et al.* (2007) whereby it was demonstrated that ethanolic *S. frutescens* plant extracts inhibited MCF-7 cell growth to 50% at 1.5mg/ml after 24h and 26% after 48h [38]. Tai *et al.* (2004) demonstrated that the 50% inhibitory concentration (IC_{50}) of ethanolic extracts of *S. frutescens* tablets occurred at a 1/250 (0.55mg/ml) dilution, however variation between plant samples is to be expected [32]. 1.5mg/ml was the TGI concentration in the MCF-7 cells and the GI_{50} concentration in the MCF-12A cells (Chapter 3.1.1). Mitotic indices were calculated from the H&E stained slides by counting 1000 cells on each slide (3 repeats) and the mitotic indices were expressed as percentage of cells in mitosis. Cells were categorized into mitotic (prophase, metaphase, anaphase, telophase, tripolar metaphase) and non-mitotic cells (interphase and hypercondensed chromatin).

A decrease in cell density was observed after 48h exposure to 1.5mg/ml *S. frutescens* extract in both cell lines and the decrease in cell density was more pronounced in the MCF-7 cells (Figures 3.8 and 3.9). Increased cytoplasmic shrinking, hypercondensed chromatin and vacuolarization were observed in both cells lines after 48h exposure to 1.5mg/ml *S. frutescens* extract (Figures 3.10 and 3.11). An increase in the number of cells in prophase and a decrease in number of cells in metaphase, anaphase and telophase were observed in both cell lines (Tables 3.1 and 3.2).

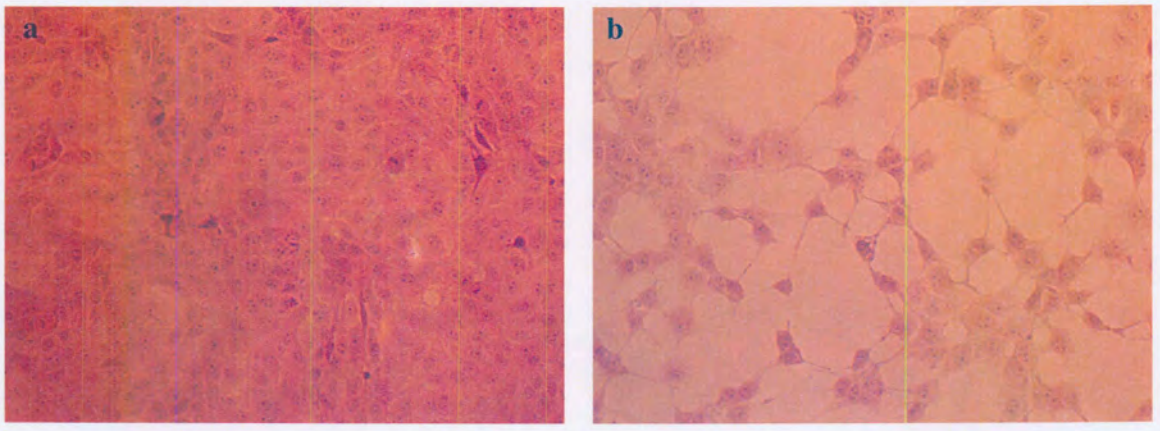

Figure 3.8: Haematoxylin and eosin staining of MCF-7 control cells exposed to 0.3% ethanol (vehicle) (a) and MCF-7 cells exposed to 1.5mg/ml *S. frutescens* (b) for 48h at 100x magnification. A decreased cell density is observed in treated cells compared to the vehicle-treated control. Cells in various stages of mitosis are observed in vehicle-treated controls.

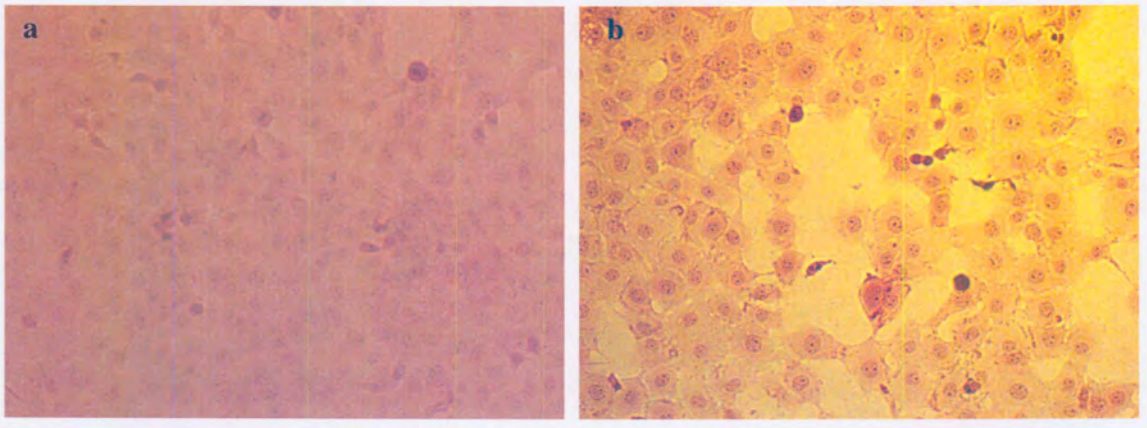

Figure 3.9: Haematoxylin and eosin staining of MCF-12A control cells exposed to 0.3% ethanol (vehicle) (a) and MCF-12A cells exposed to 1.5mg/ml *S. frutescens* (b) for 48h at 100x magnification. A decreased cell density is observed in treated cells compared to the vehicle treated control and is less pronounced when compared to MCF-7 *S. frutescens*-treated cells. Cells in various stages of mitosis are observed in vehicle-treated controls.

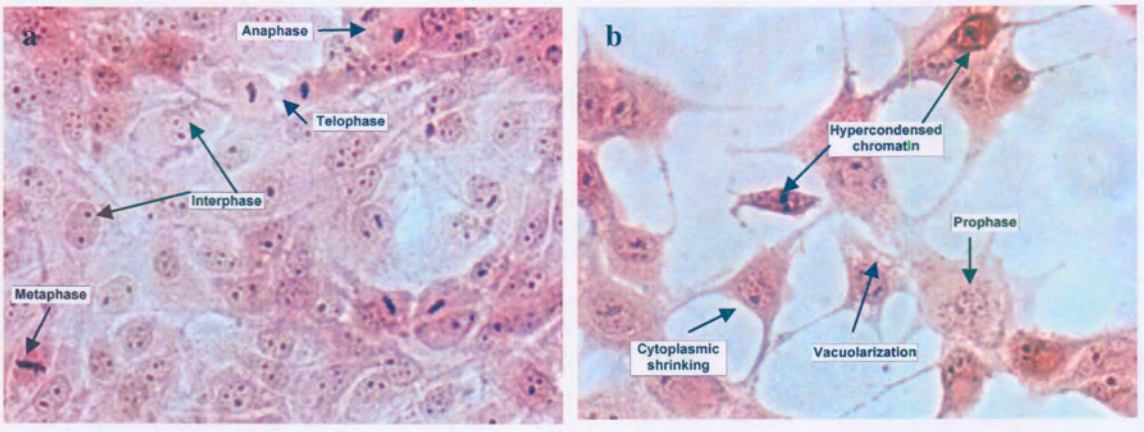

Figure 3.10: Haematoxylin and eosin staining of MCF-7 control cells exposed to 0.3% ethanol (vehicle) (a) and MCF-7 cells exposed to 1.5mg/ml *S. frutescens* (b) for 48h at 400x magnification. Cells in various stages of mitosis are observed in vehicle-treated controls. Cytoplasmic shrinking, the formations of hypercondensed chromatin increased vacuolarization are observed in *S. frutescens*-treated cells.

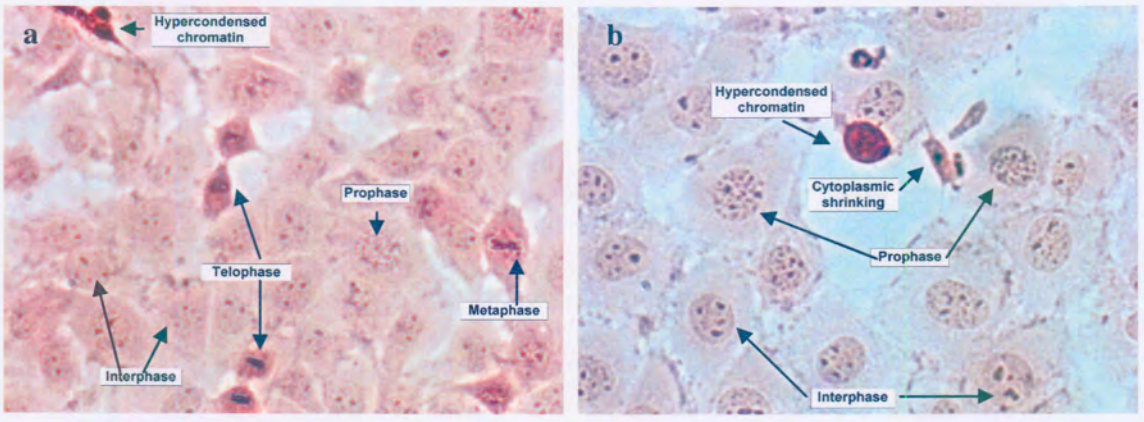

Figure 3.11: Haematoxylin and eosin staining of MCF-12A control cells exposed to 0.3% ethanol (vehicle) (a) and MCF-12A cells exposed to 1.5mg/ml *S. frutescens* (b) for 48h at 400x magnification. Cells in various stages of mitosis are observed in vehicle-treated controls. Formation of hypercondensed chromatin and a higher proportion of cell in prophase are seen in *S. frutescens*-treated cells when compared to vehicle-treated controls.

Table 3.1: MCF-7 mitotic index. Cells in interphase, prophase, metaphase, anaphase, telophase and cells presenting with hypercondensed chromatin were expressed as a percentage after 48h exposure to 1.5mg/ml *S. frutescens* extracts.

	Vehicle control (mean)	**1.5mg/ml *S. frutescens* (mean)**	**Difference (Exp-Control)**	***p*-value**
Mitotic cells				
Prophase	1.3	1.8	0.5	0.059
Metaphase	1.266	0.233	-1.033	<0.05
Anaphase	0.766	0	-0.766	<0.05
Telophase	1.6	0.133	-1.467	<0.05
Tripolar metaphase	0	0	0	0
Non-mitotic cells				
Interphase	94.4	94.266	-0.134	0.83
Hypercondensed chromatin	1.6	3.566	1.966	<0.05

Table 3.2: MCF-12A mitotic index. Cells in interphase, prophase, metaphase, anaphase, telophase, cells presenting with hypercondensed chromatin as well as tripolar metaphase were expressed as a percentage after 48h exposure to 1.5mg/ml *S. frutescens* extracts.

	Vehicle control (mean)	**1.5mg/ml *S. frutescens* (mean)**	**Difference (Exp-Control)**	***p*-value**
Mitotic cells				
Prophase	2.133	8.4	6.267	<0.05
Metaphase	1.466	0.233	-1.233	<0.05
Anaphase	0.966	0.1	-0.866	<0.05
Telophase	1.466	0.333	-1.133	<0.05
Tripolar metaphase	1.66	0.86	0.8	0.55
Non-mitotic cells				
Interphase	90.7	85.733	-4.967	<0.05
Hypercondensed chromatin	2.9	5.1	2.2	<0.05

3.2.2 Fluorescent microscopy – apoptosis, autophagy and oncosis detection

Fluorescent microscopy was employed to differentiate between viable, apoptotic, autophagic and oncotic cells. A triple fluorescent dye staining method was developed utilizing acridine orange (green), Hoechst 33345 (blue) and propidium iodide (red) fluorescent dyes were used in the technique. Acridine orange is a lysosomotropic fluorescent compound that serves as a tracer for acidic vesicular organelles including autophagic vacuoles and lysosomes [218]. Cells undergoing autophagy will have an increased tendency for acridine orange staining when compared to viable cells, however acridine orange is not a specific marker for autophagy and therefore other techniques are needed to verify the appearance of increased autophagic activity. Hoechst 33342 is a fluorescent dye that can penetrate intact cell membranes of viable cells and cells undergoing apoptosis and stain the nucleus. Propidium iodide is a fluorescent dye that is unable to penetrate an intact membrane and therefore stains the nucleus of cells that have lost their membrane's integrity due to oncotic or necrotic processes.

MCF-7 and MCF-12A vehicle-treated control cells presented with normal nuclear morphology and residual acridine orange staining (Figures 3.12a and 3.14a). *S. frutescens*-treated and amino acid-starved (positive control) MCF-7 cells presented with an increase in acridine orange staining. Amino acid starvation is a known inducer of autophagy (Figures 3.12b and 3.13). *S. frutescens*-treated MCF-7 cells also exhibited hallmarks of hypercondensed chromatin and cytoplasmic shrinking (Figure 3.12b). Increased formation of large vacuoles was also observed and the vacuoles did not appear to be acidic as they did not show an affinity for acridine orange. *S. frutescens*-treated and amino acid-starved MCF-12A cells also presented with an increase in acridine orange staining when compared with vehicle-treated controls (Figures 3.14 and 3.15). The lack propidium iodide staining indicated that the cell membranes were intact and oncotic processes were absent.

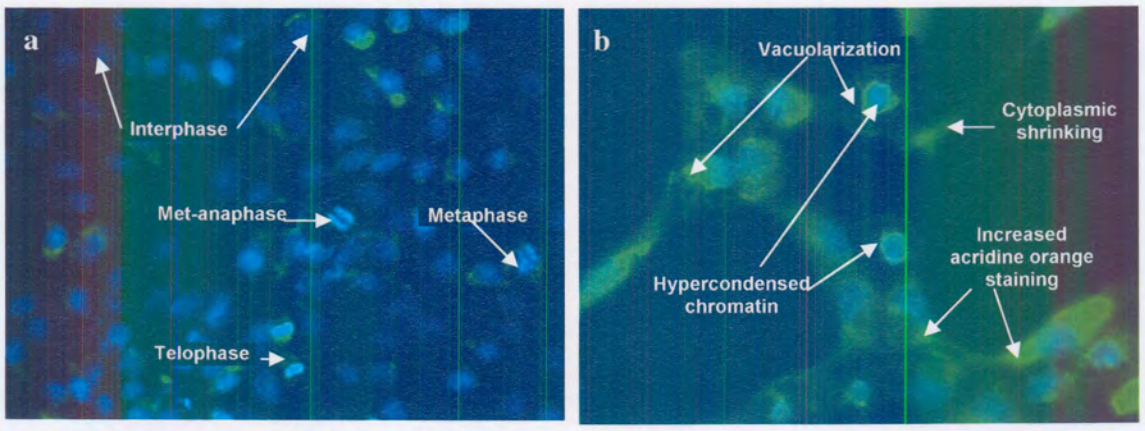

Figure 3.12: Hoechst 33342 (blue), acridine orange (green) and propidium iodide (red) staining of MCF-7 control cells exposed to 0.3% ethanol (vehicle) (a) and MCF-7 cells exposed to 1.5mg/ml *S. frutescens* (b) for 48h at 400x magnification. An increased staining of acridine orange in treated cells is observed compared to the vehicle-treated control. Increased vacuolarization of the cytoplasm as well as hypercondensed chromatin is observed.

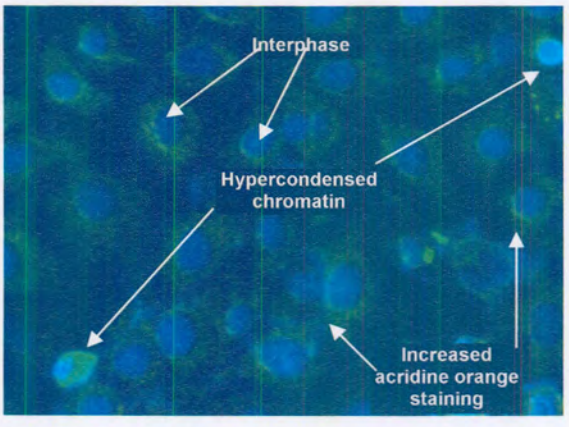

Figure 3.13: Hoechst 33342 (blue), acridine orange (green) and propidium iodide (red) staining of amino acid starved (autophagy positive control) MCF-7A cells. An increased staining of acridine orange in treated cells is observed compared to the vehicle-treated control (Figure 3.13a).

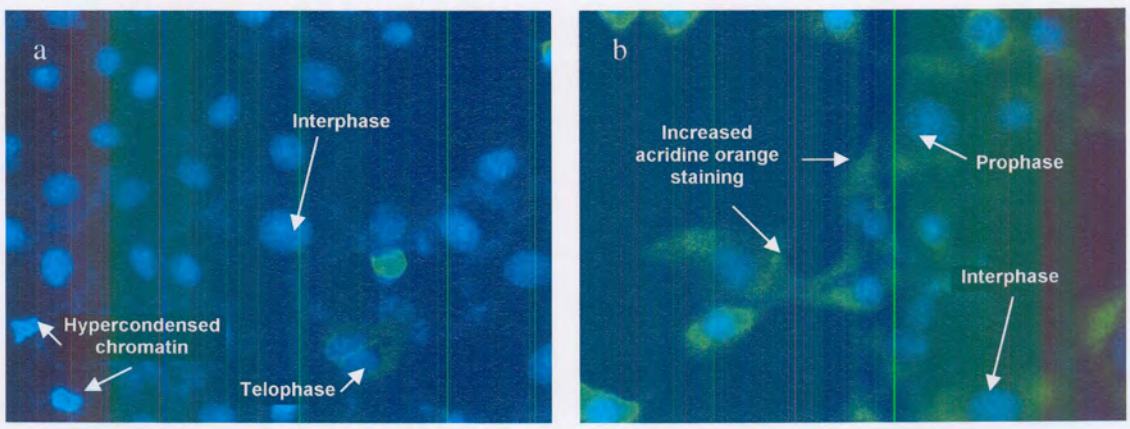

Figure 3.14: Hoechst 33342 (blue), acridine orange (green) and propidium iodide (red) staining of MCF-12A control cells exposed to 0.3% ethanol (vehicle) (a) and MCF-12A cells exposed to 1.5mg/ml *S. frutescens* (b) for 48h at 400x magnification. An increased staining of acridine orange in treated cells is observed compared to the vehicle-treated control.

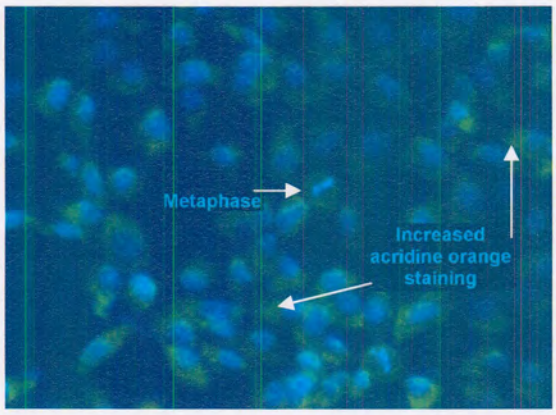

Figure 3.15: Hoechst 33342 (blue), acridine orange (green) and propidium iodide (red) staining of amino acid-starved (autophagy positive control) MCF-12A cells for 48h at 400x magnification. An increased staining of acridine orange in treated cells is observed compared to the vehicle-treated control (Figure 3.15a).

3.2.3 Transmission electron microscopy

Transmission electron microscopy (TEM) was used to determine the ultrastructure of intracellular components of exposed and control cells. TEM is currently the best and most reliable method for verifying autophagy [218]. Morphological hallmarks of autophagy were observed in both cell lines after 48h of *S. frutescens* exposure, confirming the fluorescent microscopy observations. At a low magnification (Figure 3.16a at 9000x magnification, Figure 3.16b at 7500x magnification) an increase in vacuolarization was observed in *S. frutescens*-treated MCF-7 and MCF-12A cells and was more pronounced in the MCF-7 cells (Figures 3.16, 3.18a and 3.19).

Morphological hallmarks of autophagy including autophagosome, autolysosome, endosomes and increased lysosomal formation was observed in both the MCF-7 and MCF-12A *S. frutescens*-treated cells (Figures 3.17, 3.18 and 3.20).

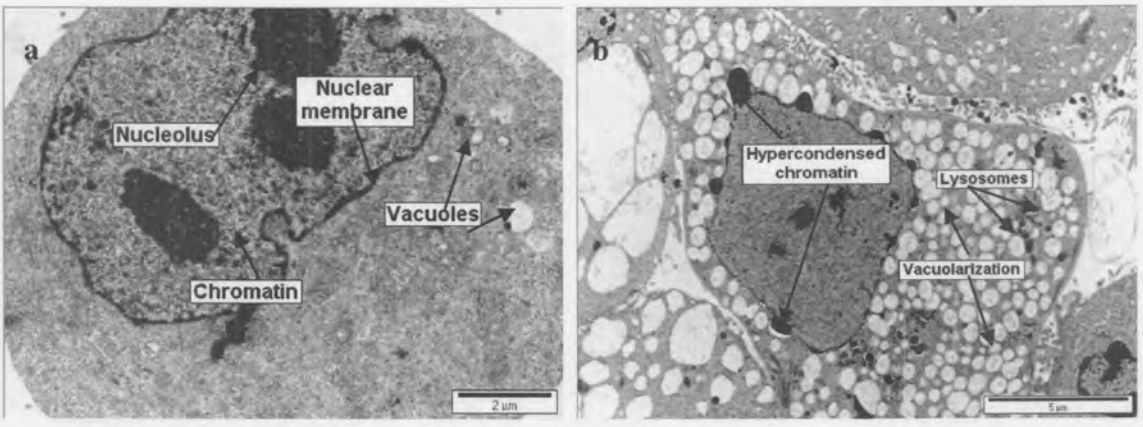

Figure 3.16: Transmission electron micrographs of MCF-7 vehicle-treated control cells (a) and MCF-7 cells exposed to 1.5mg/ml *S. frutescens* (b) for 48h. Hypercondensed chromatin and increased vacuolarization were observed in *S. frutescens*-treated cells.

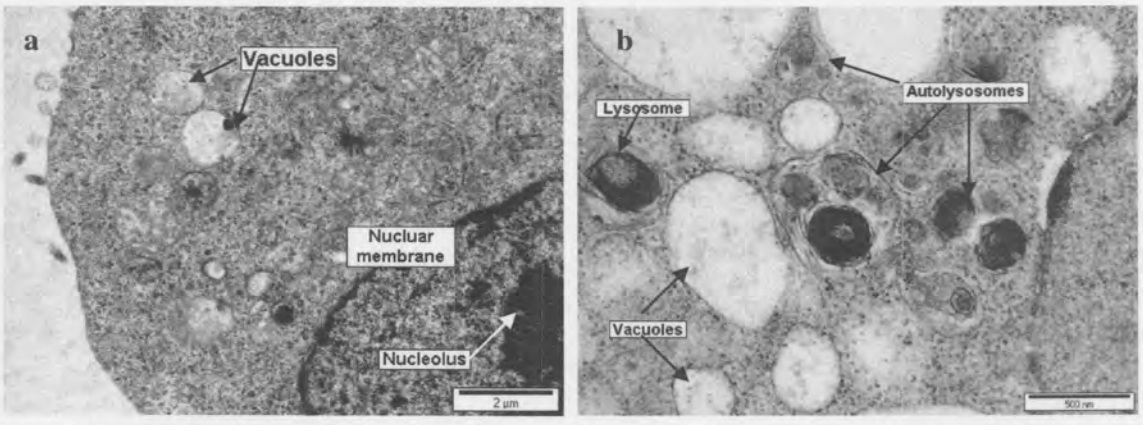

Figure 3.17: Transmission electron micrographs of MCF-7 vehicle-treated control cells (a) and MCF-7 cells exposed to 1.5mg/ml *S. frutescens* (b) for 48h. Increased autolysosome, lysosome and vacuole formation were observed in *S. frutescens*-treated cells.

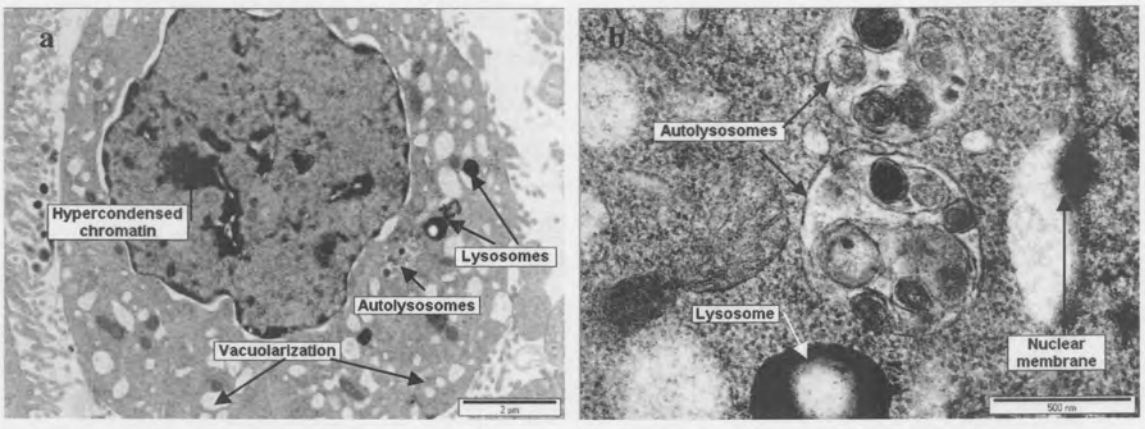

Figure 3.18: Transmission electron micrographs of MCF-7 cells exposed to 1.5mg/ml *S. frutescens* (a and b) for 48h. Hypercondensed chromatin and autolysosome-, lysosome- and vacuole formation were observed in *S. frutescens*-treated cells.

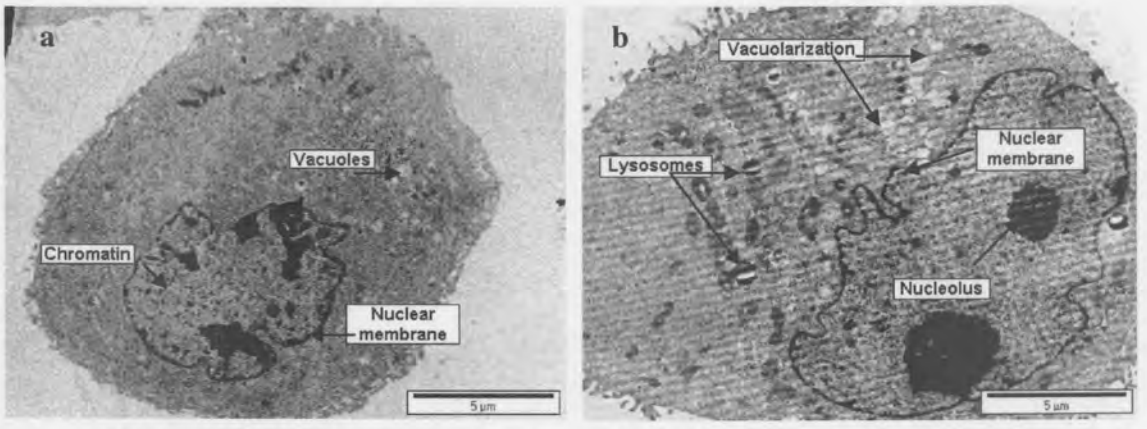

Figure 3.19: Transmission electron micrographs of MCF-12A vehicle-treated control cells (a) and MCF-12A cells exposed to 1.5mg/ml *S. frutescens* (b) for 48h. Slightly increased vacuolarization was observed in *S. frutescens*-treated cells.

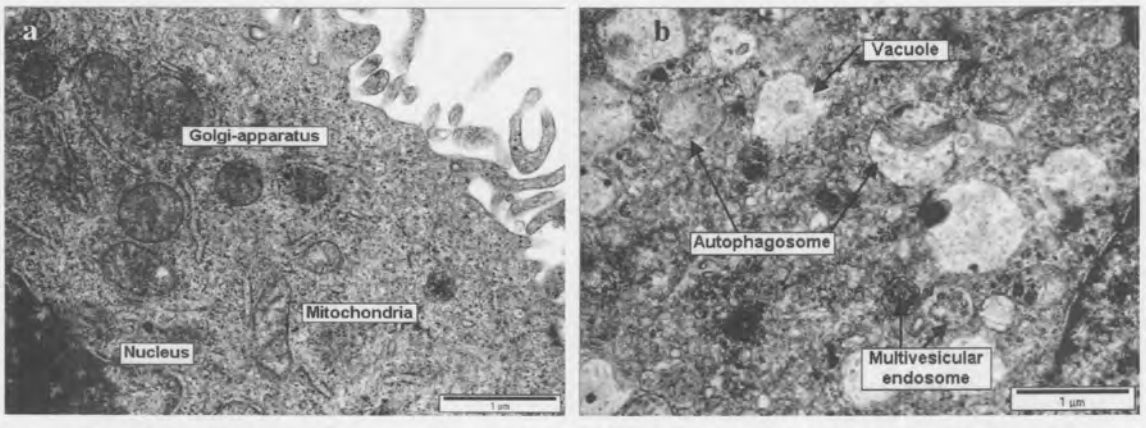

Figure 3.20: Transmission electron micrographs of MCF-12A vehicle-treated control cells (a) and MCF-12A cells exposed to 1.5mg/ml *S. frutescens* (b) for 48h. Autophagosome-, vacuole and multivesicular endosomal-formation were observed in *S. frutescens*-treated cells, however not as pronounced as MCF-7 *S. frutescens*-treated cells.

3.2.4 Scanning electron microscopy

Scanning electron microscopy was used to determine surface features of the exposed and control cells. In figures 3.21 and 3.23, a decrease in cell density in both MCF-7 and MCF-12A *S. frutescens*-treated cells were observed, however the decrease in cell density was more pronounced in the MCF-7 cells when compared to the MCF-12A cells, thereby confirming the observations found with light-and fluorescent microscopy when compared to vehicle-treated control cells. Cytoplasmic shrinking and hypercondensed chromatin was observed in the MCF-7 and MCF-12A *S. frutescens*-treated cells (Figures 3.22b and 3.24b).

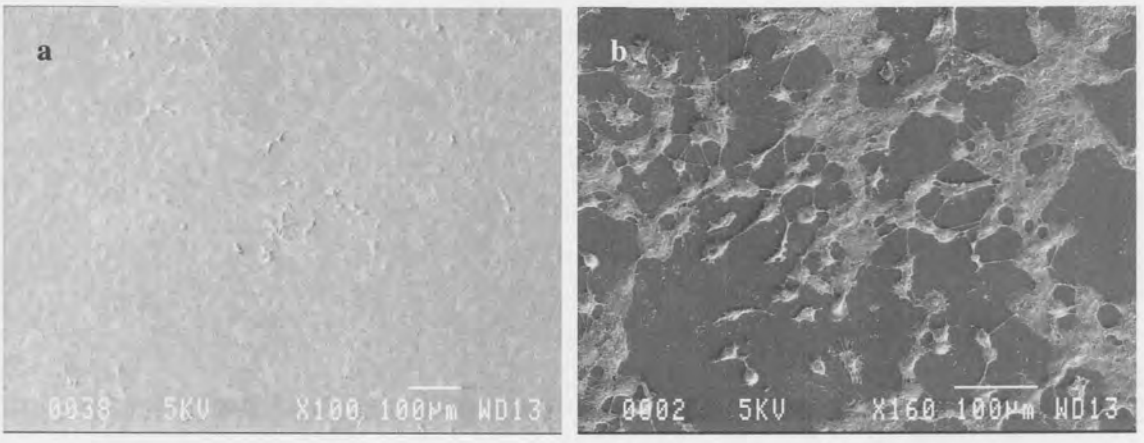

Figure 3.21: Scanning electron micrographs of MCF-7 vehicle-treated control cells (a) and MCF-7 cells exposed to 1.5mg/ml *S. frutescens* (b) for 48h. A marked decrease in cell density and an increase in the number of cells exhibiting signs of cytoplasmic shrinking were visible in *S. frutescens*-treated cells when compared to vehicle-treated control cells.

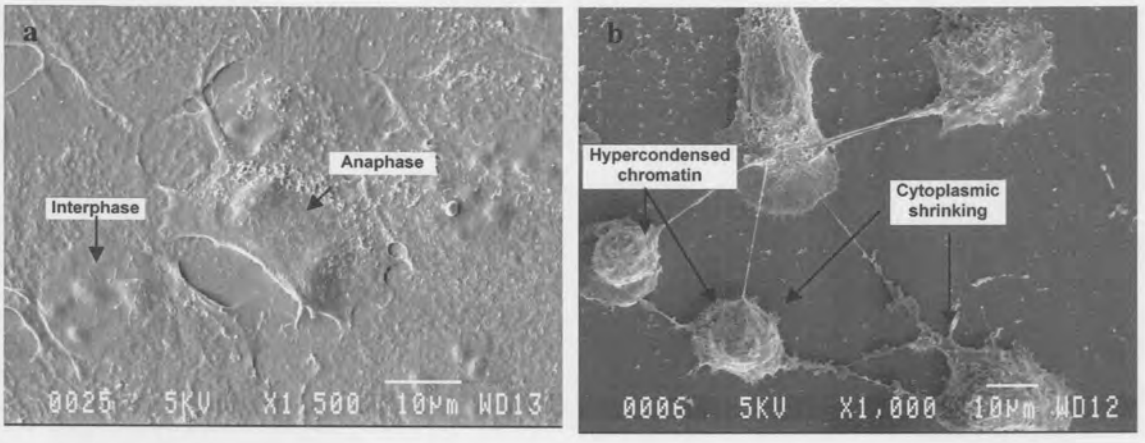

Figure 3.22: Transmission electron micrographs of MCF-7 vehicle-treated control cells (a) and MCF-7 cells exposed to 1.5mg/ml *S. frutescens* (b) for 48h. Cells in anaphase were observed in MCF-7 vehicle-treated control cells and cytoplasmic shrinking was visible in *S. frutescens*-treated cells.

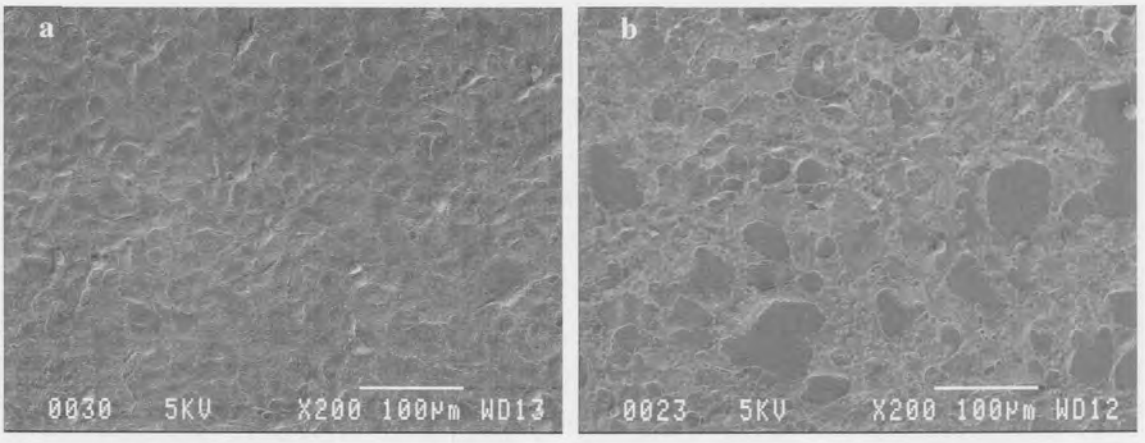

Figure 3.23: Scanning electron micrographs of MCF-12A vehicle-treated control cells (a) and MCF-12A cells exposed to 1.5mg/ml *S. frutescens* (b) for 48h. A slight decrease in cell density was visible in *S. frutescens*-treated cells when compared to vehicle-treated control cells.

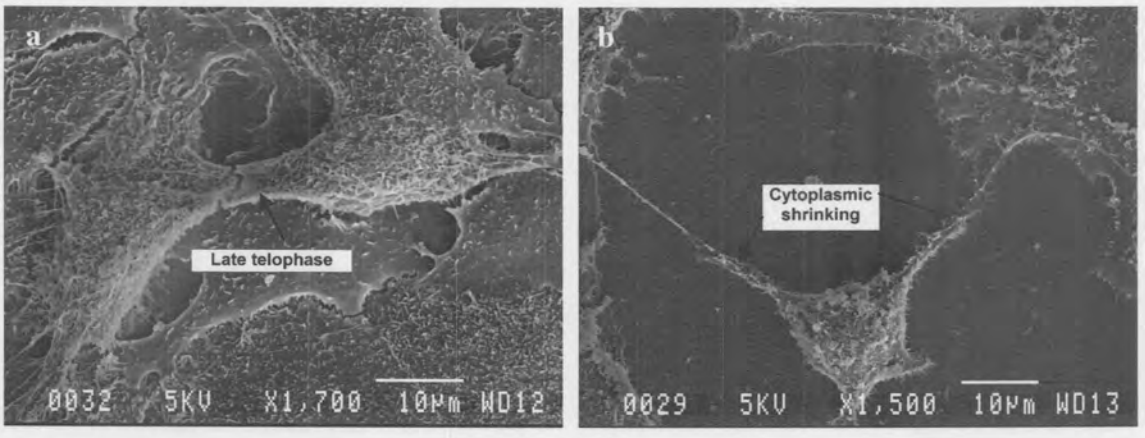

Figure 3.24: Transmission electron micrographs of MCF-12A vehicle-treated control cells (a) and MCF-12A cells exposed to 1.5mg/ml *S. frutescens* (b) for 48h. Cells in late telophase were observed in MCF-12A vehicle-treated control cells and cytoplasmic shrinking was visible in *S. frutescens*-treated cells.

3.3 Flow cytometry studies

3.3.1 Cell cycle analysis

DNA content of cells was measured as an indication of cells in the various stages of the cell cycle in order to determine the effect that *S. frutescens* extracts have on cell cycle progression (Figures 3.25 and 3.26). A more than two-fold (22%) increase of cells in the G_2/M-phase and 25% decrease of cells in the G_1-phase were observed in *S. frutescens*-treated MCF-7 cells. A small, yet statistically significant increase (2.79%) in the S-phase of *S. frutescens*-treated MCF-7 cells was also observed (table 3.3). No significant difference in the sub-G_1 *S. frutescens*-treated MCF-7 cells was observed.

A 12% increase in the G_2/M-phase, 2.63% increase in the sub-G_1 phase, a 7.29% decrease in the G_1-phase and a 7.87% decrease in the S-phase of *S. frutescens*-treated MCF-12A cells was observed (Table 3.4). Both cell lines exhibited an increase in the G_2/M-phase when treated with *S. frutescens* extracts; however the increase was not as pronounced in the MCF-12A cells when compared to the MCF-7 cells (Tables 3.3 and 3.4). The MCF-12A cells also had an increase in the sub-G_1 phase when exposed to *S. frutescens* extracts, indicating an increase in apoptosis.

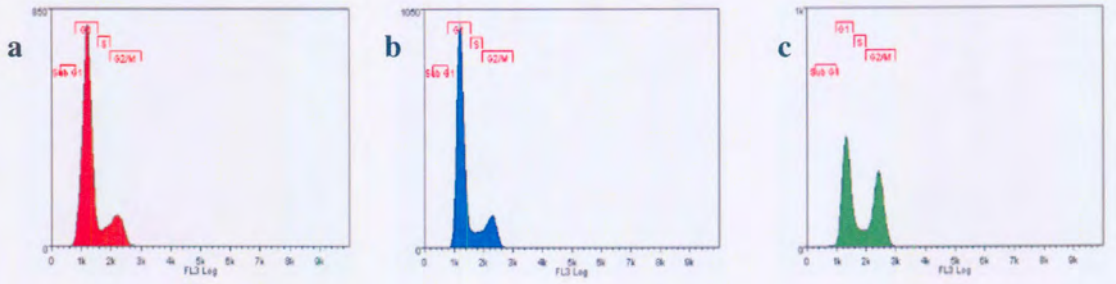

Figure 3.25: Cell cycle histograms (FL3 Log) of MCF-7 medium only control (a), vehicle-treated cells (b) and 1.5mg/ml *S. frutescens*-treated cells (c) for 48h. No differences between medium only and vehicle-treated cells were observed. *S. frutescens*-treated cells exhibited an increased proportion of cells in the G_2/M phase.

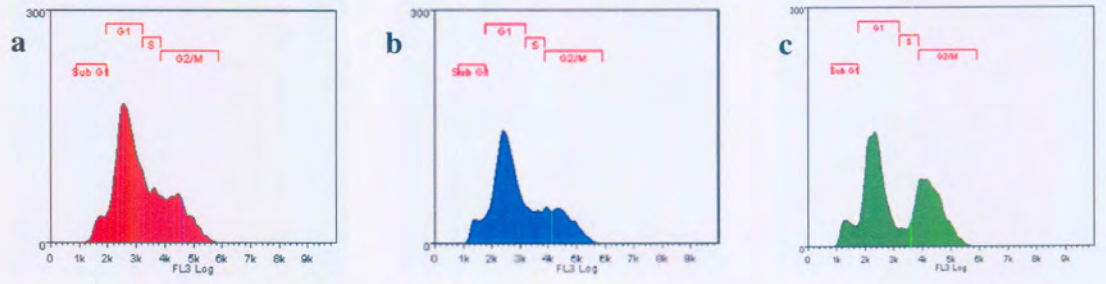

Figure 3.26: Cell cycle histograms (FL3 Log) of MCF-12A medium only control (a), vehicle-treated cells (b) and 1.5mg/ml *S. frutescens*-treated cells (c) for 48h. No differences between medium only and vehicle-treated cells were observed. *S. frutescens*-treated cells exhibited an increased proportion of cells in the G_2/M phase, but was not as pronounced when compared to MCF-7 *S. frutescens*-treated cells.

``**Table 3.3:** Measurement of DNA content of vehicle-treated control and *S. frutescens*-treated MCF-7 cells as an indication of cells in various stages of the cell cycle.

Cell cycle phase	Vehicle control (mean)	1.5mg/ml *S. frutescens* (mean)	Difference (Exp-Control)	*p*-value
G_1	76.95	51.09	-25.86	< 0.05
S	6.95	9.74	2.79	0.035
G_2/M	16.05	38.68	22.63	< 0.05
Sub G_1	0.32	0.49	0.44	0.14

Table 3.4: Measurement of DNA content of vehicle-treated control and *S. frutescens*-treated MCF-12A cells as an indication of cells in various stages of the cell cycle.

Cell cycle phase	Vehicle control (mean)	1.5mg/ml *S. frutescens* (mean)	Difference (Exp-Control)	*p*-value
G_1	54.76	47.47	-7.29	< 0.05
S	14.76	6.89	-7.87	< 0.05
G_2/M	24.45	36.98	12.53	< 0.05
Sub G_1	6.03	8.66	2.63	< 0.05

3.3.2 Apoptosis detection analysis

Translocation of the membrane PS from the inner to the outer leaflet of the plasma membrane is normally one of the earliest indications of apoptosis and was measured with fluorescein isothiocyanate conjugated Annexin V. Annexin V is a 35-36 kDa, Ca^{2+}-dependent, phospholipid binding protein with a high affinity for PS. Propidium iodide is used to distinguish between necrotic and apoptotic cells. Late apoptotic cells are Annexin V- and propidium iodide positive. A decrease in early and late apoptosis was observed in *S. frutescens*-treated MCF-7 cells when compared to the vehicle-treated and Actinomycin D-treated positive control (Figures 3.27 and 3.28). The differences, however, were minimal and not statistically significant (Table 3.5). An increase in the number of cells in early apoptosis and a decrease in the number late apoptosis were observed in *S. frutescens*-treated MCF-12A cells when compared to the vehicle-treated cells (Figures 3.29 a and b), confirming the mitotic index results. The differences were statistically significant (Table 3.6). The population of *S. frutescens*-treated MCF-12A cells shifted slightly towards early apoptosis, confirming the cell cycle analysis analyses (Figure 3.29c).

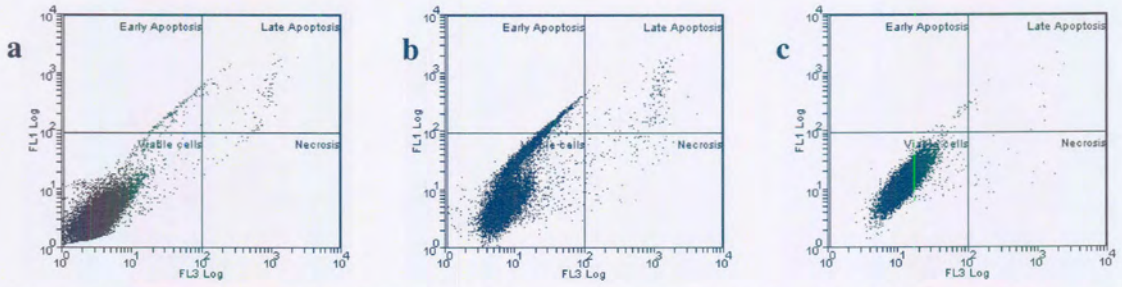

Figure 3.27: Propidium iodide (FL3 Log) vs Annexin V (FL1 Log) dot-plot of MCF-7 vehicle-treated control (a), Actinomycin D-treated positive control (b) and 1.5mg/ml *S. frutescens*-treated cells (c) for 48h.

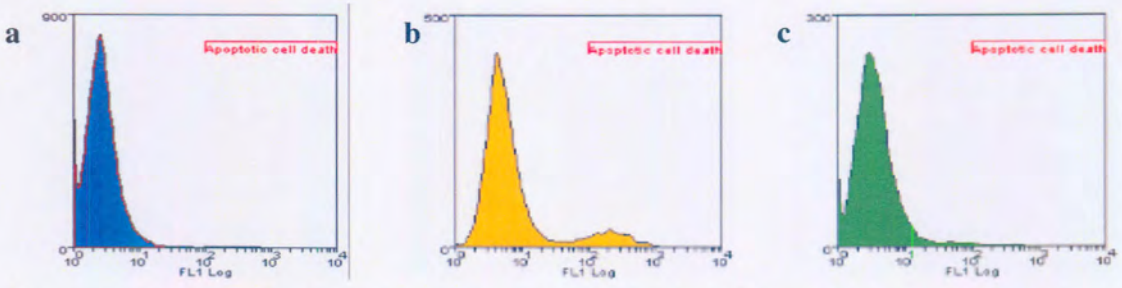

Figure 3.28: Annexin V (FL1 Log) histograms of MCF-7 vehicle-treated control (a), Actinomycin D-treated positive control and 1.5mg/ml *S. frutescens*-treated cells for 48h.

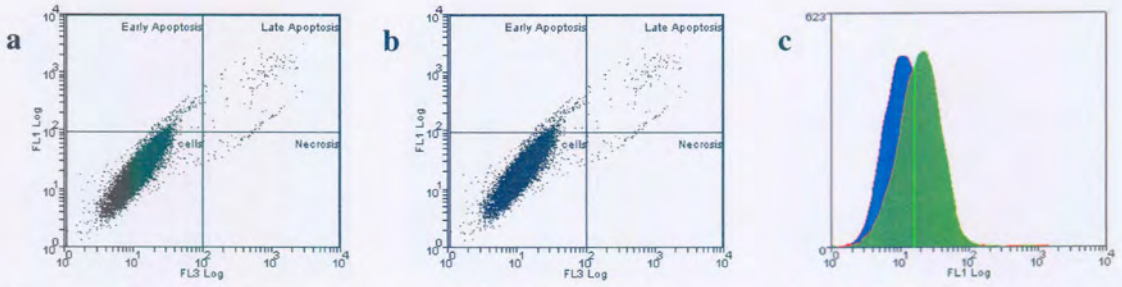

Figure 3.29: Propidium iodide (FL3 Log) vs Annexin V (FL1 Log) dot-plot of MCF-12A medium only control (a) and 1.5mg/ml *S. frutescens*-treated cells (b) for 48h and MCF-12A medium only control (blue) and 1.5mg/ml *S. frutescens*-treated cells (green) Annexin V (FL1 Log) histograms (c).

Table 3.5: Measurement of phosphatidylserine externalization and membrane permeability of vehicle-treated control and *S. frutescens*-treated MCF-7 cells as an indication of cells in various stages of cell death.

	Vehicle control (mean)	**1.5mg/ml *S. frutescens* (mean)**	**Difference (Exp-Control)**	***p*-value**
Early Apoptosis	0.49	0.28	-0.21	0.34
Late Apoptosis	0.57	0.26	-0.31	0.15
Necrosis	0.09	0.22	0.13	0.1
Viable cells	98.39	99.26	0.87	0.052

Table 3.6: Measurement of phosphatidylserine externalization and membrane permeability of vehicle-treated control and *S. frutescens*-treated MCF-12A cells as an indication of cells in various stages of cell death.

	Vehicle control (mean)	**1.5mg/ml *S. frutescens* (mean)**	**Difference (Exp-Control)**	***p*-value**
Early Apoptosis	1.52	2.15	0.63	0.027
Late Apoptosis	1.53	0.96	-0.57	<0.05
Necrosis	0.56	0.84	0.28	0.49
Viable cells	96.55	95.25	-1.3	0.032

3.4 Gene expression analysis

3.4.1 Microarray

3.4.1.1 RNA extraction

High quality pure total RNA was extracted from vehicle-treated and 1.5mg/ml *S. frutescens*-treated MCF-7 and MCF-12A cells respectively by using a combined protocol utilizing Qiagen's Qiazol reagent and RNeasy plant Mini kit. RNA quantification and purity was measured with a Nanodrop. RNA was considered pure of organic contamination (*e.g.* ethanol or phenol) with a 260/230 ratio greater than 1.5 (Table 3.7). RNA was considered pure of protein contamination with a 260/280 ratio greater than 2. Only pure total RNA was used for amino-allyl labeled cDNA synthesis. 20µg total RNA from each repeat of vehicle-treated and *S. frutescens*-treated cells was used for amino-allyl labeled cDNA synthesis. Pure total RNA samples were combined when needed. 0.75µg total RNA from each repeat of vehicle-treated and *S. frutescens*-treated cells was used to test the integrity of the RNA with electrophoresis.

Table 3.7: Measurement of total RNA quantity and quality directly after extraction.

Sample ID	Nucleic acid concentration (ng/ml)	260/280	260/230
MCF-7 *S. frutescens* samples			
MCF-7 Repeat 1 sample 1	17.21	2.14	1.75
MCF-7 Repeat 1 sample 2	24.50	2.10	1.69
MCF-7 Repeat 2 sample 1	23.40	1.97	1.80
MCF-7 Repeat 2 sample 2	42.68	1.97	1.85
MCF-7 Vehicle-treated samples			
MCF-7 Repeat 1 sample 1	79.24	2.11	1.69
MCF-7 Repeat 1 sample 2	98.91	2.04	1.78
MCF-7 Repeat 2 sample 1	58.15	2.07	1.79
MCF-7 Repeat 2 sample 2	55.23	1.98	1.88
MCF-12A *S. frutescens* samples			
MCF-12A Repeat 1 sample 1	17.56	2.21	1.86
MCF-12A Repeat 1 sample 2	21.22	1.98	1.74
MCF-12A Repeat 2 sample 1	16.95	2.05	1.90
MCF-12A Repeat 2 sample 2	18.16	2.02	1.76
MCF-7 Vehicle-treated samples			
MCF-12A Repeat 1 sample 1	72.70	2.05	1.79
MCF-12A Repeat 1 sample 2	66.29	2.04	1.76
MCF-12A Repeat 2 sample 1	70.36	2.01	1.90
MCF-12A Repeat 2 sample 2	81.39	2.04	1.84

3.4.1.2 RNA integrity

Verification of RNA integrity was conducted directly after extraction. The integrity of isolated RNA was verified by electrophoresis through 1.0% agarose-formaldehyde gel. Approximately 0.75µg total RNA from each repeat of vehicle-treated and *S. frutescens*-treated cells was loaded into each well. RNA was considered completely intact when clear 28S and 18S rRNA bands, with a 28S:18S intensity ratio was approximately 2:1, were observed (Figure 3.30a and b).

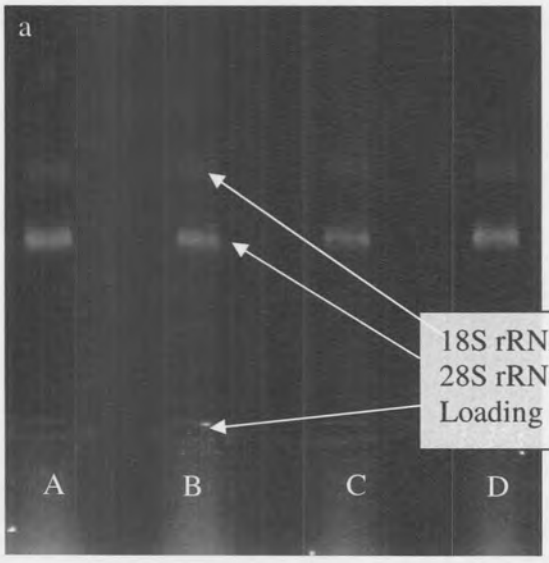

Figure 3.30a: Randomly selected MCF-7 control and exposed RNA samples

Lane A & B: Control samples

Lane C & D: Exposed samples

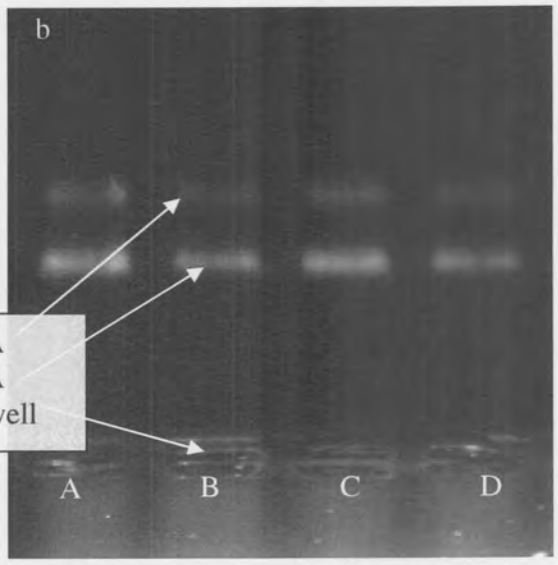

Figure 3.30b: Randomly selected MCF-12A control and exposed RNA samples

Lane A & B: Control samples

Lane C & D: Exposed samples

3.4.1.3 Amino-allyl labeled cDNA synthesis

20µg of pure and intact total RNA extracted from the *S. frutescens* and vehicle-treated control MCF-7 and MCF-12A cells were each separately annealed to oligo(deoxythymidine) and reverse transcribed in the presence of amino-allyl labeled deoxy-UTP. Amino-allyl labeled cDNA quantity and purity was verified with the Nanodrop after RNA degradation and purification. A 260/280 ratio greater than 1.8 and a 260/230 ratio greater than 1.5 was considered pure of protein and organic contamination (Table 3.8).

Table 3.8: Measurement of cDNA quantity and quality directly after RNA degradation and purification.

Sample ID	Nucleic acid concentration (ng/ml)	260/280	260/230
MCF-7 *S. frutescens* repeat 1	52.74	1.84	1.82
MCF-7 Vehicle-treated control repeat 1	71.04	1.80	1.79
MCF-7 *S. frutescens* repeat 2	64.98	1.89	1.91
MCF-7 Vehicle-treated control repeat 2	40.49	1.91	1.98
MCF-12A *S. frutescens* repeat 1	51.22	1.93	1.74
MCF-12A Vehicle-treated control repeat 1	38.68	1.91	1.78
MCF-12A *S. frutescens* repeat 2	34.53	1.82	1.72
MCF-12A Vehicle-treated control repeat 2	55.55	1.93	1.63

3.4.1.4 cDNA post-labeling coupling reaction

1.5µg of pure amino-allyl labeled cDNA from the *S. frutescens*-treated MCF-7 and MCF-12A cells were each labeled with Cy-3 (green) fluorescent dye and vehicle-treated control MCF-7 and MCF-12A cells were each labeled with Cy-5 (red) fluorescent dye. Amino-allyl Cy-dye labeled cDNA quantity, purity and incorporation was verified with the Nanodrop after purification. A 260/280 ratio greater than 1.8 was considered pure of protein contamination (Table 3.9). Quality of incorporation was measured by calculating the percentage difference of the nucleic acid concentration:Cy-dye concentration ratio of complimentary cDNA to be hybridized to the same slide. Incorporation was considered sufficient when the percentage difference of incorporation of complimentary cDNA to be hybridized to the same slide did not differ by more than 10% (Table 3.9). Percentage difference was calculated by the following formula:

Percentage difference = [Absolute value of (Experiment Nucleic acid - Cy-dye ratio)/Control Nucleic acid:Cy-dye ratio)] / (Experiment Nucleic acid 4 Cy-dye ratio)/Control Nucleic acid:Cy-dye ratio) * 100.

Table 3.9: Measurement of Cy3- and Cy5-labeled cDNA quantity, quality and Cy3 and Cy5 incorporation directly after purification.

Sample ID	Nucleic acid concentration (ng/ml)	Cy3 dye concentration (pmol/µl)	Cy5 dye concentration (pmol/µl)	260/280	Nucleic acid:Cy-dye ratio	% Difference
MCF-7 *S. frutescens* repeat 1	29.95	8.16	-0.02	1.89	3.670343	9.39
MCF-7 Vehicle-treated control repeat 1	33.55	1.29	7.48	1.80	4.431818	
MCF-7 *S. frutescens* repeat 2	32.58	9.81	-0.05	1.84	3.321101	6.10
MCF-7 Vehicle-treated control repeat 2	32.84	0.65	8.75	1.83	3.753143	
MCF-12A *S. frutescens* repeat 1	12.21	0.68	0.12	1.94	17.95588	8.14
MCF-12A Vehicle-treated control repeat 1	11.59	0.27	0.76	1.81	15.25	
MCF-12A *S. frutescens* repeat 2	21.90	1.31	0.08	1.81	16.71756	0.57
MCF-12A Vehicle-treated control repeat 2	12.89	0.15	0.78	1.84	16.52564	

3.4.1.5 Hybridization of Cy-dye labeled cDNA and scanning of Agilent microarray slides

A hybridization mixture was prepared by adding 40pmol of Cy-3 and Cy-5 labeled cDNA to a final volume of 28µl. 7µl 10x control targets was added together with 35µl 2x hybridization buffer to provide a final volume of 70µl. This hybridization mixture was pipetted onto an Agilent 22k 60-mer human oligo slide with a cover slip on. The mixture propagated over the whole slide as a result of capillary action of the liquid and cover-slip. The slides were sealed in an incubation chamber and incubated for 16h at 42°C. Afterwards the slides were washed twice and scanned with an Axon Genepix 4000B Scanner (Figures 3.31, 3.32 and 3.33). A preview scan was performed in order to adjust the count ratio of the spotted-area as close to 1 as possible. For count ratios greater than 1, the photomultiplier (PMT) gain for the 635nm channel was increased and the PMT gain for the 532nm channel was decreased until the count ratio approximated 1 for the spotted area. For count ratios smaller than 1, the PMT gain for the 635nm channel was decreased and the PMT gain for the 532nm channel was increased until the count ratio approximated 1 for the spotted area.

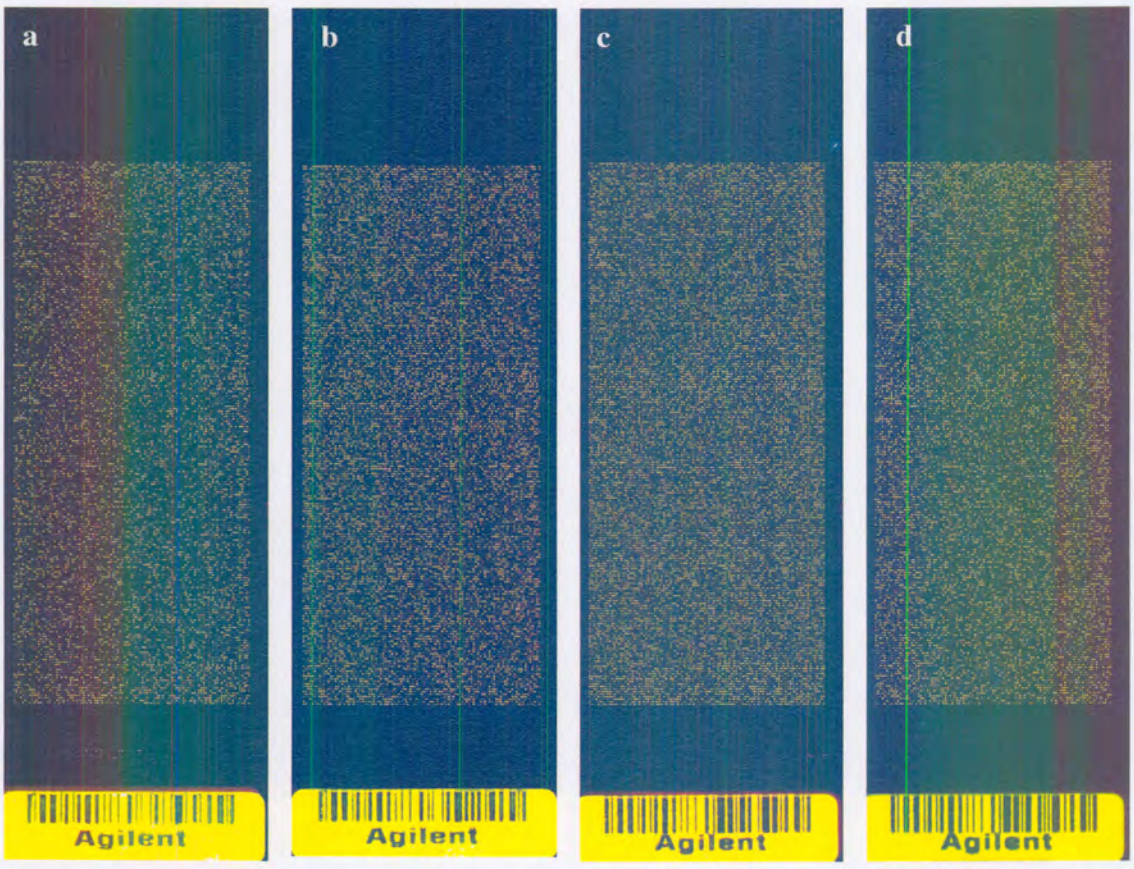

Figure 3.31: Images of PMT-corrected scanned microarray slides of MCF-7 slide 1 (Control=Cy5) (a), MCF-7 slide 2 (Control=Cy5) (b), MCF-12A slide 1 (Control=Cy5) (c) and MCF-12A slide 2 (Control=Cy5) (d).

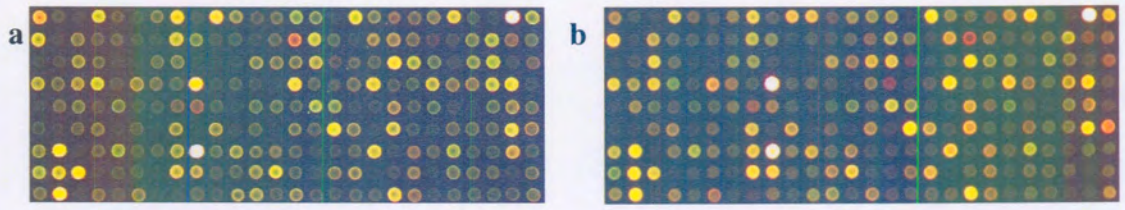

Figure 3.32: Images of PMT-corrected scanned microarray slides of MCF-7 slide 1 (Control=Cy5) (a) and MCF-7 slide 2 (Control=Cy5) of the same region at a higher magnification.

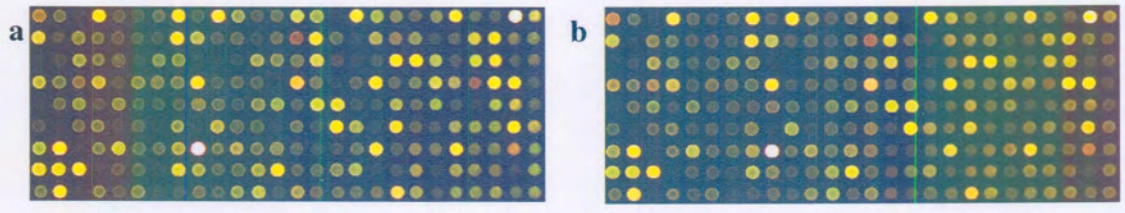

Figure 3.33: Images of PMT-corrected scanned microarray slides of MCF-12A slide 1 (Control=Cy5) (a) and MCF-12A slide 2 (Control=Cy5) of the same region at a higher magnification.

3.4.2 Bioinformatics

3.4.2.1 Spotfinding

Spotfinding was conducted with Genepix Pro 6.1. Less than 5% of spots in all the analyzed slides were excluded from further analysis. The majority of excluded genes were genes that had a low intensity vs. back ground ratio. These genes were not expressed in both the treated and untreated samples.

3.4.2.2 Limma statistical analysis

Statistical analysis after spotfinding was conducted with Limma using the LimmaGUI interface [230]. Pre-normalized MA-plots with Loess curves of the slides are represented by Figure 3.34. Global LOESS normalized MA-plots with Loess curves of the slides are represented by Figure 3.35. Figure 3.36 represents the MA-plot using the fitted M-values after normalization.

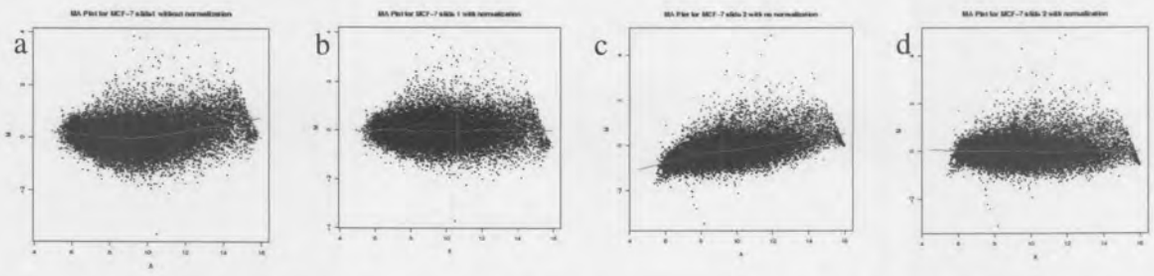

Figure 3.34: MCF-7 MA plots of pre-normalized data (a and c) whereby Cy3- and Cy5-fluorescent dye biases at high and low intensities are unaccounted for. b and d indicate MA plots of Global LOESS normalized data whereby Cy3- and Cy5-fluorescent dye biases at high and low intensities are corrected.

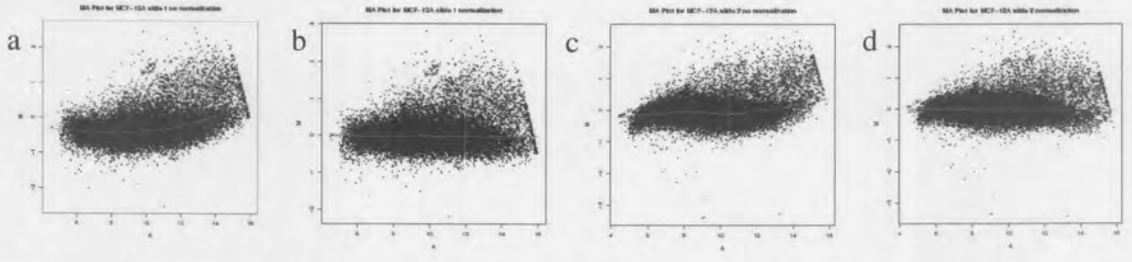

Figure 3.35: MCF-12A MA plots of pre-normalized data (a and c) whereby Cy3- and Cy5-fluorescent dye biases at high and low intensities are unaccounted for. b and d indicate MA plots of Global LOESS normalized data whereby Cy3- and Cy5-fluorescent dye biases at high and low intensities are corrected.

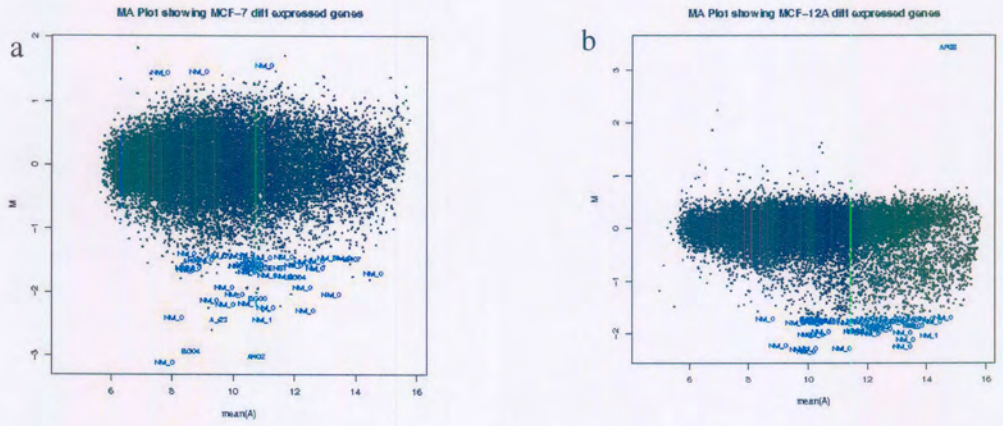

Figure 3.36: Microarray plots of Loess normalized data of MCF-7 (Treated)-(Control) (a) and MCF-12A (Treated)-(Control) (b) showing the top 50 differentially expressed genes.

3.4.2.3 Gene expression analysis

325 genes were considered statistically significantly differentially expressed in MCF-7 cells and 74.4% of *S. frutescens*-treated genes were down-regulated when compared to the vehicle-treated control. 1467 genes were considered statistically significantly differentially expressed in MCF-12A cells. 83.5% of *S. frutescens*-treated genes were down-regulated when compared to the vehicle-treated control. Mapping of differentially expressed genes to biochemical pathways and GO categories was performed using GENECODIS [224]. Differentially expressed genes exclusively responsive in *S. frutescens*-treated MCF-7 and MCF-12A cells were mapped to apoptosis, cell cycle, signal transduction and metabolism and are summarized in Tables 3.10 and 3.11 respectively. The statistically differentially expressed genes responsive to *S. frutescens* in both cell lines were compared with GeneVenn and 90 genes were found to be affected in both cell lines after 48h exposure to 1.5mg/ml *S. frutescens* extracts (Figure 3.37). The 90 genes were mapped to apoptosis, cell cycle, signal transduction and metabolism (Table 3.12).

Table 3.10: Selected genes (gene name in brackets) responsive to *S. frutescens* ethanol extracts specific to MCF-7 cells revealed by cDNA microarray and bioinformatics analyses.

Genes	M-Value (Log-2 expression ratio)	B-value (Log-odds)
Apoptosis		
Cystatin A (stefin A) (CSTA)	1.17	0.59
Cell cycle		
MCM5 minichromosome maintenance deficient 5, cell division cycle 46 (*S. cerevisiae*) (MCM5)	1.14	0.77
Tuberous sclerosis 2 (TSC2)	1.09	0.25
Proliferating cell nuclear antigen (PCNA)	-3.22	2.39
SMC1 structural maintenance of chromosomes 1-like 1 (yeast) (SMC1L1)	-1.23	1.06
Anaphase promoting complex subunit 4 (ANAPC4)	-1.51	1.58
Signal transduction		
Mitogen-activated protein kinase 9 (MAPK9), transcript variant 1	1.03	0.18
v-akt murine thymoma viral oncogene homolog 2 (AKT2)	-3.11	4.04
Nuclear factor of kappa light polypeptide gene enhancer in B-cells 1 (p105) (NFKB1)	-1.23	1.40
Protein phosphatase 1, subunit 3D (PPP1R3D)	-2.10	2.65
Protein phosphatase 1, subunit 12C (PPP1R12C)	-1.64	2.59
Mitogen-activated protein kinase kinase kinase 2 (MAP3K2)	-1.40	0.53
Transcription elongation factor A (SII)-like 4 (TCEAL4)	-1.14	0.07
Regulation of transcription		
TAF1 RNA polymerase II, TATA box binding protein (TBP)-associated factor, 250kDa (TAF1)	1.02	0.92
Nuclear transcription factor Y, gamma (NFYC)	1.01	0.04
IMP4, U3 small nucleolar ribonucleoprotein, homolog (yeast) (IMP4),	1.21	1.28
Polymerase (RNA) II (DNA directed) polypeptide L, 7.6kDa (POLR2L)	-1.29	0.27
v-myc myelocytomatosis viral oncogene homolog 1, lung carcinoma derived (avian) (MYCL1)	-1.02	0.07
Metabolism		
Cytochrome P450, family 3, subfamily A (CYP3A7)	1.07	5.31
Mitochondrial ribosomal protein S18B (MRPS18B)	-1.51	1.50
Mitochondrial ribosomal protein S36 (MRPS36)	-1.48	1.28
Mitochondrial ribosomal protein S34 (MRPS34)	-1.21	0.77
Small nuclear ribonucleoprotein polypeptide (SNRP70)	-1.64	2.59
Metalloproteases		
Disintegrin and metalloprotease domain 23 (AY545641)	-1.93	0.78

Table 3.11: Selected genes (gene name in brackets) responsive to *S. frutescens* ethanol extracts specific to MCF-12A cells revealed by cDNA microarray and bioinformatics analyses.

Genes	M-Value (Log-2 expression ratio)	B-value (Log-odds)
Apoptosis		
Growth arrest and DNA-damage-inducible, beta (GADD45B)	0.57	0.22
V-myc myelocytomatosis viral oncogene homolog (MYC)	-0.99	8.78
Cell cycle		
Cyclin A2 (CCNA2)	0.92	7.53
Cyclin B1 (CCNB1)	0.58	0.03
RecQ protein-like (DNA helicase Q1-like) (RECQL)	-2.26	35.77
Topoisomerase (DNA) I, mitochondrial (TOP1MT)	-1.50	20.52
Signal transduction		
Protein inhibitor of activated STAT1 (PIAS1)	0.97	8.62
Phosphatase and tensin homolog (mutated in multiple advanced cancers 1) (PTEN)	0.59	0.34
E74-like factor 3 (epithelial-specific) (ELF3)	-2.21	35.42
AKT1 substrate 1 (proline-rich) (AKT1S1)	-1.16	13.28
Dual specificity phosphatase 6 (DUSP6)	-1.11	18.67
Mitogen-activated protein kinase kinase 1 (MAP2K1)	-0.81	6.85
v-myc myelocytomatosis viral oncogene homolog (avian) (MYC)	-1.06	16.47
Metastasis associated 1 (MTA1)	-1.06	8.28
Regulation of transcription		
Heterogeneous nuclear ribonucleoprotein D (AU-rich element RNA binding protein 1, 37kDa) (HNRPD)	0.71	3.75
Tumor protein p73 (TP73)	-0.90	10.06
E4F transcription factor 1 (E4F1)	-1.13	12.46
E2F transcription factor 2 (E2F2)	-0.96	12.48
Mediator of RNA polymerase II transcription, subunit 25 (MED25)	-1.72	54.63
Mediator of RNA polymerase II transcription, subunit 9 (MED9),	-0.72	4.04
Polymerase (RNA) III (DNA directed) polypeptide G (32kD) like (POLR3GL),	-1.32	29.24
B double prime 1, subunit of RNA polymerase III transcription initiation factor IIIB (BDP1)	-1.72	54.65
Polymerase (DNA directed), sigma (POLS)	-0.87	6.45
Polymerase (DNA directed), epsilon 3 (p17 subunit) (POLE3)	-1.36	12.51
Primase, polypeptide 1, 49kDa (PRIM1)	-0.61	0.91
General transcription factor IIH, polypeptide 2, 44kDa (GTF2H2)	-1.05	16.05

Table 3.11: Selected genes (gene name in brackets) responsive to *S. frutescens* ethanol extracts specific to MCF-12A cells revealed by cDNA microarray and bioinformatics analyses **(continued)**.

Genes	M-Value (Log-2 expression ratio)	B-value (Log-odds)
Metabolism		
Acyl-CoA-desaturase	3.60	39.08
Ribosomal protein L3-like (RPL3L)	-1.59	22.73
Mitochondrial ribosomal protein S2 (MRPS2)	-1.97	30.94
Mitochondrial ribosomal protein L50 (MRPL50)	-1.47	20.27
Ribosomal protein L6 (RPL6)	-1.56	19.29
Mitochondrial ribosomal protein L46 (MRPL46)	-1.31	16.63
Ribosomal protein L28 (RPL28)	-1.04	10.49
Metalloproteases		
Matrix metalloproteinase 3 (stromelysin 1, progelatinase) (MMP3)	-1.19	22.60

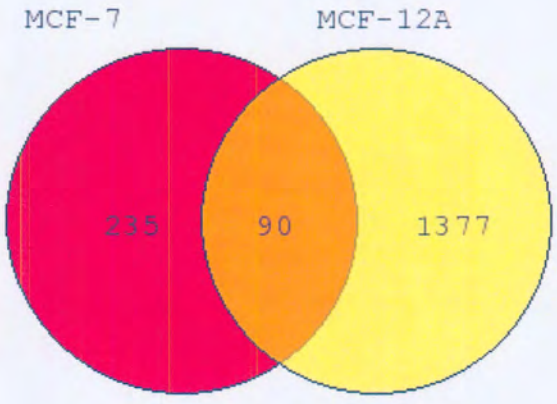

Figure 3.37: GeneVenn diagram showing common genes affected in *S. frutescens*-treated MCF-7 and MCF12A cells. 90 differentially expressed genes were affected in both cell lines after 48h exposure to 1.5mg/ml *S. frutescens* plant extracts.

Table 3.12: Selected genes (gene name in brackets) responsive to *S. frutescens* ethanol extracts in MCF-7 and MCF-12A cells revealed by cDNA microarray and bioinformatics analyses.

	MCF-7			MCF-12A	
Genes	**M-Value** (Log-2 expression ratio)	**B-value** (Log-odds)		**M-Value** (Log-2 expression ratio)	**B-value** (Log-odds)
Signal transduction					
RAB18, member RAS oncogene family (RAB18)	-1.31	1.94		-1.94	71.26
Rho family GTPase 1 (RND1)	-1.08	0.18		-0.78	5.73
Mitogen-activated protein kinase 15 (MAPK15)	-1.42	2.54		-0.88	9.41
Misshapen-like kinase 1 (MINK1)	-1.14	0.50		-0.78	5.84
Cell cycle					
Citron (rho-interacting, serine/threonine kinase 21) (CIT)	-1.29	0.13		-1.76	57.68
Polymerase (DNA directed) sigma (POLS)	-1.17	0.79		-0.99	13.67
Poly (ADP-ribose) polymerase family, member 2 (PARP2)	-2.14	5.69		-1.00	13.83
START domain containing 13 (STARD13)	-1.30	1.29		-1.05	15.88
Regulation of transcription					
CCAAT/enhancer binding protein (C/EBP), beta (CEBPB)	-1.62	2.89		-1.70	53.15
Transcription factor 19 (SC1) (TCF19)	1.39	0.99		-0.88	9.10
Jun D proto-oncogene (junD)	-1.33	1.23		-0.82	7.18
Small nuclear ribonucleoprotein 70kDa polypeptide (RNP antigen) (SNRP70)	-1.14	0.44		-1.05	16.18
Mediator of RNA polymerase II transcription, subunit 6 (MED6)	-1.74	0.74		-0.72	3.99
Steroid hormone receptor hERR2.	-1.38	1.82		-0.82	7.14
Metabolism					
ATPase, Ca^{2+} transporting, plasma membrane 3 (ATP2B3)	1.25	1.40		-0.87	8.80
Aspartyl-tRNA synthetase (DARS)	-2.29	1.29		-1.164	21.10
Mitochondrial ribosomal protein S18B (MRPS18B)	-1.35	1.52		-0.62	7.15
Mitochondrial ribosomal protein S30 (MRPS30)	-1.73	4.10		-0.69	3.20
Aldolase A, fructose-bisphosphate (ALDOA)	-1.02	0.06		-0.87	9.06
Metalloproteases					
Disintegrin-like and metalloprotease (reprolysin type) with thrombospondin type 1 motif, 20 (ADAMTS20)	1.06	0.37		0.80	6.38

3.5 mTOR kinase activity

Morphological observations of autophagy in MCF-7 and MCF-12A *S. frutescens*-treated cells, as well as the observation of an overall decrease in mRNA expression in both *S. frutescens*-treated cell lines implicated the mTOR kinase as a possible signaling kinase being affected by *S. frutescens* extracts. mTOR kinase is involved in pathways controlling mRNA synthesis, protein synthesis, cell cycle progression, apoptosis and autophagy [152]. Abrogated mTOR kinase activity is associated with autophagy and attenuated mRNA translation and ribosome biogenesis [157].

The activity of the mTOR kinase was indirectly measured by its ability to phosphorylate a p70S6K-GST fusion protein, a specific mTOR substrate, at Thr389. The ability of the immunoprecipitated mTOR kinase to phosphorylate the p70S6K-GST fusion protein substrate was 53.4% lower in *S. frutescens*-treated MCF-7 cells after 48h (Figure 3.38) and 45.2% lower in *S. frutescens*-treated MCF-12A cells after 48h of exposure (Figure 3.39).

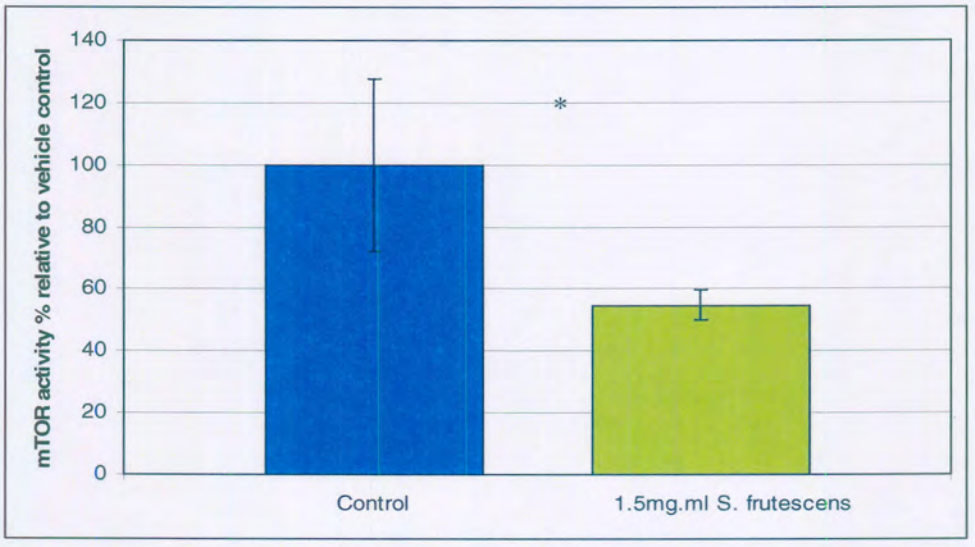

Figure 3.38: mTOR kinase activity of *S. frutescens*-treated (green) and vehicle-treated (blue) MCF-7 cells as a percentage activity relative to 100% control after 48h. mTOR kinas activity was 53.4% lower in *S. frutescens*-treated MCF-7 cells after 48h. * Indicates a p-value < 0.05 for mTOR kinase inhibition between vehicle-treated and *S. frutescens*-treated MCF-7 cells.

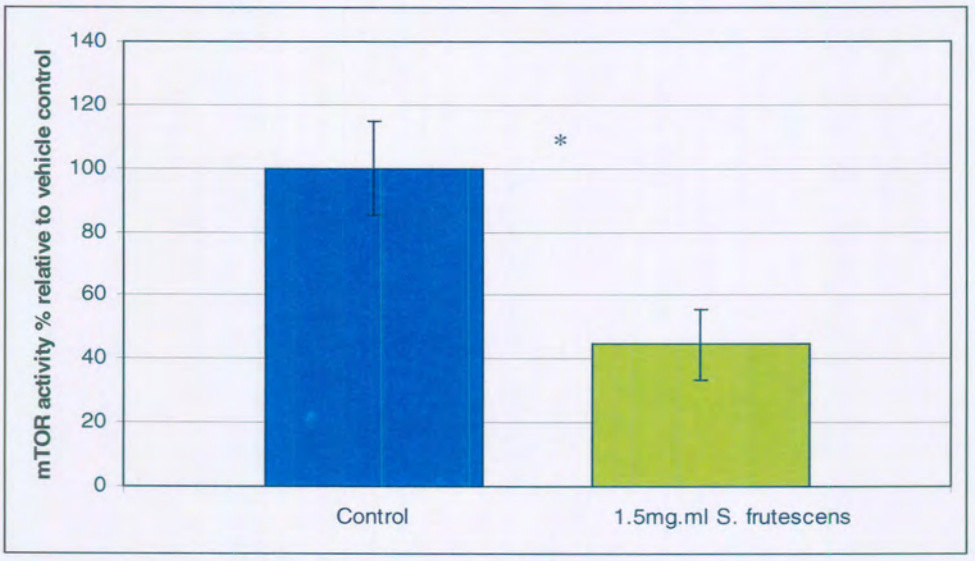

Figure 3.39: mTOR kinase activity of *S. frutescens*-treated (green) and vehicle-treated (blue) MCF-12A cells as a percentage activity relative to 100% control after 48h. mTOR kinase activity was 45.2% lower in *S. frutescens*-treated MCF-7 cells after 48h. * Indicates a p-value < 0.05 for mTOR kinase inhibition between vehicle-treated and *S. frutescens*-treated MCF-12A cells.

Chapter 4

4. Discussion

In the present study, the differential effects of *S. frutescens* extracts on cell numbers, metabolic activity, morphology, cell cycle progression, cell death, gene expression and mTOR kinase activity were investigated in MCF-7 and MCF-12A cells. The purpose of the study was to elucidate possible mechanisms of action of whole plant extracts in order to stimulate further research into isolating compounds that might be of clinical significance.

Cell growth studies employing crystal violet as a DNA stain revealed that *S. frutescens* extracts inhibited cell proliferation in a dose-dependent manner in both the tumorigenic MCF-7 and non-tumorigenic MCF-12A cell lines. *S. frutescens* extracts inhibited growth at lower concentrations in the tumorigenic MCF-7 cell line when compared to the MCF-12A cell line. Cell growth was inhibited to 24% at 1.5mg/ml in MCF-7 cells and 62% at 1.5mg/ml in MCF-12A cells after 48h of exposure. These findings are consistent with other studies indicating that *S. frutescens* display antiproliferative actions in various cell lines. Stander *et al.* (2007) demonstrated that ethanolic *S. frutescens* plant extracts inhibited MCF-7 cell growth to 50% at 1.5mg/ml after 24h and 26% after 48h of exposure [38]. Tai *et al.* (2004) demonstrated that ethanolic extracts of *S. frutescens* tablets exhibited concentration-dependent antiproliferative activities on several human cancer cell lines including the MCF-7 and MDA-MB-468 human breast adenocarcinoma and leukemia (Jurkat and HL60) cell lines [32]. The MCF-7 cell line was the most susceptible of the tested cell lines, with a 50% inhibitory concentration (IC_{50}) at a 1/250 (0.55mg/ml) dilution, and an IC_{50} at 1/200, 1/150 and 1/200 dilutions for, MDA-MB-468, Jurkat and HL60 cells, respectively [32]. The present study revealed that tumorigenic MCF-7 cells are more susceptible to growth inhibition as a result of *S. frutescens* plant extract treatment than non-tumorigenic MCF-12A cells.

The MTT assay utilizing a standard protocol for both cell lines was employed to measure the metabolic activity of vehicle-treated and *S. frutescens*-treated cells by measuring the

cellular dehydrogenase activity. Studies indicate that the reduced pyridine nucleotide cofactor, NADH, is responsible for most MTT reduction and MTT reduction is associated not only with mitochondria, but also with the cytoplasm and with non-mitochondrial membranes including the endosome/lysosome compartment and the plasma membrane [228,229]. NADH is produced in cells through glycolysis in the cytoplasm and the tricarboxylic acid cycle in mitochondria, therefore the reduction of MTT to purple formazan crystals is an indication of metabolic activity. Metabolic activity was inhibited by *S. frutescens* extracts in a dose-dependent manner in tumorigenic MCF-7 and non-tumorigenic MCF-12A cells. 1.5mg/ml *S. frutescens* extracts inhibited metabolic activity relative to the vehicle-treated control to 19% in MCF-7 cells and 72% in MCF-12A cells, thereby confirming the results at the 1.5mg/ml concentration level found by cell growth studies employing the crystal violet staining method. However, at concentrations lower than 1.5mg/ml, *S. frutescens* extracts had a greater negative effect on metabolic activity than on growth in MCF-7 and MCF-12A cells. Discrepancies between the MTT assay and other measures of cell growth have been observed [229]. Liu *et al.* (1997) demonstrated that cellular MTT reduction is confined to perinuclear vesicles including endosomes/lysosomes and the reduced formazan are transported to the cell surface through exocytosis [229]. Therefore, the reduced MTT reduction at lower concentrations can be explained through either in an increase in endosomal/lysomal activity, an increase in exocytosis and/or reduced intracellular NADH concentrations as a result of impaired glycolysis and/or mitochondrial dehydrogenase activity.

The 1.5mg/ml *S. frutescens* extract concentration was employed in all subsequent studies for both cell lines in order to determine the differential effects of *S. frutescens* extracts. The concentration is the same ethanolic plant extract concentration employed by Stander *et al.* (2007) and three times less than the MCF-7 cell line IC_{50} ethanolic tablet extract concentration used by Tai *et al.* (2005) (32,38). Morphological studies were employed in order to determine the effect that 1.5mg/ml *S. frutescens* plant extract has on tumorigenic MCF-7 and non-tumorigenic MCF-12A cells. Morphological characteristics of cytoplasmic shrinking, hypercondensed chromatin and vacuolarization were observed in both cell lines with H&E staining after 48h treatment of 1.5mg/ml *S. frutescens* plant

extract. However, these characteristics were more pronounced in the MCF-7 cell line when compared to the MCF-12A cell line. These findings are consistent with the observations made by Chinkwo (2005) whereby a 3.5mg/ml plant water extract of *S. frutescens* resulted in vacuolated CHO and Caski cells with condensed nuclei after 24h of treatment [33]. Cytoplasmic shrinking, hypercondensed chromatin and autophagic vacuoles are morphological characteristics of increased autophagic activity, as well as apoptosis in cells [149]. Observations of autophagy have not been associated with *S. frutescens*-treated cells in previous studies, therefore further studies where employed in order to determine whether autophagic activity was present or increased in *S. frutescens*-treated cells.

Acridine orange was employed during fluorescent microscopy as a lysosomotropic fluorescent compound that serves as a tracer for acidic vesicular organelles including autophagic vacuoles and lysosomes. An increase in acridine orange cytoplasmic staining of MCF-7 and MCF-12A cells was observed after 48h treatment of *S. frutescens* plant extracts, indicating either increased autophagic or lysosomal activity or both. Increased vacuolarization was observed, however, the vacuoles did not have an affinity for acridine orange. These observations can in part explain the reduced MTT at lower concentrations whereby an increase in endosomal/lysomal activity will have an effect on MTT reduction at *S. frutescens* plant extract concentrations below 1.5mg/ml without affecting cell growth.

Autophagic activity was confirmed by transmission electron microscopy in MCF-7 and MCF-12A cells. Increased autolysosomal and endosomal formation was observed after 48h treatment of 1.5mg/ml *S. frutescens* plant extracts in both cell lines and was more pronounced in MCF-7 cells. Increased vacuole formation was also observed in both cell lines and the vacuolarization was more prominent in *S. frutescens*-treated MCF-7 cells. Scanning electron microscopy confirmed observation of cytoplasmic shrinking in both cell lines after 48h treatment to *S. frutescens* plant extracts. These are the first observations of autophagy attributed to *S. frutescens* extracts and provide an additional mechanism of growth inhibition together with apoptosis and possibly cell cycle arrest.

Cell cycle analyses determined that a greater fraction of the dividing cells of MCF-7 as well as MCF-12A cells were in the G_2/M fraction after 48h treatment with 1.5mg/ml *S. frutescens* plant extracts. Consequently, a lower fraction of the cells were in the G_1 fraction. The increase in the G_2/M fraction of MCF-7 treated cells was more than two-fold (from 16.05% to 38.68%), while the increase in MCF-12A cells where from 24.45% to 36.98%.

Mitotic indices indicated an increase in the number of cells with morphological characteristics of prophase and a decrease in the number cells with morphological characteristics of metaphase, anaphase and telophase in both *S. frutescens*-treated cell lines. The observations of increased numbers of cells in prophase and an increase in the number of cells with an elevated DNA content (G_2/M) in both cell lines leads to the conclusion of a possible intra-S-phase block as a result of unreplicated DNA caused by inadequate DNA replication, or as a result of DNA damage or both. Unreplicated and damaged DNA is sensed by sensor proteins (*e.g.* ATM/ATR) that transduce the signal to effector proteins (*e.g.*CHK1/2, CDC25A) that induce cell cycle arrest and prevents cells from entering mitosis in order to complete DNA replication and repair damaged DNA. DNA polymerases (*e.g.* poly (ADP-ribose) polymerase family members 1 and 2), human replication protein A, PCNA and topoisomerases play important roles in DNA replication, DNA repair and cell cycle control and are possible candidates of proteins whose activity might be affected by *S. frutescens* plant extracts.

Possible mechanisms of growth inhibition include apoptosis, cell cycle arrest, autophagy, oncosis, metabolic catastrophe and mitotic catastrophe. Hallmarks of autophagy and cell cycle arrest have been observed in *S. frutescens*-treated MCF-7 and MCF-12A cells. Chinkwo (2005) reported hallmarks of apoptosis in CHO, Caski and Jurkat T lymphoma cells after treatment with 3.5mg/ml *S. frutescens* plant water extracts [33]. Tai *et al.* (2005) on the other hand found a statistically insignificant increase in the apoptosis/death fraction during cell cycle analysis in MCF-7 breast tumor cells treated with a 1/200 (0.68mg/ml) dilution of an ethanolic *S. frutescens* tablet extract [32]. These results

indicate a possible difference in the mechanism of action between ethanolic and water extracts of *S. frutescens*. Stander *et al.* (2007) reported an increase in the number of cells exhibiting morphological characteristics of apoptosis and hypothesized that it might be as a result of increased intracellular levels of ceramide attributed to the increased expression of neutral sphingomyelinase-2 [38]. However, the morhological characteristics of hypercondensed chromatin and cytoplasmic shrinking observed by Stander *et al.* (2007) are also hallmarks of autophagy [38,149]. In addition, ceramide is able to induce autophagy by inhibiting the mTOR activating activities of protein kinase B/Akt, and several genes involved in the positive regulation of apoptosis including, tumor necrosis factor receptor superfamily, member 10a (TNFRSF10A), tumor necrosis factor receptor superfamily, member 10b (AF018658) and caspase recruitment domain family, member 11 (CARD11), were down-regulated in response to *S. frutescens* treatment [38]. It is therefore conceivable to reinterpret the morphological studies from Stander *et al.* (2007) as hallmarks of autophagy. In the present study, apoptosis analyses revealed a statistically insignificant decrease in early and late apoptosis in *S. frutescens*-treated MCF-7 cells and the population of *S. frutescens*-treated MCF-12A cells shifted slightly towards early apoptosis with a slight increase in early apoptosis and a decrease in late apoptosis. Also, cell cycle analysis revealed an increase in the sub-G_1 fraction in *S. frutescens*-treated MCF-12A cells, confirming the apoptosis analyses. Insignificant differences in the sub-G_1 fraction observed in *S. frutescens*-treated MCF-7 cells confirmed the apoptosis analysis and are consistent with the findings of Tai *et al.* (2005) [32]. These findings indicate that apoptosis plays a part in growth inhibition in *S. frutescens*-treated MCF-12A cells and an insignificant part in growth inhibition in *S. frutescens*-treated MCF-7 cells.

Gene expression analyses using microarrays revealed a global down-regulation of genes in *S. frutescens*-treated MCF-7 and MCF-12A cells when compared to vehicle-treated cells. Microarrays, as implemented in the present study, measure the relative amounts of polyadenylated mRNA between *S. frutescens*-treated and vehicle-treated control cells at the time of termination. Cytoplasmic and nuclear mRNA levels of specific genes are controlled by transcription factors and various post-transcriptional regulatory mechanisms including mRNA splicing, mRNA polyadenylation and capping, mRNA

trafficking, mRNA stability [231]. Thus transcriptional and post-transcriptional modification of mRNA will dictate intracellular levels of mRNA. Heterogeneous nuclear ribonucleoprotein D (HNRPD) is involved in post-transcriptional regulation of mRNA and was up-regulated in MCF-12A cells in response to *S. frutescens* extracts. HNRPD binds to and destabilizes AU-rich element mRNAs, such as those of c-myc [232]. c-Myc (MYC) expression is also positively regulated by the E2F transcription factor [233]. Thus, the observations of up-regulated HNRPD and down-regulated E2F transcription factor 2 (E2F2) can in part explain the down-regulated c-Myc expression observed in *S. frutescens*-treated MCF-12A cells. In *S. frutescens*-treated MCF-7 cells the MYCL1 oncogene was down-regulated. Deregulated Myc transcription factor expression is often associated with aggressive, poorly differentiated tumors in a wide range of human cancers and has also been reported to regulate as many as 10% to 15% of all cellular genes [234,235]. Myc proteins are a group of transcription factors that regulate a variety of cellular processes including cell growth and proliferation and cell cycle progression and various strategies are aimed at targeting myc transcription factors for cancer treatment [234]. Stander *et al.* (2007) reported the down-regulation of v-myc myelocytomatosis viral oncogene homolog 2 (MYCL2) in MCF-7 cells after 24h of *S. frutescens* exposure [38]. Therefore, down-regulation of myc genes associated with *S. frutescens* treatment is likely to play an important role in growth inhibition associated with *S. frutescens*.

Several genes involved in regulation of transcription were down-regulated in both cell lines in response to *S. frutescens* exposure. Of particular interest is CCAAT/enhancer binding protein beta (C/EBPB) and the Jun D proto-oncogene (junD). Increased expression of C/EBPB has been detected in breast cancer, ovarian tumors, and colorectal tumors [236,237]. C/EBPB has been shown to be required for Ras-mediated tumorigenesis in the skin and C/EBPB expression was identified as a general feature of tumors with cyclin D1 overexpression [238,239]. Kundu *et al.* (2005) concluded that methanol extracts of *S. frutescens* inhibited TPA-induced COX-2 expression in mouse skin, which appeared to be mediated by the inhibition of the activation of activator protein 1 (AP-1) and CREB [31]. The 5'-untranslated region of the human COX-2

promoter gene harbors binding sites for several transcription factors including C/EBPB [240]. The C/EBP site plays an important role in COX-2 transcriptional activation and is a key transactivator for COX-2 expression induced by proinflammatory mediators [240]. Therefore attenuation of C/EBPB activity as a result of decreased expression caused by *S. frutescens*-extracts may play a role in mammary epithelial cell proliferation as well as the anti-inflammatory properties associated with *S. frutescens*-extracts. The JunD proto-oncogene,

down-regulated in both cell lines, binds to an AP-1 site and upon cotransfection stimulates the activity of a promoter that bears an AP-1 site [241]. The expression and activity of junD is linked to breast cancer cell motility and invasiveness and the functional involvement of AP-1 activity in cancer invasion is evident in the regulation of metalloproteinase (MMP) gene expression [242,243]. Stander *et al.* (2007) reported the down-regulation of several MMP's and in the present study, disintegrin and metalloprotease domain 23 (AY545641) was down-regulated in *S. frutescens*-treated MCF-7 cells and matrix metalloproteinase 3 (stromelysin 1, progelatinase) (MMP3) was down-regulated in *S. frutescens*-treated MCF-12A cells, while disintegrin-like and metalloprotease (reprolysin type) with thrombospondin type 1 motif, 20 (ADAMTS20) was up-regulated in both cell lines after *S. frutescens* exposure [38]. MMPs are a family of zinc endopeptidases capable of digesting various extracellular matrix components and control cell migration, proliferation and apoptosis and regulate tumor expansion, angiogenesis and dissemination [244]. Attenuation of junD expression as a result of *S. frutescens* treatment might play a role in the in MMP activity and expression. Mitogen-activated protein kinase kinase kinase 2 (MAP3K2) phosphorylates and activates two distinct MAP kinase kinases, MKK4 and MKK7, which in turn phosphorylate the janus kinases (JNK), leading to the activation of several transcription factors, including junD [245]. *S. frutescens* treatment of MCF-7 cells resulted in the down-regulation of MAP3K2, possibly abrogating junD activity.

The observations of autophagy, cytoplasmic shrinking and the global down-regulation of genes, including several ribosomal proteins, in both cell lines after *S. frutescens* treatment implicate the mTOR kinase as a possible modulator of the observations. Also, Tuberous

sclerosis 2 (TSC2) and Phosphatase and tensin homolog (mutated in multiple advanced cancers 1) (PTEN) where up-regulated after *S. frutescens* treatment in MCF-7 and MCF-12A cells respectively. Active TSC2 and PTEN are able to attenuate the activity of mTOR. The mTOR kinase positively regulates cell growth and its inhibition causes a large decrease in cell size [157]. The raptor branch of the mTOR (mTORC1) pathway modulates a number of major processes, including mRNA translation, ribosome biogenesis, nutrient metabolism and autophagy [157]. S6 Kinase 1 (S6K1) and eukaryotic translation initiation factor 4E-binding protein 1 (4E-BP1) link mTORC1 to the control of mRNA translation. Active mTORC1 phosphorylates and activates the S6 Kinase 1 at Thr389 and leads to an increase in cell proliferation and protein synthesis by controlling translation [246]. mTORC1 also phosphorylates 4E-BP1, preventing it from interacting with and inhibiting the eukaryotic translation initiation factor 4 gamma, 1 (eIF-4G) protein and thereby inducing cap-dependent mRNA translation [246]. The ability of mTOR kinase to phosphorylate a p70S6K-GST fusion protein at Thr389 was evaluated with an ELISA. In both cell lines the, mTOR kinase was attenuated after *S. frutescens* treatment, confirming it as a modulator of the observations caused by *S. frutescens*.

Several genes involved in DNA repair were differentially expressed in both cell lines in response to *S. frutescens* exposure including Poly (ADP-ribose) polymerase family, member 2 (PARP-2) (down-regulated in both cell lines) PCNA (down-regulated in MCF-7 cells) and growth arrest and DNA-damage-inducible, beta (GADD45B) (up-regulated in MCF-12A cells). PARP-2 is stimulated by DNA strand breaks during replication and acts as a chromatin modifier by targeting DNA gaps for repair and thus is involved in the maintenance of genomic integrity [247]. Dysfunctional PARP-2 sensitizes cells to DNA damage during replication and can causes dividing cells to accumulate in G_2/M phase [246]. PCNA is the "ringmaster of the genome" [248]. It is a circular sliding clamp protein and plays a crucial part during DNA replication by providing a scaffold for consecutive attachment of various DNA nucleases, DNA polymerases, DNA ligases and others [247]. PCNA also plays a crucial role in DNA repair. Another differentially expressed gene of interest is growth arrest and DNA-damage-inducible, beta (GADD45B). Transcript levels of GADD45B are normally increased following stressful

conditions and after DNA damage [249]. Following DNA damage GADD45B forms complexes with PCNA and interacts with several p53-regulated proteins (*e.g.* p21, p57) resulting in cell cycle arrest [248]. GADD45B is also able to attenuate JNK kinase signaling by inhibiting MKK7 signaling [247]. Therefore, the observed accumulation of cells in the G_2/M phase in both cell lines after *S. frutescens* treatment can be explained by the activation of the DNA damage checkpoint as a result of abrogated DNA replicating and repair mechanisms.

Finally, it is suggested that apoptosis seems to play a less significant role in growth inhibition of MCF-7 cells after *S. frutescens* exposure. This can in part be explained by the up-regulation of Cystatin A (CSTA) in response to *S. frutescens* extracts. CSTA is a cysteine protease inhibitor capable of considerably suppressing the activity of caspase 3 and thus blocks caspase-dependent apoptosis [250]. The up-regulation of CSTA in MCF-7 cells but, not in MCF-12A cells in response to *S. frutescens* extracts can in part explain the difference in cell death responses between the cell lines.

Another traditional medicinal plant, *Astragalus membranaceus*, native to northern China, is regarded as one of the most important Chinese herbs [251]. It is commonly used as a tonic to manage conditions of fatigue, loss of appetite and diarrhea and generally to enhance the body's natural defense [251]. *S. frutescens* is a taxonomically related species also belonging to the *Astragalinae* subtribe of the *Fabaceae* family [252,253]. Both plants exhibit anti-diabetic, anti-oxidant, anti-inflammatory, antimicrobial, anti-cancer and immune modulatory properties [20,25,31,32,254,255,256,257,258,259]. In addition, several biologically active compounds are present in both plants, including GABA, L-canavanine, cycloartane triterpene glycosides, and β-sitosterols [32,260,261]. Shen *et al.* (2006) showed that a number of isoflavones present in *A. membranaceus* display dual PPARα and PPARγ agonist activity [262].

PPARs are ligand-activated transcription factors that belong to the nuclear-hormone-receptor family [263]. Three isotypes have been identified; PPARα, PPARβ/δ and PPARγ [263]. Activation of PPARα by its ligands promotes lipid metabolism and thus has a

hypolipidemic action towards affected tissues [264]. Also, PPARα agonists have anti-inflammatory effects due to the inhibition of the C/EBPB pathway and are also able to repress the transcriptional NF-κB and AP-1 pathways [265]. PPARγ agonists exert anti-carcinogenic effects in many different cell types, due to its anti-proliferation, pro-differentiation and pro-apoptotic properties [266]. In addition, PPARγ agonists display hypoglycemic and anti-inflammatory properties [264]. The dual PPARα/γ agonist, troglitazone, is able to inhibit p70S6K-mediated protein synthesis through a PP2A-dependent pathway [267]. Pioglitazone, a PPARγ specific agonist, is able to induce accumulation of ceramide in the rat heart and WY-14643, a PPARα specific agonist, is able to induce *de novo* synthesis of ceramide in the rat heart [268,269]. Furthermore, PPARγ agonists are able up-regulate the tumor suppressor PTEN in several cell lines, including the MCF-7 cell line, the human promyeloid leukemia HL-60 cell line, the human hepatocarcinoma BEL-7404 cell line and the human lung carcinoma A549 cell line [270,271,272,273].

Therefore, the possibility exist that isoflavonoic compounds that act as PPARα and/or PPARγ agonists might be present in *S. frutescens* extracts, given that *A. membranaceus* and *S. frutescens* are taxonomically related species and dual PPARα and PPARγ agonists are present in *A. membranaceus*. Both plants exhibit similar *in vitro* properties and mimic properties associated with PPARα and PPARγ agonists. It is also possible that other biological compounds present in *S. frutescens* extracts work in synergy to yield its biological effects, however further research needs to be conducted in order to isolate and characterize the possible active compounds, including possible PPAR agonists.

Thus, *S. frutescens* extracts inhibit growth in tumorigenic MCF-7 and non-tumorigenic MCF-12A cells in a dose-dependent manner with the MCF-7 cell line being the more susceptible of the two lines. Induction of autophagy and a G_2/M cell cycle arrest as a result of DNA damage caused by impaired DNA replication and repair mechanisms are likely to play an important part in the growth inhibitory properties of *S. frutescens* extracts. Abrogated mTOR kinase activity as a result of *S. frutescens*

treatment in both cell lines is suggested to be a central mediator in inducing autophagy, suppressing gene expression and inhibiting ribosome biogenesis.

Chapter 5

5. Conclusion

In conclusion, *S. frutescens* extracts inhibited cell proliferation in both tumorigenic MCF-7 and non-tumorigenic MCF-12A cells in a dose-dependent manner. The MCF-7 cells were shown to be more susceptible to the effects of these extracts compared to the non-tumorigenic cells. Induction of autophagy and a G_2/M cell cycle arrest as a result of DNA damage caused by impaired DNA replication and repair mechanisms play an important part in the growth inhibitory properties of *S. frutescens* extracts. In addition, abrogated mTOR kinase activity as a result of *S. frutescens* treatment in both cell lines can be regarded as a central mediator in inducing autophagy, suppressing gene expression and inhibiting ribosome biogenesis.

Understanding of *in vitro* molecular mechanisms of *S. frutescens* enables researchers to focus on affected cellular mechanisms and identify active compounds with subsequent evaluation as possible candidates for use in anticancer therapy. Several questions regarding *S. frutescens* extracts action mechanism, its basis for differential effects on tumorigenic and non-tumorigenic cells remain unanswered. The possibility exists that biological compounds present in *S. frutescens* extracts may act in synergy to yield these effects, however, further research needs to be conducted in order to isolate and characterize the possible active compounds. The current study contributes to the unraveling of the *in vitro* molecular mechanisms and signal transduction associated with 70% ethanolic *S. frutescens* extracts, providing a basis for further research on this multi-purpose medicinal plant in Southern Africa.

6. References

1. Funahashi A, Tanimura N, Morohashi M. Kitano H. CellDesigner: a process diagram editor for gene-regulatory and biochemical networks. BIOSILICO 2003;1:159-162.

2. Sauro HM, Hucka M, Finney A, Wellock C, Bolouri H, Doyle J, *et al.* Next generation simulation tools: the Systems Biology Workbench and BioSPICE integration. OMICS. 2003;7(4):355-372.

3. World Health Organization. Traditional medicine, Report by the Secretariat. World Health Organization. [http://www.who.int/en/]. c2007 [updated 2007 Nov 26; cited 2007 Nov 26]. Available from http://www.who.int/gb/ebwha/pdf_files/EB111/eeb1119.pdf.

4. Gilani AH, Rahmanb A. Trends in ethnopharmacology. J Ethnopharmacol 2005;100:43-49.

5. Hartwell J.L. Plants Used Against Cancer. Lawrence, Massachusetts: Quarterman Publications, Inc. 1982.

6. Cragg GM, Newman DJ. Plants as a source of anticancer agents. J Ethnopharmacol 2005;100:72-79.

7. Cassady JM, Douros JD. Anticancer Agents Based on Natural Product Models. New York: Academic Press, 1980.

8. Arnold, TH, de Wet, BC, 1993. Plants of Southern Africa: Names and Distribution. Memoirs of the Botanical Survey of South Africa No 62. National Botanical Institute, Pretoria.

9. Mulholland DA. The future of ethnopharmacology, a southern African perspective. J Ethnopharmacol 2005;100:124-126.

10. Rindl M. Preliminary note on a poisonous alkaloid from the overground portions of the Transvaal yellow bulb *Homeria pallida*. Trans R Soc of SA 1924;11: 251-256.

11. Theiler A. Stiff sickness in cattle. Agric J Un SA. 1911;1:10-21.

12. Vahrmeyer J. Gifplante van Suider Afrika. Kaapstad: Tafelberg Uitgewers, 1982.

13. Hutcheon D. Vermeersiekte or vomit sickness of sheep. Agric J Cape of Good Hope 21:39-40.

14. Marais JSC. Monofluoro-acetic acid, the toxic principle of "gifblaar", *Dichapetalum cymosum*. Onderstepoort J Vet Sci Animal Ind 1944;20:67-73.

15. Cragg GM, Kingston DGI, Newman DJ. Anticancer Agents from Natural Products. Boca Raton, Florida: Brunner-Routledge Psychology Press, Taylor & Francis Group, pp. 23-46.

16. Li Q, Sham HL. Discovery and development of antimitotic agents that inhibit tubulin polymerisation for the treatment of cancer. Expert Opin Ther Pat 2002;12:1663-1701.

17. Van Wyk BE, Gericke, N. People's plants: a guide to useful plants of southern Africa. Pretoria: Briza Publications 2000; pp. 153-155.

18. Van Wyk BE, Van Oudtshoorn B, Gericke, N. Medicinal plants of South Africa. Pretoria: Briza Publications 1997; pp. 246-247.

19. Seier J, Mdhluli M, Dhansay M, Loza J, Laubscher R. A toxicity study of *Sutherlandia* leaf powder (*Sutherlandia microphylla*) consumption. Tygerberg (South Africa): Medical Research Council; 2002.
20. Ojewole JA. Analgesic, antiinflammatory and hypoglycemic effects of *Sutherlandia frutescens* R. BR. (variety Incana E. MEY.) [*Fabaceae*] shoot aqueous extract. Methods Find Exp Clin Pharmacol 2004;26(6):409-441.

21. Johnson Q, Syce J, Nell H, Rudeen K, Folk WR. A Randomized, Double-Blind, Placebo-Controlled Trial of Lessertia frutescens in Healthy Adults. PLoS Clin Trials 2007;27;2(4):e16.

22. Morris K. Treating HIV in South Africa, a tale of two systems. The Lancet 2001;357:1190.

23. Harnett SM, Oosthuizen V, Van de Venter M. Anti-HIV activities of organic and aqueous extracts of *Sutherlandia frutescens* and *Lobostemon trigonus*. J Ethnopharmacol 2005;96:113-119.

24. Mills E, Fosterb BC, Van Heeswijkc R. Impact of African herbal medicines on antiretroviral metabolism. Research Letters:AIDS 2005;19:93-99.

25. Fernandez C, Cromarty AD, Albrecht C, Constance E, van Rensburg J. The antioxidant potential of *Sutherlandia frutescens*. J Ethnopharmacol 2004;95:1-5.

26. Valko M, Leibfritz D, Moncol J, Cronin MT, Mazur M, Telser J. Free radicals and antioxidants in normal physiological functions and human disease. Int J Biochem Cell Biol 2007;39(1):44-84.

27. Surh YJ. Cancer chemoprevention with dietary phytochemicals, Nature Rev Cancer 2003;3:768-780.

28. Wai K. Leung, KA. Cyclooxygenase-2 upregulates vascular endothelial growth factor expression and angiogenesis in human gastric carcinoma. Intl Journal of Oncology 2003;23:1317-1322.

29. Dannenberg AJ, Altorki NK, Boyle JO, Dang C, Howe LR, Weksler BB, Subbaramaiah K. Cyclo-oxygenase 2: a pharmacological target for the prevention of cancer. Lancet Oncol 2001;2:544-551.

30. Surh YJ, Chun KS, Cha HS. Han, S, Keum YS, Park KK, Lee SS. Molecular mechanisms underlying chemopreventive activities of anti-inflammatory phytochemicals: down-regulation of COX-2 and iNOS through suppression of NF-kB activation. Mutat Res 2001;480:243-268.

31. Kundu JK, Mossanda KS, Na HK. Inhibitory effects of the extracts of *Sutherlandia frutescens* (L.) R. Br. and *Harpagophytum procumbens* DC. on phorbol ester-induced COX-2 expression in mouse skin: AP-1 and CREB as potential upstream targets. Cancer Lett 2005;218:21-31.

32. Tai J, Cheung S, Hasman D. *In vitro* culture studies of *Sutherlandia frutescens* on human tumor cell lines. J Ethnopharmacol 2004;93(1):9-19.

33. Chinkwo KA. *Sutherlandia frutescens* extracts can induce apoptosis in cultured carcinoma cells. J Ethnopharmacol 2005;98:163-170.

34. Bence AK, Crooks PA. The mechanism of L-Canavanine cytotoxicity: Arginyl tRNA Synthesase as a novel target for anticancer drug discovery. J Enzyme Inhib Med Chem 2003;18(5):383-394.

35. Sparg SG, Light ME van Staden J. Biological activities and distribution of plant saponins. J Ethnopharmacol 2004;94:219-243.

36. Lui J, Henkel T. Traditional Chinese Medicine (TCM): Are polyphenols and saponins the key ingredients triggering biological activities? Curr Med Chem 2002;9:1483-1485.

37. Awad AB, Fink CS. Phytosterols as anticancer dietary components: Components and mechanism of action. J Nutr 2000;130(9):2127-2130.

38. Stander BA, Marais S, Steynberg TJ, Theron D, Joubert F, Albrecht C, *et al.* Influence of *Sutherlandia frutescens* extracts on cell numbers, morphology and gene expression in MCF-7 cells. J Ethnopharmacol 2007 Jun 13;112(2):312-318.

39. Liu B, Yang R, Wong K.A, Getman C, Stein N, Teitell MA, *et al.* Negative regulation of NF-kappaB signaling by PIAS1. Mol Cell Biol 2005;3:1113-1123.

40. Robinson K, Vona-Davis L, Riggs D, Jackson B, McFadden D. Peptide YY attenuates STAT1 and STAT3 activation induced by TNF-alpha in acinar cell line AR42J. J Am Coll Surg 2006;5:788-796.

41. Stephanou A, Latchman DS. STAT-1: a novel regulator of apoptosis Int J Exp Pathol 2003;6:239-244.

42. Wajant H.TRAIL and NFκB signaling, a complex relationship. Vitam Horm 2004;67:101-132.

43. Marchesini N, Osta W, Bielawski J, Luberto C, Obeid LM, Hannun, YA. Role for mammalian neutral sphingomyelinase 2 in confluence-induced growth arrest of MCF-7 cells. J Biol Chem 2004;24:25101-25111.

44. Miller ME, Cross FR. Cyclin specificity: How many wheels do you need on a unicycle? J Cell Sci 2001;114:1811-1820.

45. Morgan DO. Cyclin-dependent kinases. Engines, clocks, and microprocessors. Annu Rev Cell Dev Biol 1997;13:261-291.

46. Bates S, Bonetta L, MacAllan D. CDK6 (PLSTIRE) and CDK4 (PSK-J3) are a distinct subset of the cyclin-dependent kinases that associate with cyclin D1. Oncogene 1994;9:71-79.

47. Koff A, Cross F, Fisher A, Schumacher J, Leguellec K, Philippe M, *et al.* Human cyclin E, a new cyclin that interacts with two members of the CDC2 gene family. Cell 1991;66:1217-1228.

48. Draetta G, Luca F,Westendorf J, Brizuela L, Ruderman J, Beach D. Cdc2 protein kinase is complexed with both cyclin A and B: Evidence for proteolytic inactivation of MPF. Cell 1989;56:829-838.

49. Rolfe M, Chiu MI, Pagano M The ubiquitin-mediated proteolytic pathway as a therapeutic area. J Mol Med 1997;75:5-17.

50. Lolli G, Johnson LN. CAK-Cyclin-dependent Activating Kinase: a key kinase in cell cycle control and a target for drugs? Cell Cycle. 2005 Apr;4(4):572-577.

51. Deshaies RJ. SCF and Cullin/Ring H2-based ubiquitin ligases. Annu Rev Cell Dev Biol 1999;15:435-467.

52. Morgan DO. Regulation of theAPC and the exit from mitosis. Nat Cell Biol 1999;1:E47-E53.

53. Castro A, Bernis C, Vigneron S, Labbe JC, Lorca T. The anaphase-promoting complex: a key factor in the regulation of cell cycle. Oncogene 2005;24:314-325.

54. Sarkar FH, Li Y. Cell signaling pathways altered by natural chemopreventive agents. Mutat Res 2004;555(1-2):53-64.

55. Massagué J. G1 cell-cycle control and cancer. Nature 2004;432(7015):298-306.

56. Adams PD. Regulation of the retinoblastoma tumor suppressor protein by cyclin/cdks. Biochim Biophys Acta 2001;1471:123-133.

57. Sladek TL. E2F transcription factor action, regulation, and possible role in human cancer. Cell Prolif 1997;30:97-105.

58. Giacinti C, Giordano A. RB and cell cycle progression. Oncogene 2006;28;25(38):5220-5227.

59. Chan HM, Krstic-Demonacos M, Smith L, Demonacos C, La Thangue NB. Acetylation control of the retinoblastoma tumoursuppressorprotein. Nat Cell Biol 2001;3:667-674.

60. Sherr CJ, Roberts JM. CDK inhibitors: Positive and negative regulators of G_1-phase progression. Genes Dev 1999;13:1501-1512.

61. Knudsen ES, Buckmaster C, Chen TT, Feramisco JR, Wang JYJ. Inhibition of DNA synthesis by RB: Effects on G1/S transition and S-phase progression. Genes Dev 1998;12:2278-2292.

62. Pietenpol JA, Kastan MB. Control of the cell cycle. In: Abeloff MD, Armitage JO, Niedehuber JE, Kastan MB, McKenna WG, editors. Clinical Oncology. New York:Elsevier/Churchill Livingstone; 2004 pp. 1-20.

63. Bell, S. P. & Dutta, A. DNA replication in eukaryotic cells. A. Rev. Biochem 2002;71:333-374.

64. Henneke, G., Koundrioukoff, S. & Hubscher, U. Multiple roles for kinases in DNA replication. EMBO Rep 2003;4:252-256.

65. Lei M, Tye BK. Initiating DNA synthesis: from recruiting to activating the MCM complex. J Cell Sci 2001;114(Pt 8):1447-1454.

66. Morgan DO. Principles of CDK regulation. Nature 1995;374:131-134.

67. Ferrari S. Protein kinases controlling the onset of mitosis. Cell Mol Life Sci 2006;63(7-8):781-795.

68. Nigg EA. Mitotic kinases as regulators of cell division and its checkpoints. Nat Rev Mol Cell Biol 2001;2(1):21-32.

69. Hermeking H, Benzinger A. 14-3-3 proteins in cell cycle regulation. Semin Cancer Biol 2006;16(3):183-92.

70. Dai W, Huang X, Ruan Q. Polo-like kinases in cell cycle checkpoint control. Front Biosci 2003;8:d1128-d1133.

71. Nigg EA. Cyclin-dependent protein kinases: key regulators of the eukaryotic cell cycle. BioEssays 1995;17:471-480.

72. Kimura K, Hirano M, Kobayashi R. Phosphorylation and activation of 13S condensin by Cdc2 *in vitro*. Science 1998;282:487-490.

73. Lowe M. Cdc2 kinase directly phosphorylates the cis-Golgi matrix protein GM130 and is required for Golgi fragmentation in mitosis. Cell 1998;94:783-793.

74. Rubin CI, Atweh GF. The role of stathmin in the regulation of the cell cycle. J Cell Biochem 2004;93(2):242-250.

75. Kramer ER, Scheuringer N, Podtelejnikov AV, Mann M, Peters JM. Mitotic regulation of the APC activator proteins CDC20 and CDH1. Mol Biol Cell 2000;11:1555-1569.

76. Hagting A, Karlsson C, Clute P, Jackman M, Pines J. MPF localization is controlled by nuclear export. EMBO J 1998;17(14):4127-4138.

77. Baker DJ, Dawlaty MM, Galardy P, van Deursen JM. Mitotic regulation of the anaphase-promoting complex. Cell Mol Life Sci 2007;64(5):589-600.

78. Kraft C, Herzog F, Gieffers C, Mechtler K, Hagting A, Pines J, Peters JM. Mitotic regulation of the human anaphase-promoting complex by phosphorylation. EMBO J 2003;22:6598-6609.

79. Golan, A., Yudkovsky, Y. and Hershko, A. The cyclinubiquitin ligase activity of cyclosome/APC is jointly activated by protein kinases Cdk1-cyclin B and Plk. J Biol Chem 2002;277:15552-15557.

80. Kotani S, Tugendreich S, Fujii M, Jorgensen PM, Watanabe N, Hoog C, *et al.* PKA and MPF-activated polo-like kinase regulate anaphase-promoting complex activity and mitosis progression. Mol Cell 1998;1:371-380.

81. Kramer ER, Scheuringer N, Podtelejnikov AV, Mann M, Peters JM. Mitotic regulation of the APC activator proteins CDC20 and CDH1. Mol Biol Cell 2000;11:1555-1569.

82. Visintin R, Craig K, Hwang ES, Prinz S, Tyers M, Amon A. The phosphatase Cdc14 triggers mitotic exit by reversal of Cdk-dependent phosphorylation. Mol Cell 1998;2:709-718.

83. Miller JJ, Summers MK, Hansen DV, Nachury MV, Lehman NL, Loktev, *et al.* Emi1 stably binds and inhibits the anaphase-promoting complex/ cyclosome as a pseudosubstrate inhibitor. Genes Dev 2006;20:2410-2420.

84. Hansen DV, Loktev AV, Ban KH, Jackson PK. Plk1 regulates activation of the anaphase promoting complex by phosphorylating and triggering SCFbetaTrCP-dependent destruction of the APC Inhibitor Emi1. Mol Biol Cell 2004 Dec;15(12):5623-5334.

85. Uhlmann F, Lottspeich F, Nasmyth K. Sisterchromatid separation at anaphase onset is promoted by cleavage of the cohesin subunit Scc1. Nature 1999;400:37-42.

86. Zur A. and Brandeis, M. Securin degradation is mediated by fzy and fzr, and is required for complete chromatid separation but not for cytokinesis. EMBO J 2001;20:792-801.

87. Hartwell LH, Weinert TA. Checkpoints: Controls that ensure the order of cell cycle events. Science 1989;246:629-634.

88. Ishikawa K, Ishii H, Saito T. DNA damage-dependent cell cycle checkpoints and genomic stability. DNA Cell Biol 2006;25(7):406-411.

89. Houtgraaf JH, Versmissen J, van der Giessen WJ. A concise review of DNA damage checkpoints and repair in mammalian cells. Cardiovasc Revasc Med 2006;7(3):165-172.

90. Niida H, Nakanishi M. DNA damage checkpoints in mammals. Mutagenesis 2006;21(1):3-9.

91. Lew DJ, Burke DJ. The spindle assembly and spindle position checkpoints. Annu Rev Genet 2003;37:251-282.

92. Baker DJ, Dawlaty MM, Galardy P, van Deursen JM. Mitotic regulation of the anaphase-promoting complex. Cell Mol Life Sci 2007;64(5):589-600.

93. Yu H. Structural activation of Mad2 in the mitotic spindle checkpoint: the two-state Mad2 model versus the Mad2 template model. J Cell Biol 2006;173(2):153-157.

94. Danial NN, Korsmeyer SJ. Cell death: critical control points. Cell 2004;116:205-219.

95. Green DR, Evan GI. A matter of life and death. Cancer Cell 2002;1:19-30.

96. Hanahan D, Weinberg RA. The hallmarks of cancer. Cell 2000;100:57-70.

97. Thompson CB. Apoptosis in the pathogenesis and treatment of disease. Science 1995;267:1456-1462.

98. Vaux DL, Flavell RA. Apoptosis genes and autoimmunity. Curr Opin Immunol 2000;12:719-724.

99. Hergartner MO. The biochemistry of apoptosis. Nature 2000;407:770-776.

100. Hail N Jr, Carter BZ, Konopleva M, Andreeff M. Apoptosis effector mechanisms: a requiem performed in different keys. Apoptosis 2006 Jun;11(6):889-904.

101. Saraste A. Morphological criteria and detection of apoptosis. Herz 1999;24:189-195.

102. Balasubramanian K, Mirnikjoo B, Schroit AJ. Regulated externalization of Phosphatidylserine at the Cell Surface: Implications for apoptosis. Biol Chem 2007;22;282(25):18357-18364.

103. Zimmerman KC, Bonzon C, Green DR. The machinery of programmed cell death. Pharmacol Ther 2002;92:57-70.

104. Bergeron L, Perez GI, Macdonald G. Defects in regulation of apoptosis in caspase 2 deficient mice. Genes Dev 1998;12:1304-1309.

105. Fernandes AT, Armstrong RC, Krebs J, Srinivasula SM, Wang L, Bullrich F. *In vitro* activation of CPP32, and Mch3 by Mch4, a novel human apoptotic cysteine protease containing two FADD like domains. Proc Natl Acad Sci USA. 1996;93:7464-7469.

106. Duan H, Orth K, Chinnaiyan AM, Poirer GG, Dixit VM. ICE/LAP6, a novel member of the ICE/ced 3 gene family, is activated by the cytotoxic T cell protease Granzyme. J Biol Chem 1996;271:16720-16724.

107. Hitomi J, Katayama T, Eguchi Y, Kudo T, Taniguchi M, Koyama Y, *et al.* Involvement of caspase-4 in endoplasmic reticulum. J Cell Biol 2004;165:347-356.

108. Sadowski DK, Coy JF, Mier W, Hug H, Los M. Caspases-their role in apoptosis and other physiological processes as revealed by knock out studies. Arch Immunol Ther Exp 2002;50(1):9-34.

109. Rupinder SK, Gurpreet AK, Manjeet S. Cell suicide and caspases. Vascul Pharmacol 2007;46:383-393.

110. Widlak P. The DFF40/CAD endonuclease and its role in apoptosis. Acta Biochim Pol 2000;47(4):1037-1044.

111. Ashkenazi A, Dixit V. Death receptors: signaling and modulation. 1998. Science 81:1305-1308.

112. Gupta S. Molecular signaling in death receptor and mitochondrial pathways of apoptosis (Review). Int. J Oncol 2003;22:15-20.

113. Philchenkov A. Caspase: potential targets for regulating cell death. J Cell Mol Med 2004;8:432-444.

114. Almasan A, Ashkenazi A. Apo2L/TRAIL: apoptosis signaling, biology, potential for cancer therapy. Cytokine Growth Factor Rev 2003;14(3-4):337-348.

115. Shklar G. Mechanism of cancer inhibition by anti-oxidant nutrients. Oral Oncol 1998;34:24-29.

116. Green DR, Kromer G. The pathophysiology of mitochondrial cell death. Science 2004;5684:626-629.

117. Aleo E, Henderson CJ, Fontanini A, Solazzo B. Identification of new compounds that trigger apoptosome independent Caspase activation. Cancer Res 2006;66(18):9235-244.

118. Li H, Zhu H, Xu C, Yuan J. Cleavage of BID by Caspase 8 mediates the mitochondrial damage in the Fas pathway of apoptosis. Cell 1998;94: 491-501.

119. Green DR. Apoptotic pathways: paper wraps stone blunts scissors. Cell 2000;7;102(1):1-4.

120. Ruvolo PP. Intracellular signal transduction pathways activated by ceramide and its metabolites. Pharmacol Res 2003;5:383-392.

121. Lin SS, Bassik MC, Suh H, Nishino M, Arroyo JD, Hahn WC, *et al.* PP2A Regulates BCL-2 Phosphorylation and Proteasome-mediated Degradation at the Endoplasmic Reticulum. J Biol Chem 2006;281(32):23003-23012.

122. Xin M, Deng X. Protein Phosphatase 2A Enhances the Proapoptotic Function of Bax through Dephosphorylation. J Biol Chem 2006;281(45):18859-18867.

123. Berridge MJ, Bootman MD, Roderick HL. Calcium signalling: dynamics, homeostasis and remodelling. Nat Rev Mol Cell Biol 2003;4(7):517-529.

124. Orrenius S, Zhivotovsky B, Nicotera P. Regulation of cell death: the calcium-apoptosis link. Nat Rev Mol Cell Biol 2003;4(7):552-565.

125. Szalai G, Krishnamurthy R, Hajnóczky G. Apoptosis driven by IP(3)-linked mitochondrial calcium signals. EMBO J 1999;18(22):6349-6361.

126. Wang HG, Pathan N, Ethell IM, Krajewski S, Yamaguchi Y, Shibasaki F, *et al.* Ca^{2+}-induced apoptosis through calcineurin dephosphorylation of BAD. Science 1999;284(5412):339-343.

127. Penzo D, Petronilli V, Angelin A, Cusan C, Colonna R, Scorrano L, *et al.* Arachidonic acid released by phospholipase A2 activation triggers Ca^{2+}-dependent apoptosis through the mitochondrial pathway. J Biol Chem 2004;279(24):25219-25225.

128. Nakagawa T, Yuan J. Cross-talk between two cysteine protease families. Activation of caspase-12 by calpain in apoptosis. J Cell Biol 2000;150:887-890.

129. Nakagawa T, Zhu H, Morishima N, Li E, Xu J, Yankner BA, *et al.* Caspase-12 mediates endoplasmic-reticulum-specific apoptosis and cytotoxicity by amyloid-beta. Nature 2000;403:98-103.

130. Oakes SA, Opferman JT, Pozzan T, Korsmeyer SJ, Scorrano L. Regulation of endoplasmic reticulum Ca^{2+} dynamics by proapoptotic BCL-2 family members. Biochem Pharmacol 2003;66(8):1335-1340.

131. Zong WX, Li C, Hatzivassiliou G, Lindsten T, Yu QC, Yuan J, *et al.* Bax and Bak can localize to the endoplasmic reticulum to initiate apoptosis. J Cell Biol 2003;162(1):59-69.

132. Johnson DE. Noncaspase proteases in apoptosis. Leukemia 2000 Sep;14(9):1695-1703.

133. Sorimachi H, Ishiura S, Suzuki K. Structure and physiological function of calpains. Biochem J 1997;328:721-732.

134. Sharif-Askari E, Alam A, Rhéaume E, Beresford PJ, Scotto C, Sharma K, *et al.* Direct cleavage of the human DNA fragmentation factor-45 by granzyme B induces caspase-activated DNase release and DNA fragmentation. EMBO J 2001 Jun 15;20(12):3101-3113.

135. Heibein JA, Goping IS, Barry M, Pinkoski MJ, Shore GC, Green DR, *et al.* Granzyme B-mediated cytochrome c release is regulated by the Bcl-2 family members bid and Bax. J Exp Med 2000 Nov 20;192(10):1391-1402.

136. Low RL. Mitochondrial Endonuclease G function in apoptosis and mtDNA metabolism: a historical perspective. Mitochondrion 2003 Mar;2(4):225-236.

137. Widlak P, Garrard WT. Discovery, regulation, and action of the major apoptotic nucleases DFF40/CAD and endonuclease G. J Cell Biochem 2005 Apr 15;94(6):1078-1087.

138. Majeski AE, Dice JF. Mechanisms of chaperone-mediated autophagy. Int J Biochem Cell Biol 2004;36:2435-2444.

139. de Waal EJ, Vreeling, Sindelarova H, Schellens JPM, Houtkooper JM, James J. Quantitative changes in the lysosomal vacuolar system of rat hepatocytes during short-term starvation: A morphometric analysis with special reference to macro- and microautophagy. Cell Tissue Res 1986;243:641-648.

140. Mariño G, López-Otín C. Autophagy: molecular mechanisms, physiological functions and relevance in human pathology. Cell Mol Life Sci 2004;61:1439-1454.

141. Majeski AE, Dice JF. Mechanisms of chaperone-mediated autophagy. Int J Biochem Cell Biol 2004 Dec;36(12):2435-2444.

142. Dice JF. Peptide sequences that target cytosolic proteins for lysosomal proteolysis. Trends Biochem Sci 1990 Aug;15(8):305-309.

143. Wing SS, Chiang HL, Goldberg AL, Dice JF. Proteins containing peptide sequences related to Lys-Phe-Glu-Arg-Gln are selectively depleted in liver and heart, but not skeletal muscle, of fasted rats. Biochem J 1991 Apr 1;275 (Pt 1):165-169.

144. Agarraberes FA, Dice JF. A molecular chaperone complex at the lysosomal membrane is required for protein translocation. J Cell Sci 2001 Jul;114(Pt 13):2491-2499.

145. Sattler T, Mayer A. Cell-free reconstitution of microautophagic vacuole invagination and vesicle formation. J Cell Biol 2000;151:529-538.

146. Seglen PO, Berg TO, Blankson H, Fengsrud M, Holen I, Stromhaug PE. Structural aspects of autophagy. Adv Exp Med Biol 1996;389:103-111.

147. Berg TO, Fengsrud M, Stromhaug PE, Berg T, Seglen PO. Isolation and characterization of rat liver amphisomes. Evidence for fusion of autophagosomes with both early and late endosomes. J Biol Chem 1998;273(34):21883-21892.

148. Eskelinen EL. Maturation of autophagic vacuoles in mammalian cells. Autophagy 2005;1(1):1-10.

149. Assuncao Guimaraes C, Linden R. Programmed cell deaths. Apoptosis and alternative deathstyles. Eur J Biochem 2004;271(9):1638-1650.

150. Inoki K, Corradetti MN, Guan KL. Dysregulation of the TSC-mTOR pathway in human disease. Nat Genet 2005;37:19-24.

151. Hay N. The Akt-mTOR tango and its relevance to cancer. Cancer Cell 2005;8:179-183.

152. Yorimitsu T, Klionsky DJ. Autophagy: molecular machinery for self-eating. Cell Death Differ 2005;12(2):1542-1552.

153. Kadowaki M, Karim MR, Carpi A, Miotto G. Nutrient control of macroautophagy in mammalian cells. Mol Aspects Med 2006;27(5-6):426-443.

154. Proud CG. Signalling to translation: how signal transduction pathways control the protein synthetic machinery. Biochem J 2007 403(2):217-234.

155. Arsham AM, Neufeld TP. Thinking globally and acting locally with TOR. Curr Opin Cell Biol 2006;18(6):589-597.

156. Inoki K, Zhu T, Guan KL. TSC2 mediates cellular energy response to control cell growth and survival. Cell 2003;115:577-590.

157. Sarbassov DD, Ali SM, Sabatini DM. Growing roles for the mTOR pathway. Curr Opin Cell Biol 2005;17:596-603.

158. Long X, Ortiz-Vega S, Lin Y, Avruch J. Rheb binding to mammalian target of rapamycin (mTOR) is regulated by amino acid sufficiency. J Biol Chem 2005;280:23433-23436.

159. 39. Kim DH, Sarbassov DD, Ali SM, King JE, Latek RR, Erdjument-Bromage H, *et al.* mTOR interacts with raptor to form a nutrient-sensitive complex that signals to the cell growth machinery. Cell 2002;110:163-175.

160. Nobukuni T, Joaquin M, Roccio M, Dann SG, Kim SY, Gulati P, *et al.* Amino acids mediate mTOR/raptor signaling through activation of class 3 phosphatidylinositol 3OH-kinase. Proc Natl Acad Sci USA 2005;102:14238-14243.

161. Kihara A, Kabeya Y, Ohsumi Y, Yoshimori T. Beclin-phosphatidylinositol 3-kinase complex functions at the trans-Golgi network. EMBO Rep 2001;2:330-335.

162. Pattingre S, Tassa A, Qu X, Garuti R, Liang XH, Mizushima N, *et al.* Bcl-2 antiapoptotic proteins inhibit Beclin 1-dependent autophagy. Cell 2005;122:927-939.

163. Tassa A, Roux MP, Attaix D, Bechet DM. Class III phosphoinositide 3-kinase -Beclin1 complex mediates the amino acid-dependent regulation of autophagy in C2C12 myotubes. Biochem J 2003;376:577-586.

164. Scarlatti F, Bauvy C, Ventruti A, Sala G, Cluzeaud F, Vandewalle A, *et al.* Ceramide-mediated Macroautophagy Involves Inhibition of Protein Kinase B and Upregulation of Beclin 1. J Biol Chem 2004;279(18):18384-18391.

165. Pattingre S, Bauvy C, Codogno P. Amino acids interfere with the ERK1/2-dependent control of macroautophagy by controlling the activation of Raf-1 in human colon cancer HT-29 cells. J Biol Chem 2003;278:16667-16674.

166. Arico S, Petiot A, Bauvy C, Dubbelhuis PF, Meijer AJ, Codogno P, *et al*. The tumor suppressor PTEN positively regulates macroautophagy by inhibiting the phosphatidylinositol 3-kinase/protein kinase B pathway. J Biol Chem 2001;276:35243-35246.

167. Feng Z, Zhang H, Levine AJ, Jin S. The coordinate regulation of the p53 and mTOR pathways in cells. Proc Nat Acad Sci USA 2005;102:8204-8209.

168. Tsuneoka M, Umata T, Kimura H, Koda Y, Nakajima M, Kosai K, *et al*. c-myc induces autophagy in rat 3Y1 fibroblast cells. Cell Struct Funct 2003;28:195-204.

169. Komata T, Kanzawa T, Takeuchi H, Germano IM, Schreiber M, Kondo Y, *et al*. Antitumour effect of cyclin-dependent kinase inhibitors (p16(INK4A), p18(INK4C), p19(INK4D), p21(WAF1/CIP1) and p27(KIP1)) on malignant glioma cells. Br J Cancer 2003;88:1277-1280.

170. Botti J, Djahaveri-Mergny M, Pilatte Y, Codogno P. Autophagy and signaling and the cogweels of cancer Autophagy 2006;2(2):67-73.

171. Janicke RU, Sprengart ML, Wati MR, Porter AG. Caspase-3 is required for DNA fragmentation and morphological changes associated with apoptosis. J Biol Chem 1998;273:9357-9360.

172. Daido S, Kanzawa T, Yamamoto A, Takeuchi H, Kondo Y, Kondo S. Pivotal role of the cell death factor BNIP3 in ceramide-induced autophagic cell death in malignant glioma cells. Cancer Res 2004;64:4286-4293.

173. Broker LE, Huisman C, Span SW, Rodriguez JA, Kruyt FA, Giaccone G. Cathepsin B mediates caspase-independent cell death induced by microtubule stabilizing agents in non-small cell lung cancer cells. Cancer Res 2004;64:27-30.

174. Hirsimaki Y, Hirsimaki P. Vinblastine-induced autophagocytosis: the effect of disorganization of microfilaments by cytochalasin B. Exp Mol Pathol 1984;40:61-69.

175. Opipari Jr AW, Tan L, Boitano AE, Sorenson DR, Aurora A, Liu JR. Resveratrol-induced autophagocytosis in ovarian cancer cells. Cancer Res 2004;64:696-703.

176. Dutcher JP. Mammalian target of rapamycin inhibition. Clin Cancer Res 2004;10:6382-6367.

177. Majno G, Joris I. Apoptosis, oncosis, and necrosis: an overview of cell death. Am J Pathol 1995;146:3-15.

178. Golstein P, Kroemer G. Cell death by necrosis: towards a molecular definition. Trends Biochem Sci 2007;32(1):37-43.

179. Liu X, Van Vleet T, Schnellmann RG. The role of calpain in oncotic cell death. Annu Rev Pharmacol Toxicol 2004;44:349-370.

180. Lieberthal W, Menza SA, Levine JS. Graded ATP depletion can cause necrosis or apoptosis of cultured mouse proximal tubular cells. Am. J Physiol. Renal Physiol 1998;274:F315-F327.

181. Festjens, N. et al. Necrosis, a well-orchestrated form of cell demise: signalling cascades, important mediators and concomitant immune response. Biochim Biophys Acta 2006;1757, 1371-1387.

182. Kawahara A, Ohsawa Y, Matsumura H, Uchiyama Y, Nagata S. Caspase-independent cell killing by Fas associated protein with death domain. J Cell Biol 1998;143: 1353-1360.

183. Holler N, Zaru R, Micheau O, Thome M, Attinger A, Valitutti S, *et al.* Fas triggers an alternative, caspase-8-independent cell death pathway using the kinase RIP as effector molecule. Nat Immunol 2000;1:489-495.

184. Harriman JF, Liu XL, Aleo MD, Machaca K, Schnellmann RG. Endoplasmic reticulum Ca^{2+} signaling and calpains mediate renal cell death. Cell Death Differ 2002;9:734-741.

185. Liu X, Van Vleet T, Schnellmann RG. The role of calpain in oncotic cell death. Annu Rev Pharmacol Toxicol 2004;44:349-370.

186. Michetti M, Salamino F, Tedesco I, Averna M, Minafra R, Melloni E, *et al.* Autolysis of human erythrocyte calpain produces two active enzyme forms with different cell localization. FEBS Lett 1996;392:11-15

187. Liu X, Rainey JJ, Harriman JF, Schnellmann RG. Calpains mediate acute renal cell death: role of autolysis and translocation. Am J Physiol Renal Physiol 2001;81:F728-F738.

188. Liu X, Harriman JF, Schnellmann RG. Cytoprotective properties of novel nonpeptide calpain inhibitors in renal cells. J Pharmacol Exp Ther 2002;302:88-94.

189. Waters SL, Sarang SS, Wang KKW, Schnellmann RG. Calpains mediate calcium and chloride influx during the late phase of cell injury. J Pharmacol Exp Ther 1997;283:1177-1184.

190. Warburg O. On respiratory impairment in cancer cells. Science. 1956;124(3215):269-270.

191. Pedersen PL. Tumor mitochondria and the bioenergetics of cancer cells. Prog Exp Tumor Res 1978;22:190-274.

192. Fulda S, Debatin KM. HIF-1-regulated glucose metabolism: a key to apoptosis resistance? Cell Cycle 2007;6(7):790-792.

193. Flier JS, Mueckler MM, Usher P, Lodish HF. Elevated levels of glucose transport and transporter messenger RNA are induced by ras or src oncogenes. Science 1987;235:1492-1495.

194. Elstrom RL, Bauer DE, Buzzai M, Karnauskas R, Harris MH, Plas DR, *et al.* Akt stimulates aerobic glycolysis in cancer cells. Cancer Res 2004;64:3892-3899.

195. Gatenby RA, Gillies RJ. Why do cancers have high aerobic glycolysis? Nat Rev Cancer 2004;4(11):891-899.

196. Thompson CB, Bauer DE, Lum JJ, Hatzivassiliou G, Zong WX, Zhao F, *et al.* How do cancer cells acquire the fuel needed to support cell growth? Cold Spring Harb Symp Quant Biol 2005;70:357-362.

197. Shaw RJ. Glucose metabolism and cancer. Curr Opin Cell Biol 2006;18(6):598-608.

198. Zong WX, Thompson CB. Necrotic death as a cell fate. Genes Dev 20061;20(1):1-15.

199. Degenhardt K, Mathew R, Beaudoin B, Bray K, Anderson D, Chen G, *et al.* Autophagy promotes tumor cell survival and restricts necrosis, inflammation, and tumorigenesis. Cancer Cell 2006;10(1):51-64.

200. Ferrara N, Kerbel RS. Angiogenesis as a therapeutic target. Nature 2005;438(7070):967-974.

201. Carmeliet P. Angiogenesis in life, disease and medicine. Nature 2005;438(7070):932-936.

202. Zong WX, Ditsworth D, Bauer DE, Wang ZQ, Thompson CB. Alkylating DNA damage stimulates a regulated form of necrotic cell death. Genes Dev 2004;18(11):1272-1282.

203. Jin S, DiPaola RS, Mathew R, White E. Metabolic catastrophe as a means to cancer cell death. J Cell Sci 2007;120(Pt 3):379-383.

204. Castedo M, Perfettini JL, Roumier T, Andreau K, Medema R, Kroemer G. Cell death by mitotic catastrophe: a molecular definition. Oncogene 2004;23(16):2825-2837.

205. Chen Z, Xiao Z, Chen J, Ng SC, Sowin T, Sham H, *et al.* Human Chk1 expression is dispensable for somatic cell death and critical for sustaining G_2 DNA damage checkpoint. Mol Cancer Ther 2003;2(6):543-548.

206. Castedo M, Perfettini JL, Roumier T, Yakushijin K, Horne D, Medema R, *et al.* The cell cycle checkpoint kinase Chk2 is a negative regulator of mitotic catastrophe. Oncogene 2004;23(25):4353-4361.

207. Weaver BA, Cleveland DW. Does aneuploidy cause cancer? Curr Opin Cell Biol 2006;18(6):658-667.

208. Kim R, Emi M, Tanabe K. The role of apoptosis in cancer cell survival and therapeutic outcome. Cancer Biol Ther 2006;5(11):1429-1442.

209. Okada H, Mak TW. Pathways of apoptotic and non-apoptotic death in tumour cells. Nat Rev Cancer 2004;4(8):592-603.

210. Freshney RI. Animal cell cultures. 3rd ed. Oxford: URL Press; 1995.

211. Gillies RJ, Didier N, Denton M. Determination of cell number in monolayer cultures. Anal Biochem 1986;159(1):109-113.

212. Kueng W. Silber E. Eppenberger U. Quantification of cells cultured on 96-well plates. Anal Biochem 1989;182:1;16-19.

213. Berry JM, Huebner E, Butler M. The crystal violet nuclei staining technique leads to anomalous results in monitoring mammalian cell cultures. Cytotechnology 1996;21:1;73-80.

214. American Type Culture Collection [www.ATCC.org]. Manassas, USA; [updated 2007 April 31; cited 2007 November 14]. Available from: http://www.atcc.org/common/catalog/numSearch/numResults.cfm?atccNum=HTB-22

215. American Type Culture Collection [www.ATCC.org]. Manassas, USA; [updated 2007 April 31; cited 2007 November 14]. Available from: http://www.atcc.org/common/catalog/numSearch/numResults.cfm?atccNum=CRL-10782

216. Mosmann, T. Rapid Colorimetric Assay for Cellular Growth and Survival: Application to Proliferation and Cytotoxicity Assays. J. Immunol Meth 1983;65:55-63.

217. Thompson, SW. Selected Histochemical and histopathological methods. Springfield, C.C. Thomas Publications 1966, p.377-378.

218. Klionsky DJ, Cuervo AM, Seglen PO. Methods for monitoring autophagy from yeast to human. Autophagy 2007 May-Jun;3(3):181-206.

219. Burge RE. Contrast and image formation of biological specimens. Princ Tech Elec Microsc 1976;6:85-116.

220. Hayes TL, Pease RF. The scanning electron microscope: principles and applications in biology and medicine. Adv Biol Med Phys 1968;12:85-137.

221. Wettenhall JM, Smyth GK. limmaGUI: a graphical user interface for linear modeling of microarray data. Bioinformatics 2004 Dec 12;20(18):3705-3706.

222. Smyth GK, Speed T. Normalization of cDNA microarray data. Methods. 2003 Dec;31(4):265-273.

223. Benjamini Y, Hochberg Y. Controlling the false discovery rate: a practical and powerful approach to multiple testing. J R Statist Soc B 1995(1);57: 289-300.

224. Carmona-Saez P, Chagoyen M, Tirado F, Carazo JM, Pascual-Montano A: GENECODIS: A web-based tool for finding significant concurrent annotations in gene lists. Genome Biology 2007 8(1):R3

225. Pirooznia M, Nagarajan V, Deng Y. GeneVenn - A web application for comparing gene lists using Venn diagrams. Bioinformation 2007 Apr 10;1(10):420-422.

226. Grever MR, Schepartz SA, Chabner BA. The National Cancer Institute: cancer drug discovery and development program. Semin Oncol 1992 Dec;19(6):622-638.

227. Izevbigie EB, Ekunwe SI, Jordan J, Howard CB. Ethanol modulates the growth of human breast cancer cells in vitro. Exp Biol Med (Maywood) 2002 Apr;227(4):260-265.

228. Vistica DT, Skehan P, Scudiero D, Monks A, Pittman A, Boyd MR. Tetrazolium-based assays for cellular viability: a critical examination of selected parameters affecting formazan production. Cancer Res 1991 May 15;51(10):2515-2520

229. Liu Y, Peterson DA, Kimura H, Schubert D. Mechanism of cellular 3-(4,5-dimethylthiazol-2-yl)-2,5-diphenyltetrazolium bromide (MTT) reduction. J Neurochem 1997 Aug;69(2):581-593.

230. Wettenhall JM, Smyth GK. limmaGUI: a graphical user interface for linear modeling of microarray data Bioinformatics 2004 Dec 12;20(18):3705-3706.

231. Misquitta CM, Chen T, Grover AK. Control of protein expression through mRNA .stability in calcium signalling. Cell Calcium 2006 Oct;40(4):329-346.

232. Khabar KS. The AU-rich transcriptome: more than interferons and cytokines, and its role in disease. J Interferon Cytokine Res 2005 Jan;25(1):1-10.

233. Alesse E, Zazzeroni F, Angelucci A, Giannini G, Di Marcotullio L, Gulino A. The growth arrest and downregulation of c-myc transcription induced by ceramide are related events dependent on p21 induction, Rb underphosphorylation and E2F sequestering. Cell Death Differ 1998 May;5(5):381-389.

234. Vita M, Henriksson M. The Myc oncoprotein as a therapeutic target for human cancer. Semin Cancer Biol 2006 Aug;16(4):318-330.

235. Knoepfler PS. Myc goes global: new tricks for an old oncogene. Cancer Res 2007 Jun 1;67(11):5061-5063.

236. Raught B, Gingras AC, James A, Medina D, Sonenberg N. Expression of a translationally regulated, dominant-negative CCAAT/enhancer-binding protein beta isoform and up-regulation of the eukaryotic translation initiation factor 2alpha are correlated with neoplastic transformation of mammary epithelial cells. Cancer Res 1996 Oct 1;56(19):4382-4386.

237. Zahnow CA, Younes P, Laucirica R, Rosen JM. Overexpression of C/EBPbeta-LIP, a naturally occurring, dominant-negative transcription factor, in human breast cancer. J Natl Cancer Inst 1997 Dec 17;89(24):1887-1891.

238. Sterneck E, Zhu S, Ramirez A, Jorcano JL, Smart RC. Conditional ablation of C/EBP beta demonstrates its keratinocyte-specific requirement for cell survival and mouse skin tumorigenesis. Oncogene. 2006 Feb 23;25(8):1272-1276.

239. Lamb J, Ramaswamy S, Ford HL, Contreras B, Martinez RV, Kittrell FS, *et al.* A mechanism of cyclin D1 action encoded in the patterns of gene expression in human cancer. Cell 2003 Aug 8;114(3):323-334.

240. Wu KK, Liou JY, Cieslik K. Transcriptional Control of COX-2 via C/EBPbeta. Arterioscler Thromb Vasc Biol 2005 Apr;25(4):679-685.

241. Gardner K, Moore TC, Davis-Smyth T, Krutzsch H, Levens D. Purification and characterization of a multicomponent AP-1.junD complex from T cells. Dependence on a separate cellular factor for enhanced DNA binding activity. J Biol Chem 1994 Dec 30;269(52):32963-32971.

242. Byun HJ, Hong IK, Kim E, Jin YJ, Jeoung DI, Hahn JH, *et al.* A splice variant of CD99 increases motility and MMP-9 expression of human breast cancer cells through the AKT-, ERK-, and JNK-dependent AP-1 activation signaling pathways. J Biol Chem 2006 Nov 17;281(46):34833-34847.

243. Westermarck J, Kähäri VM. Regulation of matrix metalloproteinase expression in tumor invasion. FASEB J 1999 May;13(8):781-792.

244. Sounni NE, Noel A. Membrane type-matrix metalloproteinases and tumor progression. Biochimie 2005 Mar-Apr;87(3-4):329-342.

245. Heasley LE, Han SY. JNK regulation of oncogenesis. Mol Cells 2006 Apr 30;21(2):167-173.

246. Holz MK, Ballif BA, Gygi SP, Blenis J. mTOR and S6K1 mediate assembly of the translation preinitiation complex through dynamic protein interchange and ordered phosphorylation events. Cell 2005 Nov 18;123(4):569-580.

247. Huber A, Bai P, de Murcia JM, de Murcia G. PARP-1, PARP-2 and ATM in the DNA damage response: functional synergy in mouse development. DNA Repair (Amst) 2004 Aug-Sep;3(8-9):1103-1108.

248. Paunesku T, Mittal S, Protić M, Oryhon J, Korolev SV, Joachimiak A, *et al.* Proliferating cell nuclear antigen (PCNA): ringmaster of the genome. Int J Radiat Biol 2001 Oct;77(10):1007-1021.

249. Papa S, Monti SM, Vitale RM, Bubici C, Jayawardena S, Alvarez K, *et al.* Insights into the structural basis of the GADD45beta-mediated inactivation of the JNK kinase, MKK7/JNKK2. J Biol Chem 2007 Jun 29;282(26):19029-190241.

250. Takahashi H, Komatsu N, Ibe M, Ishida-Yamamoto A, Hashimoto Y, Iizuka H. Cystatin A suppresses ultraviolet B-induced apoptosis of keratinocytes. J Dermatol Sci 2007 Jun;46(3):179-187.

251. Tan BK, Vanitha J. Immunomodulatory and antimicrobial effects of some traditional chinese medicinal herbs: a review. Curr Med Chem 2004 Jun;11(11):1423-1430.

252. Germplasm Resources Information Network [http://www.ars-grin.gov/]. Beltsville (MD): National Genetic Resources Program (US); [updated 2007 October 29; cited 2007 November 21]. Available from: http://www.ars-grin.gov/cgi-bin/npgs/html/genus.pl?13428

253. Germplasm Resources Information Network [http://www.ars-grin.gov/]. Beltsville (MD): National Genetic Resources Program (US); [updated 2007 October 29; cited 2007 November 21]. Available from: http://www.ars-grin.gov/cgi-bin/npgs/html/genus.pl?11733

254. Katerere DR, Eloff JN. Antibacterial and antioxidant activity of *Sutherlandia frutescens* (*Fabaceae*), a reputed anti-HIV/AIDS phytomedicine. Phytother Res 2005 Sep;19(9):779-781.

255. Chadwick WA, Roux S, van de Venter M, Louw J, Oelofsen W. Anti-diabetic effects of *Sutherlandia frutescens* in Wistar rats fed a diabetogenic diet. J Ethnopharmacol 2007 Jan 3;109(1):121-127.

256. Yin X, Zhang Y, Wu H, Zhu X, Zheng X, Jiang S, Zhuo H, Shen J, Li L, Qiu J. Protective effects of Astragalus saponin I on early stage of diabetic nephropathy in rats. J Pharmacol Sci 2004 Jun;95(2):256-266.

257. Sinclair S. Chinese herbs: a clinical review of Astragalus, Ligusticum, and Schizandrae. Altern Med Rev. 1998 Oct;3(5):338-344.

258. Tan BK, Vanitha J. Immunomodulatory and antimicrobial effects of some traditional chinese medicinal herbs: a review. Curr Med Chem 2004 Jun;11(11):1423-1430.

259 Cho WC, Leung KN. In vitro and in vivo anti-tumor effects of Astragalus membranaceus. Cancer Lett 2007 Jul 8;252(1):43-54.

260. Olivier DK, Grabielse VS, Albrecht C, van Wyk BE, van Heerden FR. SU-1 and SU-2, triterpinoids from *Sutherlandia frutescens Microphylla.* In press 2007.

261. Mills S, Bone K. Principles and Practice of Phytotherapy. Edinburgh, Scotland: Churchill Livingstone; 2000; pp. 273-279.

262. Shen P, Liu MH, Ng TY, Chan YH, Yong EL. Differential effects of isoflavones, from Astragalus membranaceus and Pueraria thomsonii, on the activation of PPARalpha, PPARgamma, and adipocyte differentiation in vitro. J Nutr 2006 Apr;136(4):899-905.

263. Michalik L, Desvergne B, Wahli W. Peroxisome-proliferator-activated receptors and cancers: complex stories. Nat Rev Cancer 2004 Jan;4(1):61-70.

264. Balakumar P, Rose M, Ganti SS, Krishan P, Singh M. PPAR dual agonists: are they opening Pandora's Box? Pharmacol Res 2007 Aug;56(2):91-98.

265. Blanquart C, Barbier O, Fruchart JC, Staels B, Glineur C. Peroxisome proliferator-activated receptors: regulation of transcriptional activities and roles in inflammation.
J Steroid Biochem Mol Biol 2003 Jun;85(2-5):267-273.

266. Rumi MA, Ishihara S, Kazumori H, Kadowaki Y, Kinoshita Y. Can PPAR gamma ligands be used in cancer therapy? Curr Med Chem Anticancer Agents 2004 Nov;4(6):465-477.

267 Cho DH, Choi YJ, Jo SA, Ryou J, Kim JY, Chung J, *et al.* Troglitazone acutely inhibits protein synthesis in endothelial cells via a novel mechanism involving protein phosphatase 2A-dependent p70 S6 kinase inhibition. Am J Physiol Cell Physiol 2006 Aug;291(2):C317-326.

268. Baranowski M, Blachnio A, Zabielski P, Gorski J. Pioglitazone induces de novo ceramide synthesis in the rat heart. Prostaglandins Other Lipid Mediat 2007 Feb;83(1-2):99-111.

269. Baranowski M, Błachnio A, Zabielski P, Górski J. PPARalpha agonist induces the accumulation of ceramide in the heart of rats fed high-fat diet. J Physiol Pharmacol 2007 Mar;58(1):57-72.

270. Kim KY, Kim SS, Cheon HG. Differential anti-proliferative actions of peroxisome proliferator-activated receptor-gamma agonists in MCF-7 breast cancer cells. Biochem Pharmacol 2006 Aug 28;72(5):530-540.

271. Lee YR, Yu HN, Noh EM, Kim JS, Song EK, Han MK, *et al*. Peroxisome proliferator-activated receptor gamma and retinoic acid receptor synergistically up-regulate the tumor suppressor PTEN in human promyeloid leukemia cells. Int J Hematol 2007 Apr;85(3):231-237.

272. Zhang W, Wu N, Li Z, Wang L, Jin J, Zha XL. PPARgamma activator rosiglitazone inhibits cell migration via upregulation of PTEN in human hepatocarcinoma cell line BEL-7404. Cancer Biol Ther 2006 Aug;5(8):1008-1014.

273. Lee SY, Hur GY, Jung KH, Jung HC, Lee SY, Kim JH, *et al*. PPAR-gamma agonist increase gefitinib's antitumor activity through PTEN expression. Lung Cancer 2006 Mar;51(3):297-301.